Biopolymer-Based Nanofiber Mats and Their Characterization and Applications

BY

Shahrzad Mohammadtalab Khansari
BCS, Sharif University of Technology, Tehran, Iran

THESIS

Submitted as a partial fulfillment of the requirements
for the degree of Doctor of Philosophy in Mechanical Engineering
in the Graduate College of
University of Illinois at Chicago, 2013

Chicago, Illinois

Defense Committee:

Prof. Alexander L. Yarin, Mechanical and Industrial Engineering Department, Chair
Prof. Farzad Mashayek, Mechanical and Industrial Engineering Department
Dr. Suman Sinha-Ray, Mechanical and Industrial Engineering Department
Prof. Kenneth Brezinsky, Mechanical and Industrial Engineering Department
Dr. Alan W. Nicholls, Research Resources Center

This thesis is dedicated to my mother (Aniss Pezeshk) and my father (Sobhan M Khansari) whose love and support has always guided me through my life.

ACKNOWLEDGEMENTS

I would like to thank my parents for standing by my side all these years and supporting me through every single phase of my life. They have always been great mentors for me. All their lives, they have worked hard and sincerely to provide the best for me and I cannot thank them enough. Through every-day life challenges, all they cared about was my success and happiness. They have been great role models for me and they will always be my heroes.

I would like to express my profound gratitude to my advisor Prof. A.L. Yarin whose enthusiasm and passion for science has always been inspiring for me. With an undergraduate degree in Chemical Engineering, it was Prof. Yarin's sincere guidance and patience that made me through PhD program in Mechanical Engineering. He taught me how to fight for something you want the most and never give up. Working in his research group has been an honor for me and I am deeply grateful for that.

I would like to take a moment and appreciate Dr. Sinha-Ray's contribution during my PhD research. As a post-doctoral fellow, he has guided through my research and inspired me by his problem-solving skills and challenge-seeking personality. I would also want to thank my all my lab-mates in The Multiscale Mechanics and Nanotechnology Laboratory who provided a dynamic and professional learning environment in the lab and actively cooperated with me through my research.

Last but not least, I would like to appreciate my committee member's guidance and helpful comments throughout my work, which helped towards more achievements in my PhD research and made my thesis a comprehensive piece of work.

TABLE OF CONTENTS

CHAPTER **PAGE**

LIST OF TABLES

TABLE **PAGE**

LIST OF TABLES (CONTINUED)

LIST OF TABLES (CONTINUED)

LIST OF FIGURES

FIGURE **PAGE**

LIST OF FIGURES (CONTINUED)

LIST OF FIGURES (CONTINUED)

LIST OF FIGURES (CONTINUED)

LIST OF FIGURES (CONTINUED)

OVERVIEW AND SUMMARY

Biodegradable biopolymers are those degradable polymers in which their degradation is brought about as a result of natural microorganisms, such as bacterea, etc. (Shimao, 2001). Biomaterials encompass a large variety of biodegradable compounds. Biopolymers are majorly produced from renewable and sustainable biological resources such as plants and animals or they might be the products of chemical synthesis of carbohydrates, oil, etc. Biopolymers from plants and animals are typically isolated from plant- and animal-based tissues.

The introduction, functionalization and characterization of biopolymers for industrial applications have gained much attention in the recent twenty years. Due to ecological issues and high prices for petroleum-based products, there is an urgency to provide sustainable biodegradable alternatives with comparable properties with those of synthetic ones. Specifically, there is significant potential in biopolymeric films and composites and their functionalization in paper coating, adhesives, automotive and textile industry (Schiffman et al., 2008).

Apart from film and composite production, there has been a sudden increase in production and fabrication of biopolymer nanofibers since the early 1990's. This upraise revealed a significant increase from the year 2000 (Schiffman et al., 2008). Distinct properties of nano-scaled materials from those of bulk ones were the major driving force behind this sudden boom (Klabunde et al., 2001; Roduner et al., 2006). Biopolymeric nonwoven nanofibers could specifically contribute to textile industry, protective clothing, air filtration, catalysis, electrochemical cell, etc. (Huang et al., 2003; Ki et al., 2007).

Therefore, production of nano- and micro-fibers using conventional methods such as electrospinning increased.

Electrospinning as an industry-oriented process was first introduced by Formhals in the 1930's and 1940's (Formhals, 1934; 1939; 1940; 1943; 1944). Electrospinning of petroleum-derived synthetic polymer solutions gained popularity in the 1990's due to the work of (Doshi et al., 1995; Reneker et al., 2008; Bhardwaj et al., 2010). The commercialization of electrospinning is, however, hindered by its low production rate. Slow rate of nanofiber production by electrospinning, as well as the need for the electrically conductive solutions, restrict its application, especially on the industrial scale, where much higher production rates are needed in order to make the process economically feasible.

Consequently, an alternative method of solution blowing was introduced in (Sinha-Ray et al., 2010; Sinha-Ray et al., 2011), in which nanofibers are produced at least 30 times faster than in electrospinning. In solution blowing, polymeric solution is being issued from a spinneret hole and stretched using a co-axial high speed air flow. Due to the stretching and bending instability, the polymer solution jet is dragged down and rapidly thins, while the solvent evaporates. As a result, nano- and micro-fibers are formed and can be effectively collected. Since no electric forces is involved in this method, solution blowing can be applied to polymeric solutions that cannot be electrospun. It is also industrially applicable for the scale-up. Recently, this method attracted more attention and was applied to various types of biopolymer solutions (this thesis, Khansari et al., 2012; Zhuang et al., 2012).

The major part of this thesis is devoted to formation and characterization of soy protein-based nanofibers. Soy bean is an annually renewable crop that mainly grows in America. According to (Schiffman et al., 2008), in the year 2000, US had 49% of global soy bean production, and Latin America was the world's second largest producer of soy bean with 34 %. Soy bean is comprised of about 20 % oil, which can be converted into bio-diesel fuel. The remaining consists of mostly soy protein, fatty acids, and carbohydrates. Soy protein is extracted from soy bean and is used in producing soy-based films, resins, and plastics (Paetau et al., 1994a; Paetau et al., 1994b; Shih et al., 1994; Stuchell et al., 1994; Kalapathy et al., 1995; Kumar et al., 2002). These types of agricultural-based films and composites have shown promising results in such applications as automobile, marine industry, and rural infrastructures (Paul et al., 1983; Wool at al., 1999; Wool et al., 2000; Kumar et al., 2002). As a result, the by-product of soy bean oil extraction can add valuable by-products to the still expansive bio-fuel, as well as diminishing the environmental concerns.

In the present work, formation of soy protein-based monolithic and core-shell nanofibers via solution blowing is examined in Chapter 3. Collected nanofibers with the average diameters of 300-500 nm undergo tensile tests with different cross-head speeds in order to reveal their stress-strain behavior. Then their stress-strain characteristics are analyzed using two different models which are comprehensively discussed in Chapter 3. One of them, the micromechanical model is novel and relates nonwoven plasticity with the breakage of the individual nanofibers. Also, various experimental parameters that might affect nanofiber mats' mechanical properties are studied in Chapter 3.

Chapters 4 and 5 take the soy protein nanofiber processing further by chemical and physical enhancement of the mechanical properties of the collected nanofiber mats. In Chapter 4, several crosslinking agents such as formaldehyde, glyoxal, sodium borohydride, and zinc sulfate are used in order to produce more aggregated fibrous structures which result in stronger soy protein-based nanofiber mats. Chapter 5 mainly focuses on the physical alternatives for enhancing soy protein nanofiber mats' strength. Wet conglutination and thermal calendaring are among the methods applied in this chapter. Besides, sustainability of solution-blown plant-based nanofiber mats at elevated temperature and extreme humidity is studied in Chapter 5.

Due to biodegradability and biocompatibility of biopolymers, they are appropriate candidates for biomedical applications. These types of biodegradable materials diminish the need to remove the material after surgical implantation or when the injured tissue is repaired. This is of importance since the damaged tissue needs not to be exposed to the environment until it is fully recovered. It is expected that degradation of biopolymers in the human body would produce no foreign-body response (Martina et al., 2007; Khadka et al., 2012; Ratner et al., 2012). Recently, natural and synthetic biopolymers have found various applications, from artificial vessels, heart valves, and sutures to drug carriers and for damaged tissue regeneration.

Biopolymeric fibrous structures resemble that of native extracellular matrix (ECM) in human body. Therefore, biopolymer nanofibers can be functionalized as a support for cell growth and activation. Biodegradable and biocompatible micro- and nano- polymeric fibers have revealed potential in dental and orthopedic implantations, controlled drug delivery, wound dressing, antimicrobial substrates, biosensors, and protective textiles

against toxic chemicals (Fang et al., 2008; Still et al., 2008; McCullen et al., 2009; Sell et al., 2009; Wang et al., 2009; Yoo et al., 2009; Cui et al., 2010; Lee et al., 2011).

Chapter 6 examines durability of silver-coated soy protein nanofiber mats in aqueous medium. Due to the antimicrobial effect of silver, this type of solution-blown nanofiber mat can be used as antibacterial substrates in wound dressing and filtration.

Chapter 7 aims at elucidating traces of protein in the collected solution-blown soy protein-based nanofiber mats. A modification of the Bradford method is applied in order to prove the presence of protein in the nanofibers. This is a cheap, repeatable, fast, and reliable method and its efficiency in the case of solution-blown soy protein nanofibers is demonstrated.

In Chapter 8, soy protein-based monolithic and core-shell nanofibers are loaded with a model drug (a fluorescent dye) and undergo controlled release in aqueous medium. Also hydrophobic PET-based nanofibers loaded with two types of model drugs are produced via electrospinning. The kinetics and mechanism of drug release over time is studied in this chapter, as well as the effect of such porogens as poly ethylene glycol (PEG) on the release rate. It is shown that biodegradability and biocompatibility of soy protein-based nanofiber mats make them potential candidates as drug carriers in controlled release processes.

Chapter 9 encompasses a wide range of plant- and animal-based proteins as potential sources of solution-blown nanofiber mats. In this chapter, different proteins extracted from animal and plant tissues are used to prepare solutions and then undergo solution blowing. Nanofibers from cellulose acetate, lignin, zein, silk sericin, and bovine serum albumin are successfully produced using solution blowing. Also different blends of

the above-mentioned biopolymers are formed as nanofibers. Each type of biopolymer-based nanofiber mat is tested in order to reveal their tensile behavior and the corresponding parameters such as Young's modulus, yield stress, and maximum stress and strain at rupture. In addition, a part of Chapter 9 discusses the effects of drawing and pre-stretching on collected biopolymer nanofiber mats and how it can improve the overall mechanical properties of solution-blown protein nanofibers.

1. INTRODUCTION AND LITERATURE SURVEY

Biodegradability, abundance, and biocompatibility of plant- and animal-derived protein macromolecules hold great potential for them to be functionalized in a wide range of industrial applications, as well as in biomedical and pharmaceutical fields. Therefore, in the last twenty years, there has been a continuously growing interest towards biopolymers consumptions in composites, fillers, adhesives, coatings, cosmetics, bioplastics, etc. Besides, a tremendous increase in the cost of petroleum-derived materials stimulated biopolymers consumption even more, since plant proteins are evidently cheap and mostly annually renewable. Specifically, nano-scaled protein structures are of interest due to the improved characteristics and similarity to natural human tissues. This type of nano-scaled fibers and particles have initiated a new era in advanced materials and the way they are characterized and tailored for each specific application.

The following subsections discuss the importance of the nano-scaled biopolymers and how the state-of-the-art procedures are utilized in each section of this thesis in order to produce bio-derived nanofibers and characterize their mechanical properties. Relevant pre- and post-processing treatments are also applied to these biomacromolecular nanofibers in each section in order to further reveal their properties and various possible applications.

1.1. Stress-Strain Dependence for Soy Protein Nanofiber Mats

Booming SoyDiesel production (Ahmed et al., 1994; Klass, 1998) facilitates increasing production of soy, while using soy oil (which comprises only about 20% of

soy mass), and leaving behind abundant residual soy protein. In addition to the use of soy protein as a nutrient, it has great industrial value as well. In particular, developing innovative ways of utilizing residual soy protein resulting from SoyDiesel production will make the overall process more economically feasible and reduce cost of SoyDiesel. Moreover, these innovative soy protein-based products will help to significantly reduce dependence on oil, not only for transportation but also by replacing petroleum-based polymers by their biopolymer counterparts. Biopolymer products are even more attractive than those derived from petroleum, since the former are biodegradable, while the latter are not. Non-biodegradable packaging and other materials create significant problem with garbage utilization, and their burning contributes to production of greenhouse gases. Biodegradable materials produced from residual soy protein effectively eliminate this problem. The field where biodegradable materials can potentially replace petroleum-derived polymers encompasses textiles and nonwovens, biomedical, "green" construction, packaging materials and catalyst supports.

The first steps in the direction of utilization of soy protein resulting from SoyDiesel production have already delivered the first fruits. Namely, nano-textured nonwovens have already been produced using solution blowing in (Sinha-Ray et al., 2011). Moreover, a similar approach can be potentially applied to the other residuals of biofuel production: algae and other crops of interest. Soy protein nanofibers can be also produced by using a slower process, electrospinning (Phiriyawirut et al., 2008; Poole et al., 2009; Vega-Lugo et al., 2009; Cho et al., 2010). Both solution blowing and electrospinning employ blends of biodegradable soy protein and petroleum-derived polymers to sustain spinnability of solutions employed.

The present work is devoted to the mechanical characterization of nano-textured nonwovens produced by using the solution blowing process similar to that of (Sinha-Ray et al., 2011). In Chapter 3, the mechanical properties of blend or core-shell soy protein/nylon 6 nanofibers are also compared to those of pure nylon 6 nanofibers produced using solution blowing. The mechanical behavior revealed in the tensile tests is rationalized in the framework of two models, the standard phenomenological elasto-plastic model and the micromechanical model proposed in the present work. As a result, Young's modulus, the yield stress, and the corresponding micromechanical parameters of soy protein nanofiber mats are established, as well as the effect on them of such parameters as the rotational speed of the collector drum.

1.2. Effect of Cross-linking on Tensile Characteristics of Solution-Blown Soy Protein Nanofiber Mats: I- Chemical Cross-linking

Biodegradable polymers attract attention in relation to such applications as food packaging, construction materials, composite fillers, wood adhesives, particle boards, etc. (Kaplan, 1998; Ciannamea et al., 2010; Liu et al., 2010). However, most products made of biodegradable polymers possess low strength and high hydrophilicity. Such biopolymers as wheat gluten, soy protein, gelatin, casein, and corn zein are of high importance due to their abundance in nature and biodegradability. Low cost and abundance of soy protein makes it a unique plant protein attractive for many applications. Among different usages of soy protein, significant attention has been paid to extracting and using micro- and nanofibers from soybean (Alemdar et al., 2008; Karki et al., 2011). In several recent works, our group developed the method of preparing soy-based

nanofiber mats en masse by solution blowing (Sinha-Ray et al., 2011; Khansari et al., 2012).

The basic building blocks of proteins are amino acids which are linked by different covalent and ionic bridges (e.g.- amide, disulfide, etc.). Reactivity of proteins depends on the side chains of their free amino acids. The labile groups in the side chains are attacked by cross-linking agents and the resulting dints serve as the sites for efficient inter- and intra-molecular cross-linking. The chemically reactive groups in amino acids include carboxylic, primary and secondary amine groups, cystine, lysine, arginine, guanidyl, and sulfhydryl groups (Liu, 1997; Chabba et al., 2005). These reactive groups participate in cross-linking triggered by chemical cross-linkers or thermal treatment.

Solubility of soy protein in a solvent is determined by the competition of protein-protein interactions with protein-solvent interactions, which is related to the isoelectric point of soy protein. Therefore, solubility of soy protein can be effectively influenced by pH, ionic strength, temperature, and soy protein concentration (Gennadios et al., 1993). The most widely used cross-linkers for soy proteins include aldehyde groups with formaldehyde being the oldest and most common agent (Huang-Lee et al., 1990; Wong, 1991; Van Luyn et al., 1992; Gennadios et al., 1993; Friess, 1998). Formaldehyde cross-links protein polyamide chains by reacting with -NH, -OH and -SH groups. This reaction produces methylene bridges between polymer molecules (Fraonkel-Conrat et al., 1948; Friess, 1998). Glyoxal is a small molecule compared to most aldehyde compounds and mostly bonds amino acid side chains in one molecule (Murata-Kamiya et al., 1997; Vaz et al., 2003). Therefore, its cross-linking effect is restricted to inter-molecular structure. Also, the cross-linking effect of zinc ions is determined by the way they bond to protein

chains (Berg et al., 1996; Katz et al., 1996; Zhang et al., 2001). In addition to these, sodium borohydride, known as a strong reducing agent can also be used as a cross-linker.

The present work is devoted to finding ways of enhancing tensile properties of such soy protein nanofiber mats, which should be beneficial to a number of applications (cf. Chapter 4. This will facilitate utilization of soy protein isolates, which are otherwise considered as agro-waste.

1.3. Effect of Cross-linking on Tensile Characteristics of Solution-Blown Soy Protein Nanofiber Mats: II- Thermal and Wet Cross-linking

Unlike the works discussed in section 1.2 of the present survey, which aimed at enhancing mechanical properties of nanoscaled biopolymeric nonwovens via chemical crosslinking, this section emphasizes the physical bonding in the protein network of biopolymer nanofibers.

As discussed in the previous section, biodegradable polymers recently attracted great attention in order to develop biodegradable plastics, nonwovens, packaging materials, etc. Among biopolymers, wheat gluten, soy protein, gelatin, casein, and corn zein are of high importance due to their abundance and biodegradability (Rhim et al., 2007). A number of physical and mechanical properties of materials made of these proteins are to be explored and in many cases improved based on specific functionalities expected in a product. In the present work, solution-blown soy protein nanofiber mats produced as in (Sinha-Ray et al., 2011; Khansari et al., 2012), underwent thermal treatment under compression in order to elaborate on the effect of this treatment on their tensile strength, Young's modulus and the yield stress. Thermal calendar bonding is

widely used in nonwovens industry (Fedorova et al., 2007), and in a sense, thermal treatment under compression employed in the present work mimics it. Several works dealt with possible improvement of tensile strength of nonwovens after calendaring (Bhat et al., 2002; Bhat et al., 2004; Michielsen et al., 2006; Fedorova et al., 2007). It was observed that an overexposure of fabrics to the elevated temperature beyond the optimal conditions in thermal calendaring of fabrics leads to failure due to fiber breakage. Below the optimum conditions, an increase in temperature or bonding time enhances fabrics strength.

In (Wang et al., 2002), thermal and mechanical properties of extruded sheets of soy protein with different moisture contents were studied. In particular, water adsorption was evaluated and the plasticizing effect of water was explored. The results were compared to the corresponding data for cross-linker-treated sheets. The effect of water absorption on compression-molded soy protein plastics with polyphosphate as a filler was explored in (Zhang et al., 2001). It revealed an enhancement in water resistance and strength of specimen. In (Otaigbe et al., 1997), the effect of heat treatment on tensile strength, elongation at break and solubility in water of soy protein glycerin-plasticized films was reported. According to this research, heat-treated films became less water-soluble than the untreated films. The effect of moisture content on biodegradable films has been reported in (Gennadios et al., 1993; Gennadios et al., 1996; Gassan et al., 1997; Gassan et al., 1999; Cho et al., 2002; Pchat-Bohatier et al., 2006). In (Gennadios et al., 1993) the effect of such plasticizers as glycerol on the water absorption properties of soy protein films was studied. It was shown that different physical and barrier properties of soy protein films can be controlled varying the content of plasticizer.

In Chapter 5, an investigation of solution-blown soy protein/nylon 6 nanofiber mats is conducted in order to elucidate the effect of thermal bonding on tensile characteristics of nanofiber mats. We also investigate the effect of wet bonding and aging in water at an elevated temperature on mechanical properties of soy protein/nylon 6 nanofiber mats.

1.4. Antibacterial Activity of Solution-Blown Soy Protein Nanofiber Mats Decorated with Silver Nanoparticles and Silver Nanoparticles' Leakage in Aqueous Medium

Water pollution and shortage pose serious environmental problems worldwide, and interests in water purification or antibacterial treatments are growing substantially. Antimicrobial functionalities in water filtration are required in multiple applications, starting from membranes used in construction industry to bandages used for wound healing. For this reason, fabrication of antibacterial materials has become one of the most challenging global research issues (Ruppert et al., 1994; Bhatkhande et al., 2001; Arana et al., 2002; Ollis et al., 2003; Zhang et al., 2003; Pekakis et al., 2006; Mccullagh et al., 2007; Qi et al., 2008; Lu et al., 2011). Nanoparticles have recently gained significant attention due to their high surface to volume ratio which leads to specific characteristics that differ from bulk material. Both semiconducting ceramic and metal nanoparticles are of interest due to their potential to act as antibacterial agents. In previous studies (Fuhrmann et al., 1968; Slawson et al., 1992; Stoimenov et al., 2002; Pillai et al., 2004; Sileikaite et al., 2006; Maneerung et al., 2008; Kawata et al., 2009; Charis et al., 2011), it was shown that such metals as silver, titanium, zinc, and calcium act as antimicrobial agents, while titanic oxide, tin oxide, and silver oxide have also been proven to be

potential antibacterial ceramic materials (Haarstick et al., 1996; Fujishima et al., 2000; Huang et al., 2000; Sobczynski et al., 2001; Zielinska et al., 2003; Kabra et al., 2004; Fujishima et al., 2008). In particular, these metals and ceramics are sources of cations that react with hydroxyl and anionic groups of enzymes in bacteria which results in change of functionalization in bacterial cells. Of all metal particles, silver has shown the strongest antibacterial effect which has been investigated vastly (Fuhrmann et al., 1968; Pillai et al., 2004; Sileikaite et al., 2006; Maneerung et al., 2008; Kawata et al., 2009; Charis et al., 2011). As a result, silver nanoparticle-coated surfaces made their way into cosmetics, textiles, and pharmaceutical products. Growing interest in functionalizing silver nanoparticles for different applications brought about toxicity issue of these particles, yet it has been documented that moderate usage of silver in human's body would not have a major reverse impact (Pillai et al., 2004).

The use of nanoparticles for antibacterial applications is often difficult, e.g. for water purification, nanoparticles should be dispersed in a polluted aqueous medium to make best usage of their high surface to volume. However, the subsequent separation of nanoparticles from purified water is difficult as they remain in a colloidal state and do not sufficiently settle. As a result, an additional equipment is required for post-processing treatment (Ochuma et al., 2007). In lieu of this, an immobilized mode, or fabrication of films is often proposed as an alternative. However, this immobilized mode prevents the effective usage of nanoparticles by compacting them into a two-dimensional film which dramatically reduces the interfacial contact between nanoparticles and the polluted medium. Antibacterial treatments imply a significant area of contact of an active material with polluted medium. Nano-textured materials with open porosity, such as electrospun

or solution-blown nanofiber mats possess specific surface area in the range 10-100 m^2/g, which makes them attractive candidates for nanoparticle supports in water purification processes (Pillai et al., 2004; Reneker et al., 2006; Sileikaite et al., 2006; Filatov et al., 2007; Kawata et al., 2009; Reneker et al., 2008; Charis et al., 2011). In addition, nanofibers can be used as filters as pores with sizes in the range ~1-10 μm can catch pollutants more efficiently than standard filters (Qin et al., 2006). In addition to filtration, nanofibers are also shown to be effective for wound dressing (Doshi et al., 1995; Zahedia et al., 2010). Nanofibers with antimicrobial functionalities can facilitate development of very efficient membranes.

Silver nanoparticles represent themselves as one of the best possible candidates because silver is active without UV light due to its intrinsic antimicrobial capability.

In Chapter 6, solution-blown soybean-nylon nanofiber mats decorated with silver nanoparticles are formed. Their antibacterial effect does not require UV illumination. This allows us to introduce such novel biocatalyst supports which can be active without UV light.

Another part of the present work (Chapter 6) is dedicated to silver nanoparticles' durability while exposed to aqueous medium. In order to apply silver nanoparticles as anti-microbial agents for certain applications such as filtration, it is needed to investigate these nanoparticles' behavior when exposed to liquid medium over long period of time. Consequently, silver ions leakage into water or any other type of liquid can be demonstrated. Sustainability of silver nanoparticles coated on soy protein nanofibers' surface when immersed in water medium is investigated in the present work.

Silver ion release from the surface of electrospun nanofibers as well as composites has been vastly studied in the literature. In (Min et al., 2008), it was shown that about 99% of silver nanoparticles decorated on the surface of silica nanofibers were left intact after 24 h of water exposure. This value was acquired for silver nanoparticles treated with UV. Silver ions release profile from poly(L-Lactide) fibers has been reported in (Xu et al., 2006) using atomic absorption spectroscopy. Ag/PLA samples were immersed in phosphate buffered saline and after specific equal time intervals, liquid solution was tested for the trace of silver ion in it. The cumulative release amount was less than 500 ppm over 20 days of release test for 32 wt% AgNO3/PLA. In (Radetic et al., 2008), silver nanoparticles were placed on polyester and polyamide fabrics. Following specific procedure as in (Radetic et al., 2008), laundering durability of silver-coated samples after 5 consecutive washing cycles was investigated. Before undergoing washing steps, samples revealed 99.9% of bacterial removal whereas this value reduced to 85.3% after five cycles of washing treatment, which indicates reduction in the number of silver particles which act as antibacterial agent. Release profile of silver ions from extruded polyamide was shown in (Kumar et al., 2005). Silver-coated samples were immersed in water and water samples were collected to analyze presence of silver ion at specified intervals using atomic absorption spectroscopy. It is concluded in (Kumar et al., 2005) that release rate increases over time.

1.5. Protein Tracing in Soy Protein/Nylon 6 Nanofiber Mats Using Coomassie Brilliant Blue G250

Protein tracking is of immense importance especially in biological studies. A common method to stain proteins is Bradford essay in which Coomassie Brilliant Blue G250 is dissolved in ethanol and phosphoric acid. Due to the acidity condition, dye solution is brownish, yet protein exposure forms blue complex of dye-protein. Then optical absorbance is conducted at 595 nm wavelength. This method is majorly used in staining protein bands that are separated in polyacrylamide gel. The procedure of protein binding with Brilliant Blue G250 is fast and reproducible. Besides, Bradford staining interferes less with non-protein compounds in the samples and it is specifically developed for protein detection. Coomassie brilliant Blue G250 used in this method has high color intensity which makes proteins easily noticeable (Bradford, 1976).

Several different methods have been proposed in order to recognize protein, such as Standard Lowry, Lawry and biuret assays (Grassman et al., 1950; Bennett, 1967), but complicated procedures are huge drawbacks for these methods to be commonly used. A modified alternative of Bradford assay is introduced in the present work in Chapter 7 in order to trace soy protein isolate in monolithic and core-shell soy protein-based nanofiber mats.

1.6. Controlled Drug Release from Solution-Blown Soy Protein Nanofiber Mats

Recent developments for maintaining broken or diseased tissues involve biodegradable and biocompatible scaffold in order to make the scaffold function as a target tissue (Caplan et al., 2000; Cancedda et al., 2003; Tuan et al., 2003; Li et al.,

2005a). The main objective in producing tissue scaffolds is to produce a material which resembles native extracellular matrix (ECM) in case of physical and biological structure as well as chemical composition (Ma et al., 2005b). Engineered tissues provide a temporary base for cells until the ECM is regenerated or repaired (Liu et al., 2004; Sharma et al., 2004; Pham et al., 2006).

An interesting feature of native ECM is its nano-scaled structure. Fibers existing in typical tissues range from ten to a few hundred nanometers. These aggregated nanofibers present in ECM form a nonwoven nanofibrous matrix. Native ECM consists of nano-scaled compounds such as collagen. Cellular behavior and activity is directly affected by the dimension of scaffold fibers (Flemming et al., 1999; Price et al., 2003).

Nano-scaled characteristics of native tissues are of great importance while designing engineered tissues such as blood vessel tissues. Higher cell adhesion is reported for fibers with dimensions smaller than the actual cell size; as a result, cells' activity improves (Laurencin et al., 1999).

It is stated in (Price et al., 2003) that osteoblast and osteoclast were more active while exposed to spherical nano-phase alumina particles, which mimics the structure of hydroxyapatite crystals present in bone tissues. Obvious resemblance between PCL electrospun nanofiber mesh with native ECM in rat's cornea is reported in (Ma et al., 2005).

Biocompatibility of engineered tissues is an important aspect in order to prohibit major immune response due to incompatibility with the host tissue. Porosity is another major factor needed for smooth and fast transition of nutrients and cell attachment and activity. Biodegradability is another critical feature required for implanted tissue so that

another surgery is not needed to remove the scaffold after the injured tissue is repaired (Liu et al., 2004; Sharma et al., 2004; Rosso et al., 2005; Pham et al., 2006).

Biopolymer nanofibers have been utilized in cartilage and bone tissues (Li et al., 2003; Li et al., 2005a; Li et al., 2005b). Natural nanofibers such as silk, chitosan, and dextran were electrospun and functionalized as tissue scaffolds (Boland et al., 2004a; Jin et al., 2004). Silk fibers were successfully utilized in bone marrow stem cell attachment and growth (Jin et al., 2004).

In order to further enhance tissue functionalization and its biocompatibility as well as cell adhesion to them, multilayered nanofiber mats were used as scaffolds. For instance, collagen types I and III were collected as layered fiber mats so that structure of scaffold mimics native situation more closely (Matthews et al., 2002; Boland et al., 2004b).

Production of mixed biopolymer nanofibers with distinct degradation times is another method to improve cell attachment and in-growth. When one biopolymer degrades much faster than the other polymer in the scaffold, it produces voids with few hundred nanometers to micrometer scales in the tissue structure which brings about more cell adhesion to the fibrous mesh. As shown in (Kidoaki et al., 2005), mixture of PCL and gelatin nanofibers led to more porous structure due to fast degradation of gelatin.

High surface area to volume ratio of polymeric biomaterial nanofibers brings about great potential for them to be functionalized as drug delivery carriers. Drug delivery through biopolymers is of high interest since these materials are capable of delivering the drug load efficiently to a specified type of cell or compartment in the body (Gombotz et al., 1995). Besides, most of the times drug delivery should be combined with implanting

biodegradable scaffolds for disinfection and repairing of diseased or injured tissue. In general, lower dimension for the drug carrier increases the rate of dissolving the drug in the body and consequently enhances drug absorbance to the specified target.

Several drugs have been examined and delivered by controlled release process via nanofibrous scaffolds as in (Verreck et al., 2003; Ma et al., 2005b). In (Kenawy et al., 2002), tetracycline hydrochloride was released from poly(ethylene-co-vinylacetate) (PEVA) nanofibers, poly(lactic acid) (PLA) nanofiber mesh, or their 50/50 wt% blend. Also nanofibrous structure of poly(lactic acid) mat was used for loading antibiotic drug Mexofin which prevents surgery induced adhesions.

Typically, in order to produce nanofibers as drug carriers, drug is premixed with the solution before undergoing any type of nanofiber producing mechanism. After the fibers are produced, drug might be in the form of nanoparticles exposed on nanofiber surface. Another possibility is that drug and the solution turn into one type of nanofiber blend. Also they might form two distinct nanofibers. In addition, it might be possible to have the drug encapsulated inside nanofibers (Cancedda et al., 2003).

The main goals of controlled drug delivery is to optimize drug release and to minimize drug's side effects by targeting specific cells or tissues as well as high compatibility of drug with human's body (Burgess et al., 1987; Robinson et al., 1987; Li et al., 2005b). Targeted delivery is advantageous specifically for highly toxic drugs such as anticancer agents (Fung et al., 1997; Leach et al., 1999).

Cases of biocompatible and/or biodegradable polymers used in controlled drug delivery are demonstrated in (Gilding et al., 1979; Lewis et al., 1990) and several

biopolymers are discussed as potential drug carriers in (Laurencin et al., 1999; Li et al., 2005b; Ma et al., 2005b).

As reported in (Anderson et al., 1997), the first commercial product for controlled drug delivery from biodegradable polymers was revealed in 1989 termed as 'Lupron® Depot'. This product was leuprolide encapsulated in poly(D,L-lactide-co-glycolide) (PLGA) microspheres.

Several models have been proposed for controlled-drug delivery (Wise et al., 2000; Narasimhan et al., 2001; Langer et al., 2003). As stated in (Langer et al., 2003), general mechanism for drug delivery is either diffusion, chemical reaction, or solvent activation, and transport. As discussed in (Anderson et al., 1997), major mechanism for drug delivery from biodegradable polymers consists of diffusion, osmosis, and polymer degradation.

Overall, nanofiber mats hold potential of being used in biomedical applications. Both monolithic and core-shell fibers are of interest. Controlled drug release from monolithic and core-shell nanofibers was studied in (Kenawy et al., 2002; Huang et al., 2003b; Moroni et al., 2006; Srikar et al., 2008; Gandhi et al., 2009). It should be noted that core-shell nanofibers loaded with drug or dye in the core reveal reduced release. To facilitate release in such cases, a compound leachable in water, and called porogen (a pore promoter), should be added to the shell, which helps to expose drug or dye embedded in the core to the surrounding medium. As a porogen, poly (ethylene glycol), PEG, can be added to the other fiber-forming polymers (Liao et al., 2006). PEG is a non-toxic polymer which can be passed by kidney for molecular weights less than 10 KDa (Liao et al., 2006). The fact that without porogens, non-degradable nanofibers release far

less embedded compounds than 100% was attributed in (Srikar et al., 2008; Gandhi et al., 2009) to the drug/dye desorption being the limiting mechanism of the release process, while solid-state diffusion is immaterial.

All nanofiber mats used in drug release experiments so far, were obtained by electrospinning. Electrospinning is a relatively slow process, and there is a significant interest in other processes which can form nanofibers at a much higher rate. Recently, solution blowing process was introduced as an economically feasible alternative for the industrial-scale production of nanofibers, which is much faster than electrospinning (Sinha-Ray et al., 2010a). This method uses high speed air as a driving force to blow polymer solution into nanofibers. Both monolithic and core-shell nanofibers can be formed using solution blowing (Sinha-Ray et al., 2010a). This method has already been applied to produce biocompatible and biodegradable soy protein, solution-blown nanofibers (Sinha-Ray et al., 2011; Khansari et al., 2012).

In addition to biocompatible scaffolds, significant efforts aimed at development of biocompatible and biodegradable sutures, for which soy protein seems to be an attractive candidate (Sessa et al., 1998). However, the problem with the available soy protein-based sutures is in their low strength (https://engineering.purdue.edu/ABE/InfoFor/CurrentStudents/SeniorProjects/2012/MorrisonShahUstynoskiWolak). Moreover, the available methods of manufacturing soy-based sutures involve extrusion at high temperature, which excludes the possibility of loading the raw material with drugs that can facilitate healing. In this regard, isothermal solution blowing demonstrated in (Sinha-Ray et al., 2011; Khansari et al., 2012) holds great potential for biomedical sutures.

PET-based materials are widely used as surgical sutures and meshes owing to their physical and chemical properties (Ramires et al., 2000; Ma et al., 2005c; Veleirinho et al., 2008; Duzyer et al., 2011; Whelove et al., 2011). Electrospun PET nanofiber mats hold great potential, as electrospinning allows the nanofiber mat to be functionalized at room temperature (Duzyer et al., 2011). In practice the drugs intended to be used for controlled release can be either completely or partially soluble in the solvent of the host polymer resulting in a variation of surface compatibility. The drug release can be modulated by choice of porogens. To the best of our knowledge, no in-depth studies on the effect of porogens on release kinetics was conducted.

In the present work in Chapter 8, two systems are studied. The first one is soy protein-containing nanofibers with embedded Rhodamine B, a model drug which is readily soluble in the solvent and aqueous media. These nanofibers are formed by solution blowing using the host-guest approach, with nylon 6 or PVA being the host polymers, while soy protein being the guest biopolymer. The choice was done judiciously as both host polymers are used as biologically safe and proven biomaterials (Stammen et al., 2001). The second system explored is the PET-based nanofibers loaded with Rhodamine B or riboflavin. Riboflvin is used as a model drug which is poorly soluble in the solvent and aqueous media. Riboflavin and Rhodamine B are separately premixed in the polymeric solutions and riboflavin- and Rhodamine B-containing PET-based nanofiber mats are formed using electrospinning. The release kinetics of model drugs from both systems is studied, which is the main aim of the present work.

1.7. Biopolymer-derived Nanofiber Mats and Their Mechanical Characterization

Due to the technological, environmental and political considerations, substituting traditional synthetic composites and plastics made of glass, polyesters and other polymers by biodegradable natural biopolymers attracted significant attention since the 1990's. Such synthetic materials as reinforcers and fillers made of epoxy, polyurethanes, and phenolics remain stable after their usage period ends which results in severe littering, environmental problems, and recycling concerns (Mahonty et al., 2000; Andrady et al., 2007). As a case in point, biodegradation of blown poly(ethylene terephthalate) bottles is studied in (Kint et al., 1999; Wellen et al., 2012). It is shown that 50% of materials loss occurs in 30-40 years at $20^{\circ}C$ and 45-100% relative humidity. It is also mentioned that film tapes take as long as 100 years for degradation in environment under the above-mentioned conditions.

The demand to replace synthetic products by sustainable and biodegradable materials stimulated research work on high-value biopolymer-derived materials which have mechanical properties comparable to those of the petroleum-derived ones. Humidity resistance, processibility, and manufacturing costs are major issues for biodegradable materials which are produced from plant proteins, e.g. soy protein, starch, cellulose, lignin, and zein (Chandra et al., 1998; Kaplan, 1998; Huang et al., 2003a).

Soy protein is one of the low-cost and abundant bio-polymers (Liu et al., 1997; Kaplan, 1998) which is commercially used in plastics, fillers and adhesives. Compression molding and extrusion are usually employed to produce soy plastics (Paetau et al., 1994a; Sue et al., 1997; Mo et al., 1999; Zhang et al., 2001).

Cellulose is a natural polymer which had been isolated from plant structure over 150 years ago (O'Sullivan, 1997). Cellulose has a fibrous structure and comprises a significant percentage of the wood parts in plant structure. In particular, over 40% of wood and 90% of cotton fiber structure are comprised of cellulose (Krassig et al., 1993; Kamide et al., 2005; Stephen et al., 2006), which makes wood pulp and cotton major commercial sources of the industrially available cellulose. Correspondingly, cellulose is commercially utilized in paper and textile industry.

The protein structure of cellulose is heterogeneous and biocompatible and it holds great promise for biomedical and pharmaceutical applications. Cellulose had been traditionally used as a source of biofuel, albeit the current tendency is to find alternative high-value applications for it. Modern adhesives and liquid filtration industries are benefitting from cellulose utilization (Ma et al., 2005a; Chen et al., 2008; Zhou et al., 2011a). A considerable number of hydroxyl groups in cellulose structure results in formation of hydrogen bonds in its macromolecule (O'Sullivan, 1997; Mahonty et al., 2000; Peng et al., 2011). Therefore, cellulose structure becomes aggregated. The intra- and inter-connected network-like structure of cellulose is responsible for its insolubility in water and most of the organic solvents. Consequently, cellulose-containing materials, e.g. wood, possess noticeable strength associated with the aggregation and hydrogen bonds in their structure.

Cellulose insolubility in many solvents motivated the search for alternatives which possess cellulosic structure and properties but are relatively easily soluble in acid and basic solutions. For example, acetate and nitrate esters are among the most widely used derivatives of cellulose, which are used as such alternatives. Cellulose acetate is

thermally stable and non-toxic. These properties, as well as its solubility in common solvents resulted in many applications of cellulose acetate. Cellulose acetate is used in adhesives, thermoplastics, coatings, and textile industry (Liu et al., 2002; Son et al., 2004; Frey, 2008; Han et al., 2008; Zhou et al., 2011a; Zhou et al., 2011b).

Lignin is an aromatic polymer, which is found in cell walls of plants. It is responsible for their strength (Vanholme et al., 2010). Lignin also protects plants from microbial infections (Vanholme et al., 2010). It is a stable macromolecule and prevents plants from degradation due to environmental conditions, such as humidity and temperature. Typically it is found in secondary cell walls of plants where lignin wraps cellulose microfibrils. On the other hand, primary cell walls are formed of cellulose (Bhatnagar et al., 2005). Lignin is considered to be a second most abundant natural bio-polymer, while cellulose is the first one. Lignin, similarly to cellulose, had traditionally been used as a source for biofuel, albeit the current tendency is to find alternative applications for this plant-derived biopolymer. Lignin macromolecules possess a variety of different structures, being either sulfur-containing or sulfur-free. The complex aromatic structure of lignin, which also contains both hydrophilic and hydrophobic groups, is cross-linked and aggregated, which results in significant strength to this material.

Lignin is used in cosmetic and anti-bacterial materials, adhesives and surfactants (Kadla et al., 2002). Lignin is a major by-product of the paper industry, and as such is abundant, which fuels research on its novel applications, in particular, as a precursor to carbon fibers (Kadla et al., 2002; Braun et al., 2005; Kwon et al., 2011). Lightweight and

strong carbonaceous materials find applications in aerospace and aviation industries (Kim et al., 2007; Liu et al., 2012).

Zein constitutes up to 50% of protein in corn structure. It has been isolated from corn in the early 19th century. Corn structure consists of endosperm, which incorporates all zein (Shukla et al., 2001). Except human food, corn is used to extract starch and oil, as well as more recently to produce ethanol as a fuel (Shukla et al., 2001). According to (Gianazza et al., 1977; Geraghty et al., 1981), major amino acid components in zein are proline, luecine, and alanine which are hydrophobic. It is emphasized that zein does not contain majority of essential amino acids; therefore, its value as a nutritional protein is quite restricted. Significant attention was paid to development of commercially available industrial polymers from zein. Some efforts were directed at forming nanofibers by electrospinning from zein solution (Miyoshi et al., 2005; Yao et al., 2006; Kanjanapongkul et al., 2010).

Silk sericin is the major constituent of silk. Sericin is extracted from silk for different applications such as pharmaceutical and cosmetics (Zhang et al., 2002a; Padamwar et al., 2004). It is functionalized to use in contact lenses and damaged tissues. It has noticeable adhesive properties and acts as a glue bonding fibroin together in the cocoon structure of silk. Sericin is blended with synthetic polymers and resins to acquired materials with comparable properties with those of synthetic ones. Electrospinning of Bombyx mori silk with poly(ethylene oxide) was reported in (Jin et al., 2002; Li et al., 2006). The biggest usage of sericin is that it is dumped as waste in water, which in turn pollutes the water by increasing biological oxygen demand. Besides, sericin can also be used as a very useful biomaterial (Zhang, 2002b).

Bovine serum albumin (BSA) is similar to serum albumin protein in human body by properties and structure. Therefore, BSA can be used as a characteristic protein to mimic human protein environment.

Protein nanofibers comprise a structure similar to that of natural extracellular matrix (ECM). Consequently, artificial biopolymer nanofibers can be used as biocompatible agents to diminish chances that such artificial protein scaffolds would be rejected by human body.

Due to the similarity in structure and properties of BSA with natural human serum albumin protein, BSA nanofibers attracted significant attention in relation with wound dressing, cell growth, and drug carriers (Peters, 1996; Curry et al., 1999). In (Liao et al., 2006), core-shell electrospun nanofibers were formed with BSA in the core and polycaprolactone (PCL) in the shell. The shell also contained PEG as a porogen . These nanofibers were used for controlled drug release. In (Dror et al., 2008), BSA fibers were functionalized as a biosensor. Nerve growth factor (NGF) was released from BSA-PCL nanofibers in (Valmikinathan et al., 2009). Solubility of BSA in aqueous medium leads to formation of pores in the nanofibrous structure which finally results in NGF release from the fibrous carrier.

Although such plant- and animal-derived polymers as soy protein, starch, lignin, zein, sericin, and BSA have been extensively used in composites, fillers, coatings, and adhesives, their low cost, abundance and specific protein structures hold great promise for their further utilization. Prior efforts to use these biopolymers as substitutes for synthetic materials were hindered by their relatively low strength, low water resistance as well as odor and color. The present work aims at an en masse forming of nanofibers from

animal and agricultural proteins using solution blowing (cf. Chapter 9). This method is much faster than electrospinning and does not depend on the electric properties of polymer solutions as the latter. Solution blowing was recently introduced and applied to form soy protein nanofibers with rates 20-30 times faster than conventional electrospinning (Sinha-Ray et al., 2010a; Sinha-Ray et al., 2011). Solution blowing method was also used in (Zhuang et al., 2012) in which monolithic and core-shell cellulose micro/nanofibers are produced.

In the present work (cf. Chapter 9), solution blowing is applied to form nanofibers from soy protein, cellulose acetate, lignin, zein, sericin, and bovine serum albumin and it also aims at their mechanical characterization as an extension of our previous work (Khansari et al., 2012).

Beside plant- and animal-derived proteins, solution blowing is also applied to form nanofibers from poly(ethylene terephthalate) PET. PET is an aromatic polyster commercially used in packaging food and beverages as well as its wide applications in textile industry. PET is rigid and strong and also possesses a light weight. It is also used in cardiovascular surgery for blood vessels and artificial heart implantation (Karck et al., 1993; Dewanjee et al., 1999; Smith et al., 2003) due to its noticeable mechanical properties and acceptable biocompatibility in human body. As discussed in (Wang et al., 2004), artificial heart valves produced with PET are supposedly functional up to 10 years in the body. In addition, in the present work post-processing is also applied to biodegradable solution-blown nanofibers to enhance their overall mechanical properties (cf. Chapter 9).

2. RESEARCH DESIGN AND OBJECTIVES

Protein-based nanofibers hold promise for a vast range of applications from protective textiles, paper industry, adhesives, and civil infrastructure to biomedical applications, heavy metal filtration, and catalysis. In spite of research focus of many groups on developing nano-scaled bio-polymeric materials, the partial hydrophilic nature of these materials, as well as their low strength impose significant barriers to their industrial applications. The method of polymer nanofiber forming employed in the present work are cost-effective and industrially scalable. In particular, solution blowing method, which was recently introduced by our group, holds great promise.

(i) The first aim of this work in producing protein-based nanofibers and nonwoven mats.

(ii) Characterization of their mechanical strength and long-term stability is the next goal.

(iii) Theoretical work on tensile properties of such nanofiber mats is also conducted.

(iv) Chemical and physical cross-linking are employed as a means to enhance mechanical stability of soy protein nanofiber mats.

(v) Biomedical applications, such as the antimicrobial activity and drug release comprise the following step.

(vi) The investigation of a wide range of plant- and animal-derived bio-polymers as a source of useful nanofibers (lignin, zein, silk sericin, cellulose and BSA) is also undertaken.

2.1. Stress-Strain Dependence for Soy Protein Nanofiber Mats

The first part of the work is devoted to developing solution-blown soy protein-based nanofiber mats and their mechanical characterization. In our works (Khansari et al., 2012; Sinha Ray et al., 2012) which comprises Chapters 3-5 of the present thesis, soy protein/nylon 6 solution is used in order to produce monolithic and core/shell soy protein/nylon 6 nanofibers. The as-spun nanofibers are collected on rotating aluminum drum with specified linear velocity at the collector's surface which is later optimized experimentally. These nanofibers have the average diameter in the range 300-500 nm. Collected samples are cut into rectangular pieces which then undergo tensile tests in order to reveal their stress-strain dependences. These dependences are linear at low strains which correspond to the elastic behavior. Then, a plastic-like nonlinearity sets in for higher strain values, which is followed by catastrophic rupture. Parameters such as Young's modulus, yield stress, and specific strain energy are measured and used to express the mechanical characteristics of the samples. The results are rationalized in the framework of the phenomenological elastic-plastic model, as well as a novel micromechanical model (the latter attributes plasticity to bond rapture between the individual overstressed fibers in the mat). Besides, the effects of stretching history, rate of stretching, and winding velocity of the collector drum on the strength-related parameters are studied. These experiments reveal the optimum rotating velocity for the collector as it acts as a pre-stretching mechanism while the fibers are getting collected on the drum. Stretching history experiment is conducted by applying two pre-stretching steps prior to complete tensile test on the rectangular nanofiber samples. Then, the effect of pre-stretching on the overall mechanical properties of the samples are reported. Also due to

viscoelastic nature of the polymers in the sample, rate of stretching in uniaxial elongation test affects Young's modulus, yield stress, and specific energy of the samples. This effect is also elaborated using tensile test experiments.

Finally, in order to compare the overall mechanical properties of these biopolymer nanofiber mats with a synthetic material, nylon 6 nanofibers are used as control samples. A 20 wt% nylon 6 solution in formic acid is prepared and used for solution blowing similar to soy protein-based solutions. Nanofibers are then collected and cut into rectangular pieces similarly to soy protein/nylon 6 samples. Furthermore, tensile tests are conducted on pure nylon 6 nanofiber mats and the average mechanical properties are compared with those of the biopolymer based-nanofiber samples.

2.2. Effect of Cross-linking on Tensile Characteristics of Solution-Blown Soy Protein Nanofiber Mats: I- Chemical Cross-linking

Soy proteins obtained from sustainable bio-resources hold great promise as biodegradable materials which can potentially replace petroleum-derived polymers in many high-value products, e.g. in nano-textured nonwovens. Such nonwovens and the enhancement of their tensile properties and longevity are tackled in the present work. The collected fiber mats are chemically bonded using four different cross-linking agents. The experiments in Chapter 4 are conducted using two covalent cross-linkers (formaldehyde and glyoxal) and two ionic cross-linkers (zinc sulfate and sodium borohydride).

Such mechanical properties of soy-protein-containing nanofiber mats as Young's modulus, yield stress, and maximum stress and strain at rupture are measured for different cross-linkers at different contents. Overall, higher contents of cross-linking

agents in soy protein nanofiber mats result in nanofibers with higher strength which is accompanied by a less plastic behavior. Treatment with ionic cross-linkers results in nanofiber mats with higher Young's modulus of the mats. Covalent bonds formed by aldehyde groups have a smaller effect on the mat strength. 20 wt/wt % formaldehyde/mat revealed 3-4 times increase in the samples' Young's modulus. Same glyoxal/mat content leads to 5 times increase in the strength of the samples. Both zinc sulfate and sodium borohydride reveal a 7-fold increase in the average Young's modulus of the samples that undergo tensile test for the similar crosslinking content to mat weight ratio.

The second part on this topic in Chapter 4 deals with the effect of heat treatment on soy protein nanofiber samples which are chemically treated with three different agents. Formalehyde and glyoxal are used as covalent bond producers. Also zinc sulfate-treated samples undergo heat treatment in order to reveal how ionic bonds resist heat exposure. As cross-linked nanofibers are exposed to heat, the bonds formed between amino groups in the fibers are broken and they become less aggregated. Therefore, they gain their mobility and rotate back partially.

In the following part related to this topic, soy protein-based nanofiber mats which do not undergo any further treatment, as well as the ones that undergo chemical bonding treatment with different covalent and ionic agents, are immersed in de-ionized water for 24 h under certain conditions which is applied as a standard test to examine their sustainability in aqueous medium. Material's loss when exposed to water for a long time is of importance in order to further introduce these materials to various applications in packaging, filtration, and antibacterial items.

2.3. Effect of Cross-linking on Tensile Characteristics of Solution-Blown Soy Protein Nanofiber Mats: II- Thermal and Wet Cross-linking

Chapter 5 specifically deals with physical cross-linking mechanisms that could be applied to soy protein-based nanofiber mats in order to enhance their overall mechanical properties. Thermal treatment under compression is a common procedure used in industry in order to improve characteristics of nonwovens. Modified version of such industrial process is done in the present work. Nanofibers are produced and collected, and then undergo thermal calendaring under compression at $55^{o}C$ for 1 min. After that, the samples undergo uniaxial elongation after cooling at room temperature. This leadd to an increase of about 50% in the Young's modulus of tested samples.

In addition, non-treated samples are tested using wet conglutination procedure as a post-treatment method to enhance their average mechanical characteristics. Wet soy protein-based nanofiber samples are loaded with 6 kPa pressure for 24 h and then left at room condition to dry out completely. Consequently, 65% increase in materials' strength is observed due to physical crosslinking of the nanofibers at intersection points.

Last part of the work on this topic is devoted to a test termed as 'aging' which is applied to these biopolymer-based nanofiber samples. The samples are subjected to water at $80^{o}C$ for 1 h. It is of interest to observe that the samples do not lose their strength as a result of water exposure at elevated temperature, only they gain plasticity due to water exposure; that is, samples fail at higher strain values under tensile experiment.

2.4. Antibacterial Activity of Solution-Blown Soy Protein Nanofiber Mats Decorated with Silver Nanoparticles and Silver Nanoparticles' Leakage in Aqueous Medium

In Chapter 6 highly porous solution-blown soy protein-based nanofiber mats are decorated with silver nanoparticles. These coated nanofibers demonstrate significant antibacterial activity against E. coli colonies without exposure to UV light (as it is shown in the thesis of my collaborator Y. Zhang). The nano-textured materials developed in this work can find economically-viable applications in water purification technology and in biotechnology. Also in another set of experiments conducted in my work, silver- coated nanofibrous surfaces are tested in order to reveal their durability in water. In other words, silver-coated soy protein-based nanofibers are tested for leaching to examine how much of silver nanoparticles are lost while water exposure during long period of time. Possible silver leaching is tested, and no reliable evidence of it is found in 24 h. These antibacterial nanofibers can be combined in water purification industry as the materials used for making nanofibers that are not soluble in water. In addition, nanofibers prepared in this work are biocompatible, which allows using them in bandages for wound healing.

2.5. Protein Tracing in Soy Protein/Nylon 6 Nanofiber Mats Using Coomassie Brilliant Blue G250

Protein tracing method via Bradford staining is among the widely used methods to uncover protein presence in a sample. This method is fast, inexpensive, and it works precisely while tracking proteins (Compton et al., 1985). The mechanism involved in dye

binding with protein macromolecules is due to the formation of complexes between the dye and some primary amino acids in the protein structure. Arginine is mainly responsible for bond formation with the dye, yet other amino acids show lower effect.

Tracing of soy protein in the monolithic solution-blown soy protein/nylon 6 nanofiber mats is demonstrated in Chapter 7 using a modified version of Bradford assay. Protein presence can be determined via binding Coomassie brilliant Blue G250 with protein structure. Due to the complex formation between Bradford assay and the protein, absorbance wavelength alters from 465 nm to 595 nm which results in the color alteration in the complex. The change in the color of the samples is indicative of protein presence in the samples which is discussed in this part of the thesis.

2.6. Controlled Drug Release from Solution-Blown Soy Protein Nanofiber Mats

Biopolymer nanofibers are promising materials to be used in tissue engineering and biomedical applications. Porosity, biodegradability, and biocompatibility bring about significant potential for them to be functionalized as engineered tissues, artificial vessels, or drug carriers in the body. Plant- and animal-derived protein micro- and nanofibers are among the best candidates to be utilized in biomedical applications, implants, and different areas in which an artificial object should be embedded inside human body. The plant and animal proteins possess biodegradability, biocompatibility as well as high porosity which are the critical conditions for the artificial tissues. These properties bring about similarity between these materials and the native ECM inside the body. Therefore, the chances for the artificial vessels or tissues to be rejected by the body reduce tremendously.

Biopolymer nanofibers have already been used in drug delivery applications. Due to the nano-scale dimensions of these fibers, the drug loaded into the fibers is more prone to be dissolved inside the body, whereas in the traditional methods of delivering the drug for the specified tissue, only few portion of the drug actually gets through the target tissue.

In the present work in Chapter 8 using monolithic or core/shell nanofibers are produced in which a model drug fluorescent dye is a part of the original polymer solution.

The nanofibers used as model drug carriers, biodegradable nanofibers consisting of high percentage of soy protein are produced via solution blowing (Sinha-Ray et al., 2010; Khansari et al., 2012). Fluorescent dye Rhodamine B and riboflavin are used as model drugs. Rhodamine B is mixed in the soy protein isolate solution. Then it undergoes solution blowing procedure in order to produce monolithic soy protein/nylon 6 nanofibers which contained 1wt% Rhodamine B. Besides, core/shell soy protein nanofiber mats are produced in which Rhodamine B is premixed in the core solution. Consequently, the dye release decreases due to the prohibition provided by shell structure incorporating core nanofibers.

In addition, monolithic electrospun PET-based nanofibers are produced, in which riboflavin that is a partially soluble model drug and Rhodamine B that is a water-soluble model drug are separately premixed with the PET solutions.

Mixing dye-containing biopolymer nanofibers with a leachable compound that has a much faster degradation time than the biopolymer can further enhance the dye release rate over time. In this work, poly (ethylene glycol), PEG, is used as leachable material also termed as porogen. Fast degradation of PEG in aqueous environment results in

higher exposure of dye on the nanofibrous surface to the water. Therefore, higher percentage of dye on the surface is released over time. The same type of experiment is conducted in the core/shell nanofibers where the dye is embedded in the core structure. Presence of PEG in the shell nanofibers results in the production of pores in the shell fibers while immersed in water. Therefore, the core nanofibers which contain the dye have more exposure to water medium which results in higher release for the dye.

As a part of the work on drug release in Chapter 8, we discuss the mechanism responsible for the drug release saturation over time. Recently, a work done by another student in our group (Srikar et al., 2008) showed that dye desorption is the main limiting mechanism for the release of dye from the nanofibers' surface. In the present work, this model is used to demonstrate the release mechanism from soy protein nanofibers' surface, and it is shown that it cannot fully predict the release kinetics in time. This is due to the presence of porogen in the system which should be accounted for. Therefore, the model proposed in (Srikar et al., 2008) is modified and the new expression is derived to fully describe the dye release kinetics from degradable nanofibers with leachable porogen.

2.7. Biopolymer-Based Nanofiber Mats and Their Mechanical Characterization

High production costs for petroleum-derived materials and environmental problems caused by their vast exploitation in humans' lives, stimulated researchers to find applicable substitutes for synthetic and petroleum-based products. Among biodegradable materials plant proteins are most suitable candidates as alternatives for synthetic polymers. They are annually renewable, abundant, and cost-effective. These plant

proteins possess the potential to be used in packaging, filtration, nonwovens, adhesives, and cosmetics products. Recently, soy protein, cellulose, zein, lignin, and starch have been used as reinforcers and fillers in composites. Significant efforts were directed toward using soy protein as fillers in plastics since 1950's.

Cellulose acetate is a derivative of cellulose which possesses its properties, yet it can be dissolved in common organic solvents. It is also thermally stable. Therefore, it is widely used in textile and thermoplastic industry.

Lignin is the second most abundant natural polymer after cellulose and there is immense interest for it to be utilized in cosmetic products and adhesives. Also lignin has shown promising results to be functionalized as precursor to carbon fibers.

Zein and silk sericin are also of interest due to high percentage of protein macromolecules in their structure. These materials have already been electrospun and used in biomedical applications.

Bovine serum albumin possesses similar structure to native ECM in human body. Therefore, its major potential is in controlled drug release and wound dressing.

Due to the high surface area to volume ratio, it is of importance to produce high volumes of nanofibers from these biodegradable and abundant sources of protein. Prior efforts have been majorly focused on electrospinnig these biopolymers, even though electrospinning is a slow process.

Chapter 9 deals with producing nanofibers from these biopolymers using solution blowing as discussed in (Sinha Ray et al., 2011; Khansari et al., 2012). Solution blowing is a very fast method compared to electrospinning and it was applied to soy protein, cellulose acetate, lignin, zein, sericin, and bovine serum albumin solutions to produce

nano-scaled fiber mats. Also mechanical characterization of these biopolymers is conducted following our approach (Khansari et al., 2012) described in Chapter 3. Therefore, Young's modulus, yield stress, and maximum stress and strain at rupture of these biodegradable nanofibers are found.

3. Stress-Strain Dependence for Soy Protein Nanofiber Mats

3.1. Experimental

3.1.1. Materials

Materials used in this work include Polyamide-6 (Nylon-6) obtained from BASF (M_w=65.2 KDa), formic acid grade >95%, obtained from Sigma- Aldrich, protein isolate PRO-FAM 955 (SP 955) obtained from ADM Specialty Food Ingredients. All materials were used as received, without any further purification.

3.1.2. Solution Preparation

For solution blowing of monolithic nanofibers of blend of soy protein and nylon 6, the solution preparation was performed as described in (Sinha-Ray et al., 2011). In particular, 1 g of soy protein SP 955 was mixed with 9.5 g of formic acid and left on a hotplate at 75 °C for 24 h. Next, 1.5 g of nylon 6 was added to the solution and stirred at 75 °C for a day. For solution blowing of core-shell nanofibers, two solutions were prepared. The core solution was prepared as follows. First, 1.3 g of SP 955 was mixed with 8.7 g of formic acid and left on a hotplate at 75 °C for 24 h. Then, 1 g of nylon 6 was added to the solution and stirred on the hotplate at the same temperature for another day. The shell solution was a blend of 20 wt % nylon 6 in formic acid, which was left on a hotplate at 75 °C for a day to become homogeneous. For solution blowing of pure nylon 6 nanofibers, a 20 wt % solution of nylon 6 in formic acid was prepared.

3.1.3. Solution Blowing

In order to produce soy protein-based nanofibers, the setup described in (Sinha-Ray et al., 2010a; Sinha-Ray et al., 2010b; Sinha-Ray et al., 2011) was used. In particular, for blowing of monolithic nanofibers, solution was pumped through a 13G needle using a syringe pump with flow rate of 5 ml/h. After leaving the needle exit, the solution was subjected to a coaxial turbulent air jet at an upstream pressure of 1.5-2.5 bar through an annular nozzle surrounding the needle and the needle-to-collector distance was 19-24 cm. The upstream pressure differs from that of (Sinha-Ray et al., 2010a) since the tubing setting used in this particular experiment was 1/8", whereas the tubing in (Sinha-Ray et al., 2010a) was 1/16". Smaller tubing size caused more friction in the system; thus, higher upstream pressure was needed to obtain specific downstream velocity in (Sinha-Ray et al., 2010a). Solution blowing experiments were done at room temperature and 45-55% relative humidity.

The set-up for core-shell co-blowing is described in (Sinha-Ray et al., 2010b). In particular, to blow core-shell soy protein/nylon 6 nanofibers, two different solutions were used as described above. The core solution was pumped into a central nozzle which was surrounded by a reservoir carrying the shell solution. The shell solution was pumped through the reservoir with the flow rate of 4 ml/h. The core solution was supplied with the same flow rate. The core-shell jet was issued inside a concentric nozzle surrounded by an annular nozzle. A turbulent air jet was issued through the annular nozzle with the upstream pressure of 1.5 to 2.5 bar. It is emphasized that the exit of the core nozzle was slightly pushed inside the annular nozzle to avoid clogging. The core-shell soy

protein/nylon 6 nanofibers were collected on a rotating drum covered with aluminum foil which was located 15 cm below the nozzle exit.

For comparison, solution blowing of pure nylon 6 was conducted as follows. Pure nylon 6 solution was pumped through a 13G needle with a flow rate of 5 ml/h. The needle was surrounded by an annular nozzle. A turbulent air jet with the upstream pressure of 1.5 to 2.5 bar was issued through the annular nozzle. Nanofibers were collected on a rotating drum covered with aluminum foil located at a distance of 19-24 cm from the needle exit.

3.1.4. Sample Preparation

Nanofibers were collected on a rotating drum with diameter of 5 cm, which was covered with aluminum foil. The rotating drum (of 5 cm in diameter) had an angular velocity of 100-280 rad/s, which transcends into linear velocity of 2.5-7.0 m/s at the foil surface. Aluminum foil which was covered with nanofiber mat was taken off from the rotating drum. The nanofiber mat was cut into rectangular pieces which were 25-35 mm long and 10 to 15 mm wide and then piled off from the foil. The thickness of nanofiber mat was 0.15-0.30 mm. Nanofiber mat pieces which were used as samples in the uniaxial stretching experiments are shown in Fig. 3.1. The SEM images of the nanofiber mats are shown in Figs. 3.2 a,b,c. The samples were kept at room temperature and humidity.

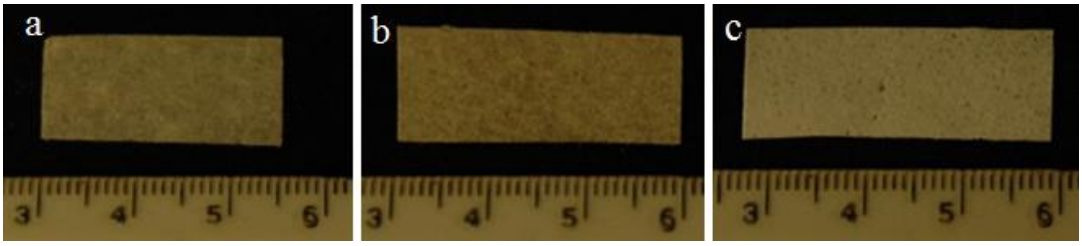

Figure 3.1. Solution blown nanofiber mat samples prepared for stretching test. Panel (a) shows soy protein/nylon 6 nanofibers. Panel (b) shows co-blown core-shell nanofibers, and panel (c) shows pure nylon 6 nanofibers.

3.1.5. Tensile Tests

The tensile test was performed using a 100 N capacity Instron machine (model 5942). The upper and lower ends of the samples were clamped by Instron's pneumatic grips. The upper end was stretched with a single stretching rate (0.1 mm/min), while the lower end was kept at its initial position. The uniaxial stretching tests were conducted until sample breakage. Tensile test with a fixed rate of stretching until sample rupture is termed protocol 1. This protocol was applied to soy protein/nylon 6 mats, pure nylon 6 mats, and core-shell nanofiber mats. Soy protein/nylon 6 nanofiber mats collected at different winding velocities of the rotating drum were also tested according to protocol 1. The corresponding mechanical properties of these nanofiber mats are reported below.

Another protocol, termed as protocol 2, was used to evaluate the effect of the stretching rate in uniaxial stretching on the mechanical behavior of nanofiber mats. Similar samples were tested with three different stretching rates; 0.1 mm/min, 0.5 mm/min, and 1.0 mm/min, and the corresponding mechanical properties were compared. This test was applied to soy protein/nylon 6 nanofiber mats.

The third set of experiment followed protocol 3, designed to evaluate the effect of pre-stretching on nanofiber mat's mechanical behavior. In particular, rectangular nanofiber samples were uniaxially stretched up to a particular strain (2%), and were held at that strain for 5 min. Then, they were released from the grips and fully unloaded. After that, they were clamped again with the initial gauge length and stretched. Then, the unloading and the following stretching were repeated once again. At the third stretching, the process was continued to the sample failure. This protocol was applied to soy protein/nylon 6 nanofiber mats.

In the experiments which followed protocol 4, samples were uniaxially stretched with incremental loads of 0.01 N and unloaded afterwards. The loading and unloading procedure continued until a sample was stretched with 0.35 N load. This test protocol was designed to evaluate reversible and irreversible components in the mechanical behavior of nanofiber mats. This test was conducted over soy protein/nylon 6 nanofiber mats.

3.1.6. Optical Observations

Morphology of solution-blown nanofibers was observed by using a Phenom scanning electron microscope (SEM). For the observation purposes, soy protein/nylon 6 nanofiber mats were sputter coated with a 6-7 nm Pd-Pt layer. The observations were done by using 5 kV accelerating voltage. The observations of soy protein/nylon 6 nanofiber mat cross-section were done by using JEOL JSM 6320F scanning microscope after a 7-8 nm Pd-Pt layer was sputter coated. In these observations a 3.5 kV accelerating voltage was applied.

Solution-blown nanofibers had cross-sectional diameters in the range 300-500 nm. The size distribution of the nanofibers corresponded to the one reported in (Sinha-Ray et al., 2011). The overall and zoomed-in SEM images of soy protein/nylon 6 nanofibers collected on a rotating drum are shown in Fig. 3.2. Compared to those of (Sinha-Ray et al., 2011), nanofibers are stretched and have preferential orientation in the direction of rotation (cf. Figs. 3.2a,b), since they were collected on a rotating drum. Due to the relatively small distance between the needle exit and rotating drum, solvent did not completely evaporate from the jet in flight. As a result, nanofibers were glued to each other in some places of the collected mat (cf. Fig. 3.2c).

The mat cross-section shown in Fig. 3.2d demonstrates that the mat's cross-section has a layered structure and is not fully filled with nanofibers. There are significant gaps between the fiber layers. This circumstance should be accounted for when calculating the stress supported by nanofiber mats in uniaxial elongation by using Instron. The images similar to the one in Fig. 3.2d taken at 30 different locations will be used for correcting the cross-sectional area and evaluating the real area which supports load. The processing of such images by using MATLAB revealed that only about 50% of the cross-sectional area in the mat contains nanofibers which support the load.

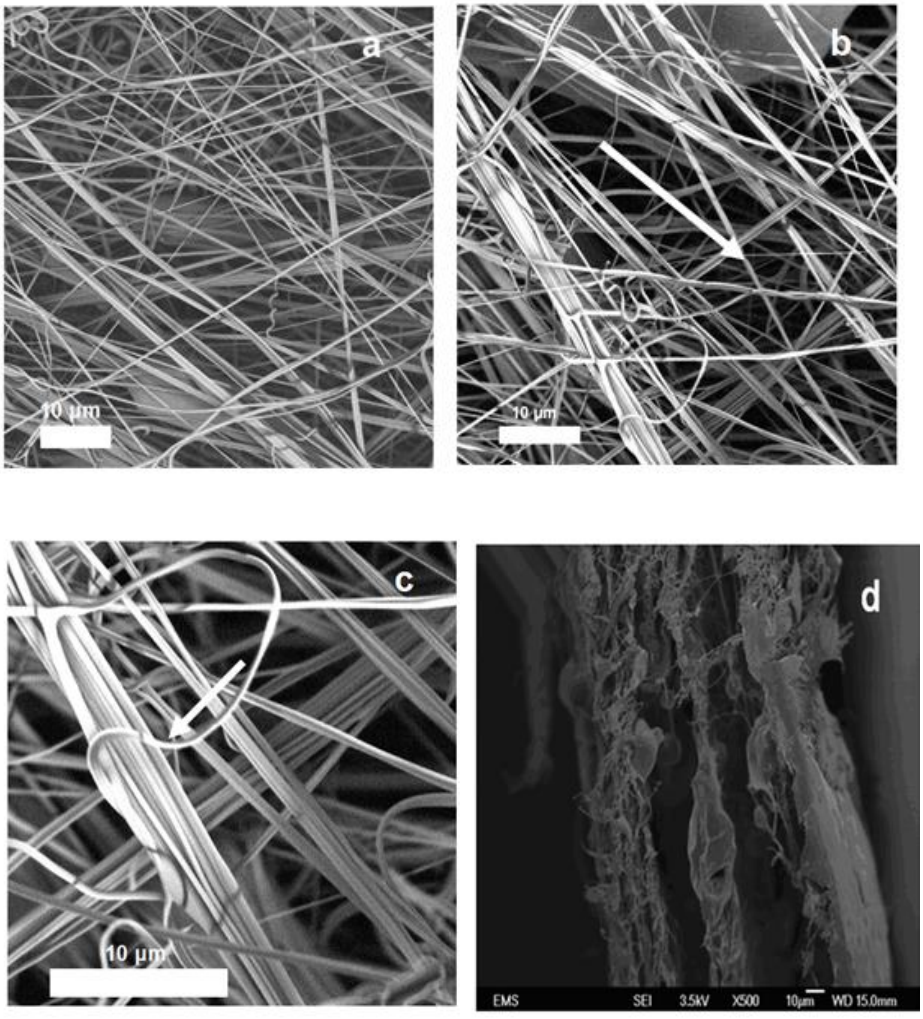

Figure 3.2. SEM images of soy protein/nylon 6 nanofiber mat. Panel (a) shows that nanofibers collected on rotating drum are oriented. A zoomed-in image shown in panel (b) illustrates that stretched nanofibers are mostly oriented in the winding direction shown by an arrow. Panel (c) shows that some nanofibers are glued together, which is a result of an incomplete evaporation of solvent from the jet in flight. Panel (d) shows that nanofiber mats have a layered structure, and only about one half of the cross-section supports load in the uniaxial stretching tests.

3.1.7. The Theoretical Background

The phenomenological equation for the uniaxial stretching of a planar strip as in the experiments in the present work, the stress-strain dependence is given by the following equation

$$\sigma_{xx} = \sqrt{\frac{8}{3}} Y \tanh\left(\sqrt{\frac{2}{3}} \frac{E}{Y} \varepsilon \right) \tag{3.1}$$

which encompasses the elastic and plastic behavior (see 3.3 Theory). In Eq. (3.1), E is Young's modulus, Y is the yield stress, σ_{xx} is the tensile stress and ε is the tensile strain. In the following section Eq. (3.1) will be compared to the experimental data to establish the values of Young's modulus E and the yield stress Y for solution blown soy protein nanofiber mats.

The micromechanical stress-strain relation for nanofiber mats under uniaxial elongation derived in Appendix B reads

$$\sigma_{xx} = E_m \varepsilon \frac{1}{2\pi} \exp(2\varepsilon) \int_0^{2\pi} \cos^4 \varphi \left(1 + \frac{2E_f \varepsilon \cos^2 \varphi}{\sigma_*} \right) \exp\left(- \frac{2E_f \varepsilon \cos^2 \varphi}{\sigma_*} \right) \times \frac{d\varphi}{\left[\cos^2 \varphi + \exp(4\varepsilon) \sin^2 \varphi \right]} \tag{3.2}$$

The dimensionless tensile strength σ_*/E_f in Eq. (3.2) affects the character of deviation of the dependence of σ_{xx} on ε from the linear Hooke's law, and thus effectively controls mat plasticity.

In the limit of small strains when $\varepsilon \to 0$, Eq. (3.2) reduces to $\sigma_{xx} = (3/8) E_m \varepsilon$. The latter corresponds to Hookean behavior. The Hookean limit should correspond to that of the phenomenological model of Eq. (3.1), which means that $E_m = (32/9)E$. Equation (3.2) is compared to the experimental data in the following section.

3.2. Experimental Results & Discussion

3.2.1. Stress-strain Curves from the Experiments According to Protocol 1 (Monolithic Fibers)

A typical stress-strain dependence for soy protein/nylon 6 nanofiber mats measured in the tests following protocol 1, is shown in Fig. 3.3. It is seen that at relatively small deformations, σ_{xx} depends on ε practically linearly demonstrating an elastic Hookean response. At higher strains, ε>3%, the response becomes nonlinear which can be attributed to the onset of plasticity.

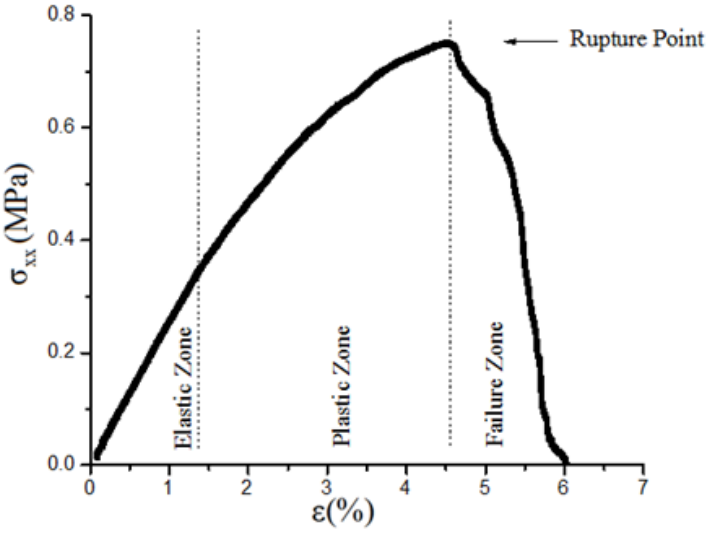

Figure 3.3. Tensile stress versus strain acquired for a sample of soy protein/nylon 6 solution blown nanofiber mat. Symbols-experimental data. Sample rupture occurs at $\sigma_{xx,rupture}$=0.7 MPa and $\varepsilon_{rupture}$=4.5% .

The morphology of sample failure corresponding to Fig. 3.3, is illustrated in Fig. 3.4. In most cases, samples failed in the sample middle (cf. Fig. 3.4). Typically, the failure stress and strain were in the range of $\sigma_{xx,rupture}$=0.4-0.9 MPa and $\varepsilon_{rupture}$=4-10%, respectively.

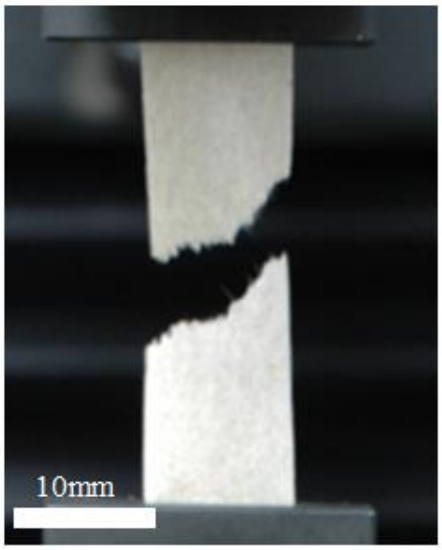

Figure 3.4. Typical sample rupture pattern for soy protein/nylon 6 nanofiber mat.

Fitting Eq. (3.1) to the experimental stress-strain curve in the elastic and plastic zone, the values of Young's modulus E and the yield stress Y can be determined (cf. Fig. 3.5).

The average values of E and Y found for several samples of soy protein/nylon 6 nanofiber mats are listed in Table 3.1. The table also contains the specific strain energy defined as $u = \int_0^{\varepsilon} \sigma_{xx} d\varepsilon$.

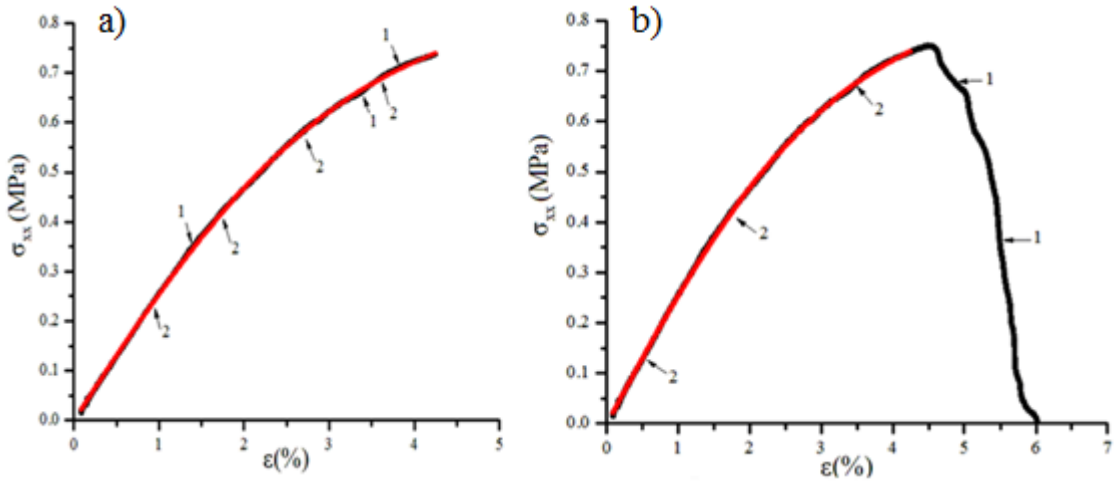

Figure 3.5. Comparison of phenomenological elastic-plastic model [Eq. (3.1)] with the experimental stress-strain data for soy protein/nylon 6 nanofiber mat. In panel (a), Eq. (3.1) is fitted to the experimental data up to the rupture point. Panel (b) shows the overall stress-strain data corresponding to panel (a). Black symbols 1 - experimental data, red line 2- phenomenological model, Eq. (3.1).

Table 3.1. Average mechanical properties of soy protein/nylon 6 nanofiber mats.

Average width of the samples (mm)	Average thickness of the samples (mm)	Average Young's modulus E (MPa)	Average yield stress Y (MPa)	Average specific strain energy u (MPa)	Average maximum strain at rupture $\varepsilon_{rupture}$(%)	Average maximum stress at rupture $\sigma_{xx,rupture}$
12.07	0.20	19.56±6.48	0.56±0.15	2.26±0.71	4.52±0.92	0.67±0.10

The micromechanical model (3.2) was also fitted to the data, and one case of such fitting is shown in Fig. 3.6. It is seen that the micromechanical model fits the data in the elastic and plastic part of the stress-strain dependence as good as the phenomenological

model (3.1), albeit as the latter is incapable to describe the last part corresponding to the catastrophic rupture of the sample. Similar comparisons were done for 20 different samples and the results are presented in Table 3.2. The fitted values of E_m of the micromechanical model were recalculated into the values of Young's modulus E of the phenomenological model using the relation $E_m = (32/9)E$, and found to be in full agreement with the values of E found directly by fitting the phenomenological model (Table 3.2). It is emphasized that the micromechanical model (3.2) does not involve the yield stress Y. Instead, it involves the relative characteristic bond-breaking stress σ_*/E_f, which is responsible for plastic effects. Its values for the 20 samples are also presented in Table 3.2.

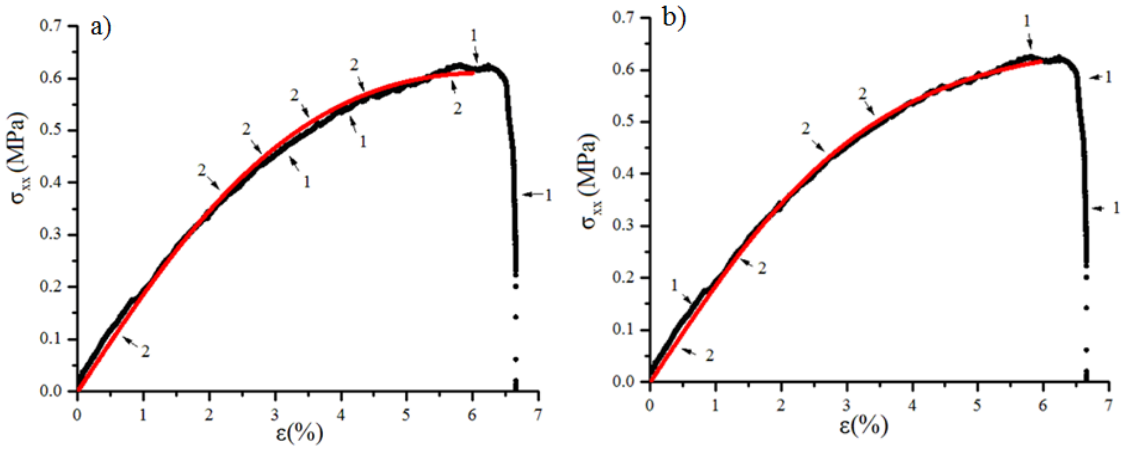

Figure 3.6. Soy protein/nylon 6 stress-strain curve fitted with (a) phenomenological and (b) micromechanical models. Sample No. 1 from Table 3.2. Black symbols (1) depict the experimental data, red lines (2) the corresponding theoretical results.

Table 3.2. Young's modulus, yield stress, and the relative bond-rupture stress σ_*/E_f. Soy protein/nylon 6 nanofiber mats.

Sample	Width (mm)	Thickness (mm)	Young's modulus E (phenomenological model); MPa	Young's modulus E corresponding to the micromechanical model; MPa	Yield stress of the phenomenological model, Y (MPa)	Relative bond rupture stress of the micromechanical model, σ_*/E_f
1	11.91	0.22	12.8	12.8	0.53	0.071
2	11.47	0.22	17.58	17.58	0.46	0.047
3	12.43	0.22	14.26	14.26	0.46	0.058
4	11.47	0.22	20.88	20.88	0.53	0.047
5	11.21	0.22	19.69	19.69	0.6	0.055
6	11.38	0.24	24.01	24.01	0.6	0.047
7	11.53	0.2	38.02	38.02	0.78	0.038
8	11.65	0.22	24.25	24.25	0.53	0.041
9	11.99	0.22	14.87	14.87	0.49	0.058
10	12.01	0.16	21.79	21.79	0.79	0.060
11	11.59	0.16	21.58	21.58	0.69	0.062
12	11.68	0.22	17.62	17.62	0.59	0.057
13	10.87	0.22	21.93	21.93	0.49	0.042
14	11.6	0.22	14.55	14.55	0.56	0.062
15	12.72	0.22	18.74	18.74	0.67	0.062
16	13.38	0.16	14.58	14.58	0.69	0.076
17	14.14	0.16	20.22	20.22	0.39	0.041
18	13.44	0.17	40.28	40.28	0.77	0.035
19	12.83	0.15	16.50	16.50	0.21	0.030
20	12.29	0.18	21.46	21.46	0.57	0.041

The effect of the relative fiber rupture parameter σ_*/E_f on the predictions of the micromechanical model is illustrated in Fig. 3.7, which shows how a particular value of this parameter is chosen to fit the data in the plastic part when the value of E_m (or E) has already been established using the elastic part of the stress-strain curve.

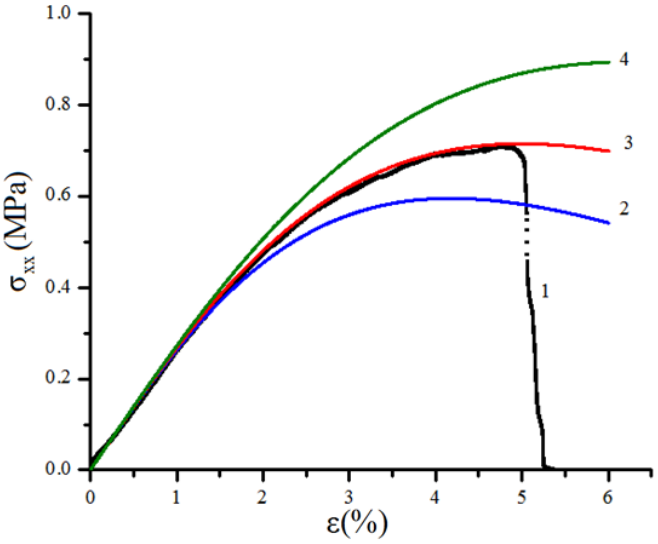

Figure 3.7. The effect of the relative fiber rupture stress, σ_*/E_f on modeling plastic behavior of soy protein/nylon 6 nanofiber mats. Black symbols (1) depict the experimental data. Curves 2, 3 and 4 show the results of the micromechanical model with different values of the ratio σ_*/E_f: 2- $\sigma_*/E_f = 0.040$, 3- $\sigma_*/E_f = 0.047$, and 4- $\sigma_*/E_f = 0.058$.

3.2.2. Effect of the Stretching Rate According to Protocol 2 (Monolithic Fibers)

Performing tensile test on soy protein/nylon 6 nanofiber mats with three different speed rates, it was found that the unaixial stretching with a higher stretching rate results in a higher value of Young's modulus corresponding to the stress-strain curve. Also, the

yield stress, strain energy, and maximum stress and strain at rupture acquire higher values for higher stretching rates. Table 3.3 contains such results for three different stretching rates. The corresponding graphic illustration of the above-mentioned trends is depicted in Fig. 3.8. The parameters listed in Table 3.3 and Fig. 3.8 were found by fitting the phenomenological Eq. (3.1) to the experimental stress-strain curves.

Table 3.3. Average mechanical properties of soy protein/nylon 6 nanofiber mats found for three different rates of stretching.

Rate of stretching (mm/min)	**Average Young's modulus E (MPa)**	**Average yield Stress Y (MPa)**	**Average specific strain energy u (MPa)**	**Average maximum strain at rupture $\varepsilon_{rupture}$(%)**	**Average maximum stress at rupture $\sigma_{xx,rupture}$**
0.1	19.56±6.48	0.56±0.15	2.26±0.71	4.52±0.92	0.67±0.10
0.5	21.52±1.82	0.57±0.03	2.85±0.36	4.57±0.14	0.75±0.08
1.0	31.13±6.88	0.65±0.12	2.99±0.02	4.04±0.2	1.12±0.41

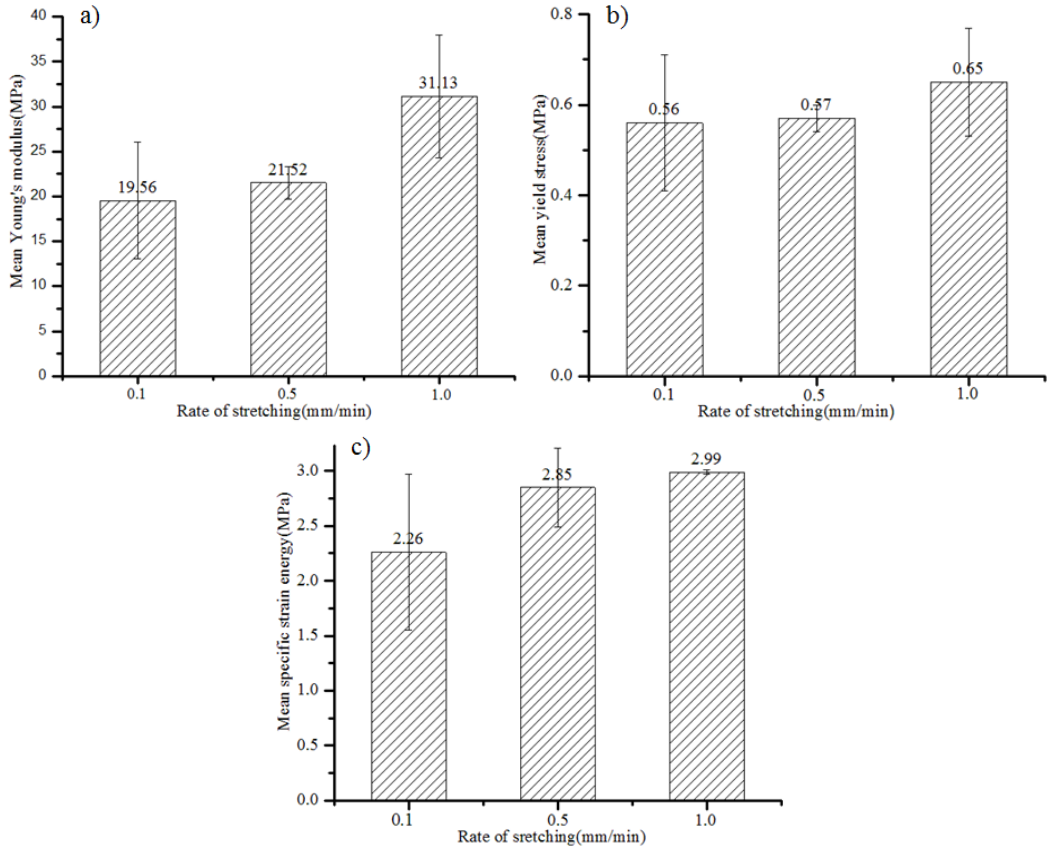

Figure 3.8. (a)Young's modulus, (b) yield stress, and (c) specific strain energy for three different rates of stretching.

3.2.3. Effect of Pre-stretching on the Stress-strain Curves of Soy Protein/Nylon 6 Nanofiber Mats According to Protocol 3 (Monolithic Fibers)

According to protocol 3, soy protein/nylon 6 nanofiber mat was loaded up to 3% strain and held at this strain for 5 min. Then, the sample was released and clamped again at the same gauge length. After that, the second pre-stretching step was done up to 3% strain where the sample was kept for 5 min. Then, it was released once again and re-clamped with the initial gauge length. After that, the sample was stretched up to its rupture. The phenomenological model (Eq. 3.1) was fitted to the stress-strain curves for

the 1st, 2nd and 3rd stretching and the corresponding values of Young's moduli found, which is reported in Table 3.4 and Figs. 3.9, 3.10. The results show that pre-stretching increases nanofiber mat's strength, and in particular, Young's modulus at each consequent stretching. Fig. 3.9 and the data for the 2nd and 3rd stretching in Table 3.4 show that the highest value of Young's modulus can be reached in the intermediate (2nd) stretching process instead of the last (3rd) one. This could be attributed to damage accumulated in the preceding two stretching tests, as a result of which many fibers in the mat can already be ruptured before the 3rd test had begun.

Table 3.4. Average Young's moduli for soy protein/nylon 6 nanofiber samples for three consequent stretching tests.

Average thickness of the samples (mm)	Average width of the samples (mm)	Average Young's modulus E (MPa), 1st stretching	Average Young's modulus E (MPa), 2nd Stretching	Average Young's modulus E (MPa), 3rd stretching
0.17	13.28	21.19±9.45	26.74±13.30	24.60±10.54

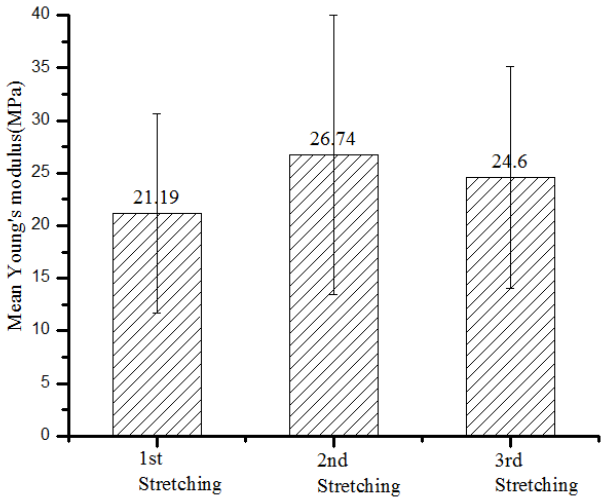

Figure 3.9. Young's moduli in three consequent stretching tests.

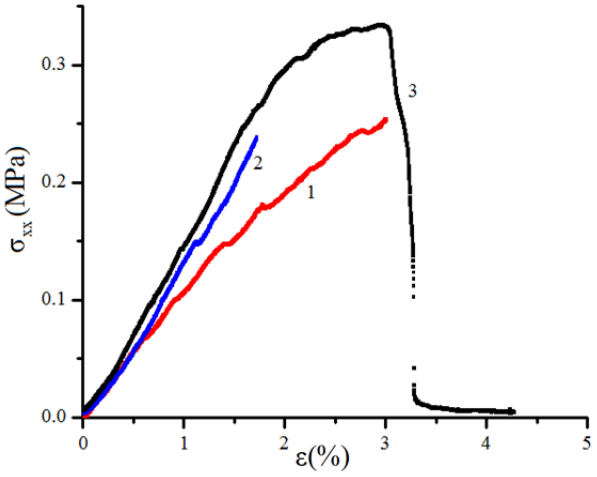

Figure 3.10. Stress-strain curve for soy protein/nylon 6 nanofiber mat in three subsequent stretching tests. Data set 1 shows the results for the 1st stretching, 2- for the 2nd stretching, and 3- for the 3rd stretching.

3.2.4. Incremental Loading-Unloading of Soy Protein/Nylon 6 Nanofiber Mats According to Protocol 4 (Monolithic Fibers)

An example of the experimental data obtained following protocol 4 with alternating loading and unloading is shown in Fig. 3.11. The experiments of this type allow evaluation of the reversibility/irreversibility of sample deformation. In particular, Fig. 3.11a shows the stress-strain curve obtained in the loading steps of the experiment, in which sample was loaded by incremental values of 0.01 N. After each loading step, the sample was unloaded, and shrank, but not to its initial length due to some irreversible changes in the mat structure. That allowed us to evaluate the irreversible strain corresponding to each stress level achieved, as is shown in Fig. 3.11b. This incremental loading and unloading was continued up to 0.35 N, which is close to the rupture point. It is seen that the irreversible part of strain corresponding to plastic component due to the damage accumulation is gradually increasing as the total strain and the applied stress increase.

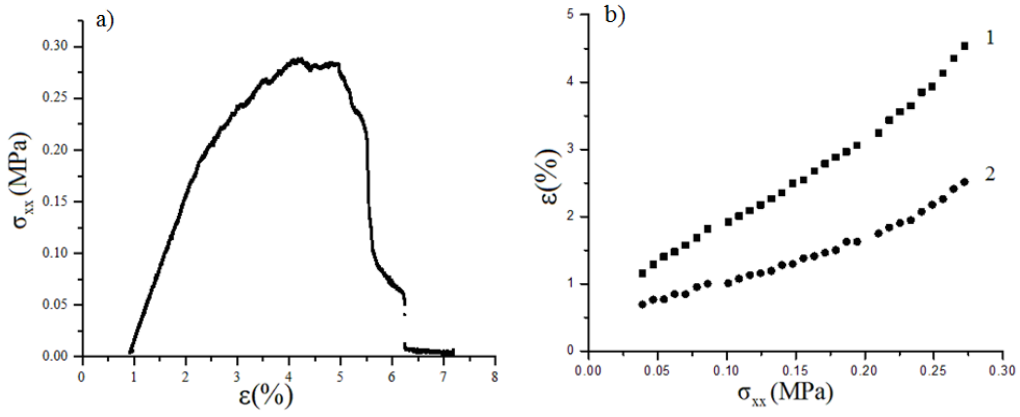

Figure 3.11. (a) Stress-strain curve corresponding to the loaded states of sample according to protocol 4. (b) Strain versus stress: square symbols (1) show the total strain

versus the applied stress, circular symbols (2) show the corresponding irreversible strain found in the unloaded sample.

3.2.5. Effect of Winding Velocity on Soy Protein/Nylon 6 Nanofiber Mats (Monolithic Fibers)

Fig. 3.12 shows stress-strain curves measured for samples corresponding to 6 different winding velocities. The stress-strain curves were fitted with the phenomenological model (Eq. 3.1) and, as a result, the values of Young's modulus and yield stress were found. They are listed in Table 3.5 together with the specific strain energy corresponding to the data sets in Fig. 3.12. These parameters are also illustrated graphically in Fig. 3.13. At the lowest values of the winding velocity the mat strength varies non-monotonously, being higher at 3.2 m/s than at 3.6 m/s. However, beginning from the velocity of about 4.5 m/s the further increase in the winding velocity practically does not affect the stress-strain curve (cf. Fig. 3.12). Overall, Figs. 3.12 and 3.13 show that the effect of the winding velocity in the intermediate range is insignificant.

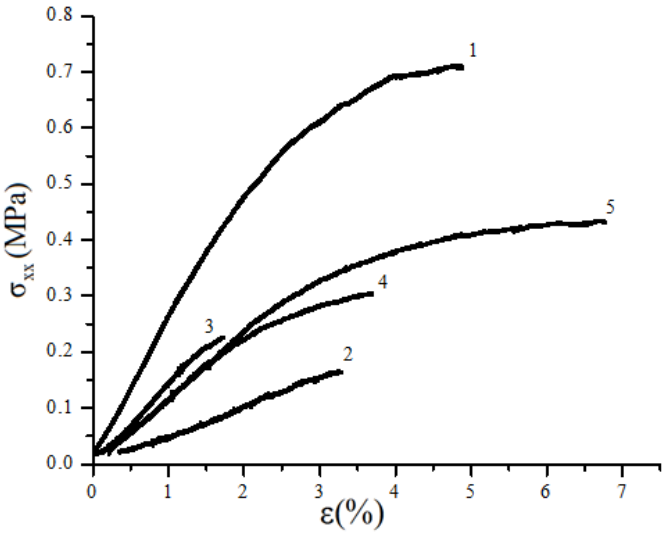

Figure 3.12. Stress-strain curves at different winding velocities at sample formation. Data set 1 corresponds to the winding velocity of 3.2 m/s, 2 - to 3.6 m/s, 3- to 4.5 m/s, 4- to 5.5 m/s, and 5- to 6.9 m/s.

Table 3.5. Young's modulus, yield stress and specific strain energy versus winding velocity at sample formation of soy protein/nylon 6 nanofiber mats.

Winding velocity (m/s)	**Average width of the samples (mm)**	**Average thickness of the samples (mm)**	**Average Young's Modulus E (MPa)**	**Average yield Stress Y (MPa)**	**Average specific strain energy u (MPa)**
2.58	11.87	0.26	6.39±2.42	0.33±0.17	0.46±0.12
3.1	12.07	0.20	19.56±6.48	0.56±0.15	2.26±0.71
3.6	12.68	0.18	8.13±4.12	0.35±0.14	0.28±0.12
4.5	11.97	0.16	10.11±5.71	0.19±0.11	0.36±0.11
5.55	13.01	0.22	7.65±2.75	0.28±0.06	1.39±0.53
6.9	13.41	0.21	9.48±1.46	0.28±0.07	1.93±0.63

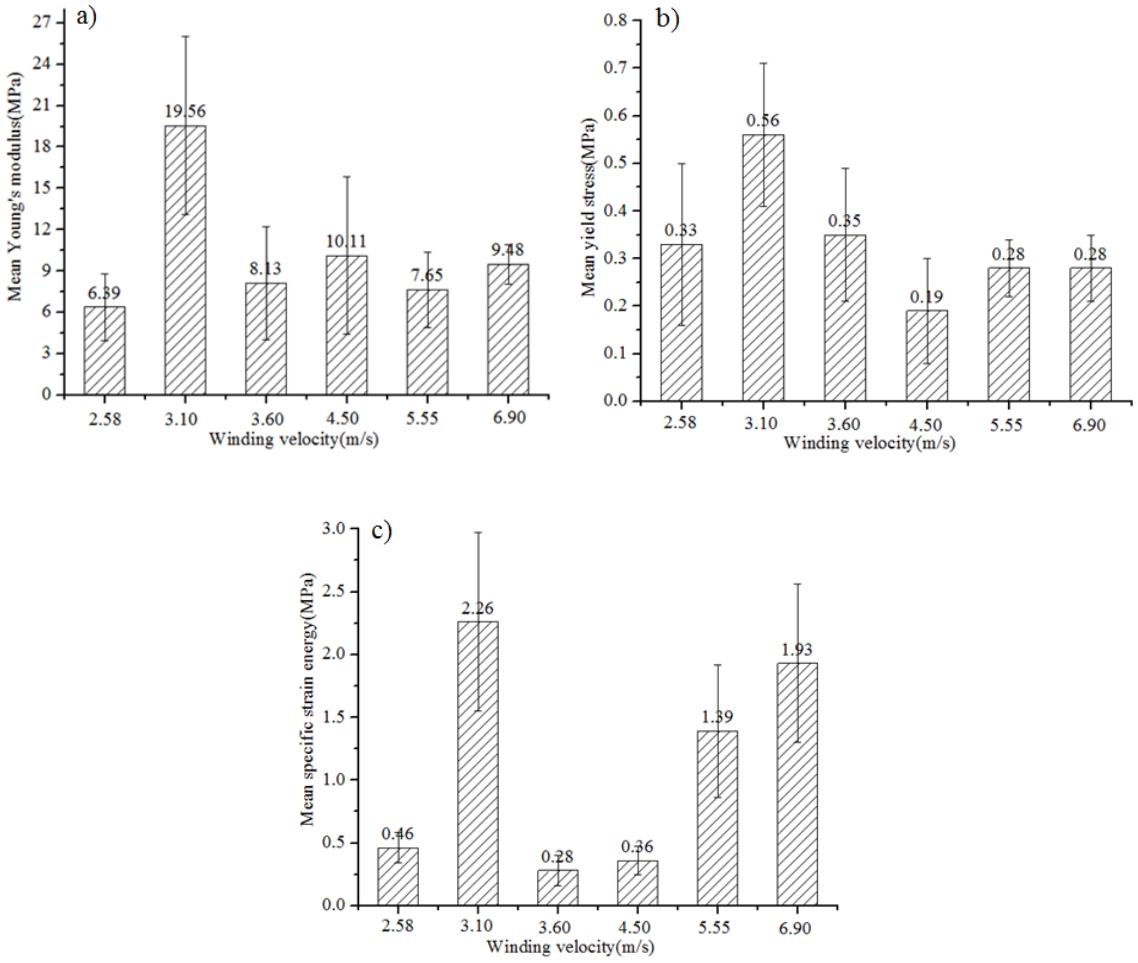

Figure 3.13. Mechanical properties of soy protein/nylon 6 nanofiber mats at different winding velocities of mat formation.

3.2.6. Stress-strain Curves from the Experiments According to Protocol 1 (Core-Shell Nanofibers)

Stretching behavior of core-shell soy protein/nylon 6 nanofiber mats was studied experimentally following protocol 1. A typical stress-strain data set is depicted in Fig. 3.14. Core-shell soy protein/nylon 6 nanofiber mats behave elastically at small strains. Plasticity is felt at the strains higher than about 1.5%, and rupture occurs at about $\sigma_{xx,rupture}$=0.4-0.7 MPa and $\varepsilon_{rupture} \approx 2.1$. Fitting the data by the phenomenological equation (3.1) revealed the values of the mechanical parameters listed in Table 3.6.

Table 3.6. Mechanical properties of core-shell soy protein/nylon 6 nanofiber mats.

Average width of the samples (mm)	Average thickness of the samples (mm)	Average Young's modulus E (MPa)	Average yield Stress Y (MPa)	Average specific strain energy u (MPa)	Average maximum strain at rupture $\varepsilon_{rupture}$(%)	Average maximum stress at rupture $\sigma_{xx,rupture}$
11.22	0.15	22.26±6.06	0.57±0.3	0.92±0.02	2.41±0.40	0.54±0.10

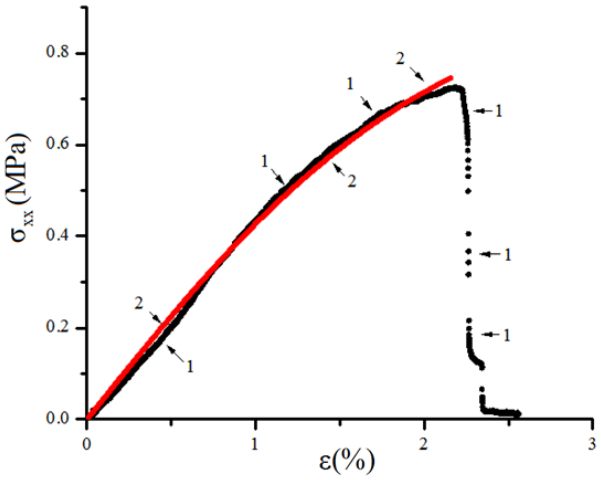

Figure 3.14. Stress-strain curve for soy protein-nylon 6 core-shell nanofiber mat (circular symbols, 1), fitted with the phenomenological model (the dashed line, 2) up to the rupture point.

3.2.7. Stress-strain Curves from the Experiments According to Protocol 1 (Nylon 6 Nanofibers)

For comparison with the data for monolithic and core-shell soy protein/nylon 6 nanofiber mats, pure nylon 6 mats were studied. A typical stress-strain curve for nylon 6 nanofiber mat is shown in Fig. 3.15. It was fitted with the phenomenological equation (3.1) and the corresponding mechanical parameters were established. Their values are listed in Table 3.7.

Table 3.7. Mechanical properties of pure nylon 6 solution-blown nanofiber mats.

Average width of the samples (mm)	Average thickness of the samples (mm)	Average Young's Modulus E (MPa)	Average yield stress Y (MPa)	Average specific strain energy u (MPa)	Average maximum strain at rupture $\varepsilon_{rupture}$(%)	Average maximum stress at rupture $\sigma_{xx,rupture}$
13.00	0.39	14.46±2.30	1.17±0.75	11.71±0.31	11.80±1.39	1.68±0.18

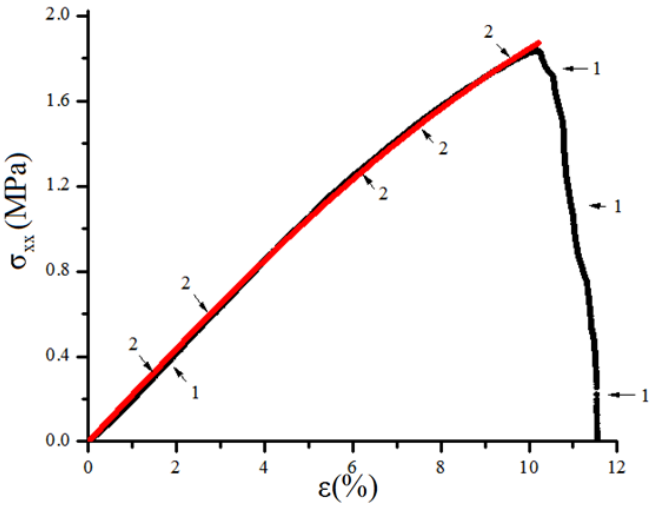

Figure 3.15. Stress-strain data (black symbols, 1) for pure nylon 6 nanofiber mat and the phenomenological model (red line, 2), fitted to up to the rupture point (practically indistinguishable from the data).

Comparing mechanical properties of soy protein/nylon 6 nanofiber mats with those of pure nylon 6 samples, shows that mean values of Young's modulus are almost the same for both types of samples (cf. Fig. 3.16a). However, Figs. 3.16b,c show that the

specific strain energy and yield stress of pure nylon 6 nanofiber mats are higher than those of soy protein/nylon 6 nanofiber mats. Therefore, pure nylon 6 nanofiber mats resist more to deformation up to rupture than the corresponding soy protein/nylon 6 nanofiber mats.

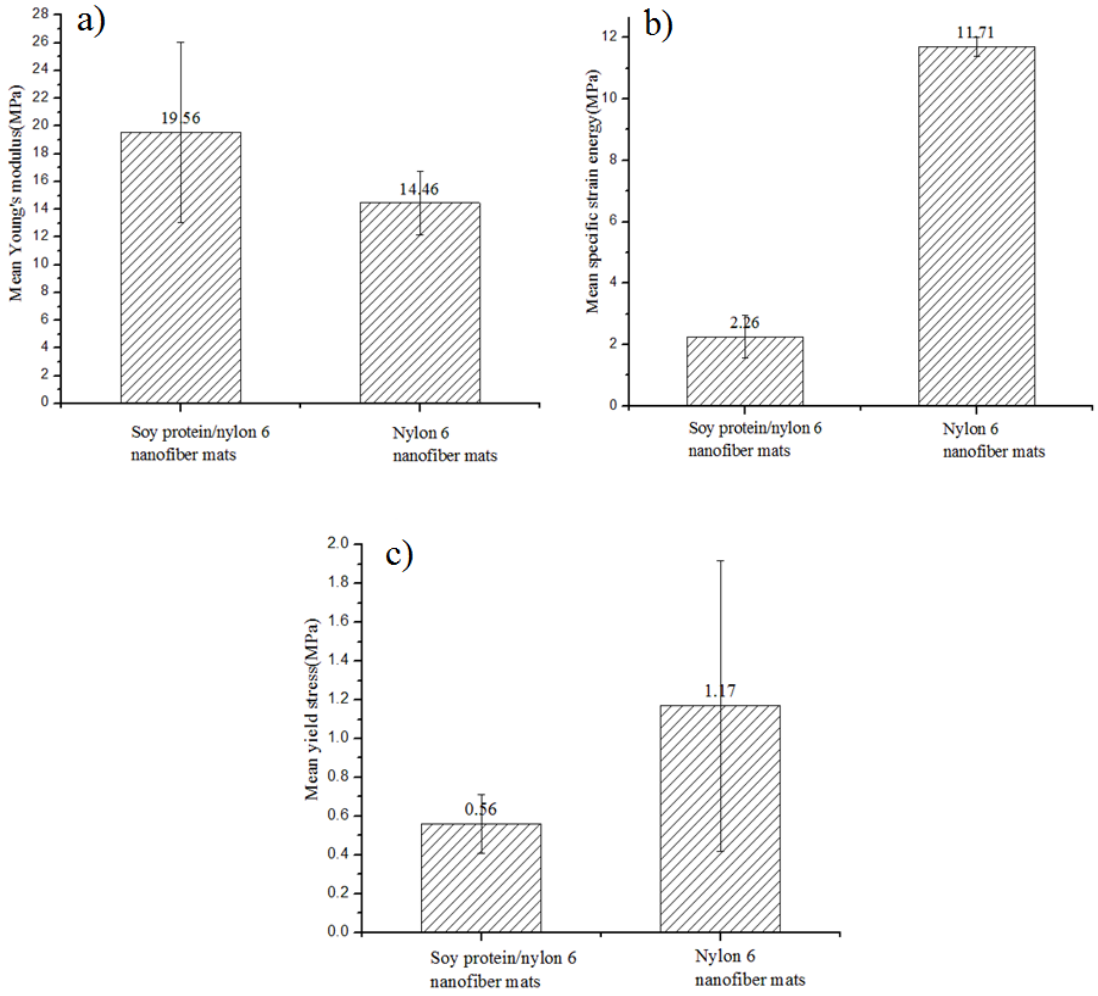

Figure 3.16. (a) Average Young's moduli, (b) average specific strain energies and (c) average yield stresses for soy protein/nylon 6 and pure nylon 6 solution-blown nanofibers.

3.3. Theory

3.3.1. Phenomenological Constitutive Equation

Phenomenological models which span the elastic and plastic ranges of stress response of solids to deformation date back to the seminal works of (Prager, 1938; Prager, 1942; Truesdell, 1952; Truesdell, 1953; Green, 1956). They bridge between the Hookean elastic body and the ideally plastic body which flows with a constant yield stress as soon as the von Mises condition is fulfilled. Different terms were applied to such materials, e.g. alternatively, hypo-elasticity or plasticity. More recently, materials of this type with deviations from the Hookean linear behavior and the associated irreversibility of deformation were understood as elastic-viscoplastic and close counterparts of viscoelastic polymeric liquids (Rubin et al., 1993; Rubin et al., 1995). Following (Rubin et al., 1993; Rubin et al., 1995), the phenomenological rheological constitutive equation prone of behavior reminiscent of that in Figs. 3.3, 3.5 and 3.6 will be taken in the form

$$\frac{d\boldsymbol{\tau}}{dt} = \nabla\mathbf{v}\cdot\boldsymbol{\tau} + \boldsymbol{\tau}\cdot\nabla\mathbf{v}^{T} - \frac{2}{3}(\boldsymbol{\tau}:\mathbf{D})\mathbf{I} + 2\mu\mathbf{D} - \Gamma\boldsymbol{\tau} - \frac{\alpha^{2}\Gamma}{\mu}\left(\boldsymbol{\tau}^{2} - \frac{1}{3}\mathbf{I}\right) \tag{3.3}$$

where d/dt denotes the material time differentiation, τ denotes the deviatoric stress tensor, $\nabla\mathbf{v}$ is the velocity gradient tensor and D its symmetric part (the rate-of-strain tensor), I is tensor unit, μ is the Lame coefficient responsible for the elastic behavior (in the case of an incompressible body assumed here, μ=E/3 with E being Young's modulus), and τ:D denotes the scalar product of two tensors. The dimensionless factor α^2 is included here for the correspondence with Green's version of plastic rheological constitutive equation in (Green, 1956).

In the uniaxial stretching of an axisymmetric specimen or a strip in the x-direction, the quantity Γ in Eq. (3.3) is determined as $\Gamma = \dot{\varepsilon}$ with $\dot{\varepsilon}$=const being the rate of strain. Then, integrating Eq. (3.3), we obtain for the longitudinal deviatoric stress

$$\tau_{xx} = \frac{2\mu}{\alpha}\tanh(\alpha\varepsilon) \tag{3.4}$$

with $\varepsilon = \dot{\varepsilon}t$ being strain.

Since $\boldsymbol{\tau} : \mathbf{D} = 0$, for an axisymmetric specimen one finds that the lateral deviatoric stresses $\tau_{yy}=\tau_{zz}=-\tau_{xx}/2$. Then, the longitudinal stress $\sigma_{xx}=\tau_{xx}-\tau_{yy}$ is equal to

$$\sigma_{xx} = \frac{3\mu}{\alpha}\tanh(\alpha\varepsilon) \tag{3.5}$$

Since as ε tends to infinity, σ_{xx}=Y with Y being the yield stress, and 3μ=E, one finds that α=E/Y and Eq. (5) reduces to the following expression established by (Green, 1956)

$$\sigma_{xx} = Y\tanh\left(\frac{E}{Y}\varepsilon\right) \tag{3.6}$$

which obviously recovers Hooke's law $\sigma_{xx}=E\varepsilon$ as ε tends to zero.

For uniaxial stretching of a planar strip similar to the experimental situation in the present work, integrating Eq. (3.3) and accounting for the fact that $\alpha>>1$, we obtain Eq. (3.1) of the main text, which obviously recovers Hooke's law for this case, $\sigma_{xx}=(4/3)E\varepsilon$ as ε tends to zero.

3.3.2. Micromechanics of Nanofiber Mats in Uniaxial Stretching

3.3.2.A. Fiber Orientation

Consider the orientational probability density function $f_{or}(\varphi,t)$ in nanofiber mats with φ being the angle relative to the stretching direction and t being time. It assumes that fiber segments cross any cross-section normal to the stretching direction with certain inclinations φ, and the corresponding probability density function $f_{or}(\varphi,t)$ varies in time as stretching goes on. At the moment stretching has begun t=0 and $f_{or}(\varphi,t) = 1/(2\pi)$ which corresponds to a random mat resulting from solution blowing. The probability density function $f_{or}(\varphi,t)$ (cf. Fig. 3.17) can be found from the following Fokker-Planck equation

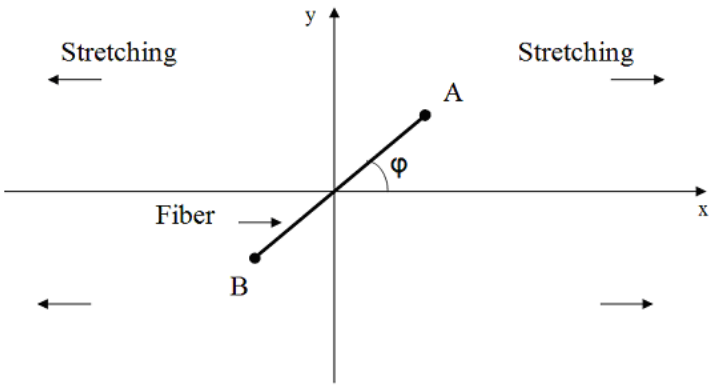

Figure 3.17. Randomly oriented fiber with the angle φ relative to the stretching direction.

$$\frac{\partial f_{or}}{\partial t} = \dot{\varepsilon}\frac{\partial}{\partial \varphi}\left(f_{or}\sin 2\varphi\right) \tag{3.7}$$

where the stretching rate $\dot{\varepsilon}$ is assumed to be constant.

The solution of Eq. (3.7) satisfying the initial condition reads

$$f_{or} = \frac{\exp(2\varepsilon)}{2\pi\left[\cos^2\varphi + \exp(4\varepsilon)\sin^2\varphi\right]} \tag{3.8}$$

It is easy to see that Eq. (3.8) automatically satisfies the normalization condition

$$\int_0^{2\pi} f_{or} d\varphi = 1 \tag{3.9}$$

3.3.2.B. Rupture of Individual Bonds in Mats Under Uniaxial Stretching

Tensile strength of different bulk materials σ_* including individual nanofibers is affected by many factors which are not under control, and therefore can be treated as a mathematical expectation of many scattered values which might be measured in repeated experiments. Following our previous works (Librovich et al., 1982; Librovich et al., 1988), consider a material with n potential defects per unit volume, which might be responsible for a local rupture. In the present context these defects are associated with the inter-fiber bonds. These bonds are formed due to conglutination of partially wet nanofibers when they deposit on top of each other in the process of mat forming. The bond strength is random in its nature, albeit an appropriate statistical law can be expected. This law is outlined below. The bonds can be ruptured due to stretching in any direction if an appropriate effective local stress arises. We can treat these bonds as potential initially conglutinated rupture surfaces (cf. Fig. 3.18). A bond is ruptured when its banks are pulled apart by an appropriate effective stress normal to its conglutinated surface. Each bond, in fact, can be considered as multiple conglutinated surfaces radiating spherically symmetrically. Any of these surfaces could be ruptured by an appropriate effective normal stress. The bond rupturing process is considered as random.

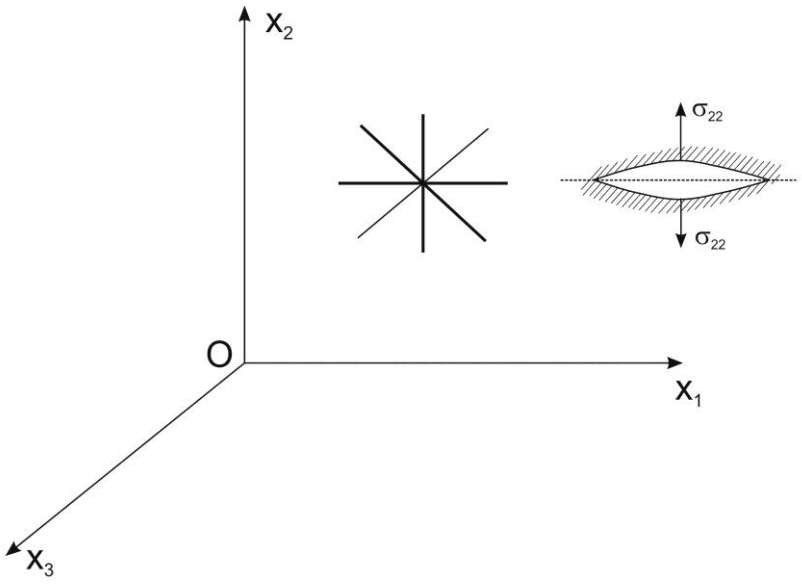

Figure 3.18. Sketch of a bond and its rupture. An intact bond with conglutinated banks is depicted on the left. A bond ruptured by stresses in the x_2 direction is shown on the right.

The calculation below in this subsection follows that of (Yarin, 2008) and is included here for completeness of discussion. The probability density function of a bond to be ruptured by an effective normal stress σ_{11} [related to stretching along the Ox_1 axis (cf. Fig. 3.18), whereas the conglutinated surface is normal to this axis] is denoted as $F(\sigma_{11})$, and the probability of the defect to be ruptured by a stress from the interval $[\sigma_{11}, \sigma_{11}+d\sigma_{11}]$ is $p_1= F(\sigma_{11})\, d\sigma_{11}$. Rupture process in different directions is considered to be mutually independent. Therefore, the number of ruptured bonds in a unit volume subjected to stretching, for example, along three normal axes Ox_1, Ox_2, and Ox_3 is

$$dN = nF(\sigma_{11})d\sigma_{11}F(\sigma_{22})d\sigma_{22}F(\sigma_{33})d\sigma_{33} \tag{3.10}$$

This number is obviously associated with the joint probability density function $f(\sigma_{11}, \sigma_{22}, \sigma_{33})$, so that

$$dN = nF(\sigma_{11})F(\sigma_{22})F(\sigma_{33})d\sigma_{11}d\sigma_{22}d\sigma_{33} = f(\sigma_{11}, \sigma_{22}, \sigma_{33})d\sigma_{11}d\sigma_{22}d\sigma_{33} \tag{3.11}$$

Therefore, the number of bonds in a unit volume which will not be ruptured at all in such three-axial stretching by stresses σ_1, σ_2, and σ_3 is given by

$$N_0 = n\int_{\sigma_1}^{\infty} F(\sigma_{11})d\sigma_{11}\int_{\sigma_2}^{\infty} F(\sigma_{22})d\sigma_{22}\int_{\sigma_3}^{\infty} F(\sigma_{33})d\sigma_{33} = n\Phi(\sigma_1)\Phi(\sigma_2)\Phi(\sigma_3) = \int_{\sigma_3}^{\infty}\int_{\sigma_2}^{\infty}\int_{\sigma_1}^{\infty} f(\sigma_{11}, \sigma_{22}, \sigma_{33})d\sigma_{11}d\sigma_{22}d\sigma_{33} = \omega(\sigma_1, \sigma_2, \sigma_3) \tag{3.12}$$

Accordingly, the number of bonds ruptured in a unit volume in this case is $N=n-N_0$.

The choice of a coordinate system is obviously arbitrary, and same rupture process can be described using an arbitrarily oriented Cartesian coordinate frame Ox, Oy and Oz. Then, the number of the intact bonds is equal to $N_0=\omega(\sigma_{xx}, \sigma_{xy}, \sigma_{xz}, \sigma_{yy}, \sigma_{yz}, \sigma_{zz})$, where σ_{xx}, etc. denote the corresponding components of the effective stress tensor σ. The previously used Cartesian axes Ox_1, Ox_2, and Ox_3 can be thought as the principal axes of the effective stress tensor σ, with σ_1, σ_2, and σ_3 being, correspondingly, the principal stresses. The number of the intact or ruptured bonds should not depend on the directions of the arbitrarily chosen axes Ox, Oy and Oz, which means that the function ω should depend only on the three invariants of the effective stress tensor σ

$$I_1 = \sigma_{xx} + \sigma_{yy} + \sigma_{zz} = \sigma_1 + \sigma_2 + \sigma_3 \tag{3.13}$$

$$I_2 = \sigma_{xx}\sigma_{yy} + \sigma_{yy}\sigma_{zz} + \sigma_{xx}\sigma_{zz} - \sigma_{xy}^2 - \sigma_{yz}^2 - \sigma_{xz}^2 = \sigma_1\sigma_2 + \sigma_2\sigma_3 + \sigma_1\sigma_3 \tag{3.14}$$

$$I_3 = \sigma_{xx}\sigma_{yy}\sigma_{zz} + 2\sigma_{xy}\sigma_{yz}\sigma_{xz} - \sigma_{xx}\sigma_{yz}^2 - \sigma_{yy}\sigma_{xz}^2 - \sigma_{zz}\sigma_{xy}^2 = \sigma_1\sigma_2\sigma_3 \tag{3.15}$$

Equations (12)-(15) result in the following functional equation

$$n\Phi(\sigma_1)\Phi(\sigma_2)\Phi(\sigma_3) = \omega(\sigma_1+\sigma_2+\sigma_3, \sigma_1\sigma_2+\sigma_2\sigma_3+\sigma_1\sigma_3, \sigma_1\sigma_2\sigma_3) \tag{3.16}$$

Its solution reads

$$\Phi(\sigma_i) = (A+B\sigma_i)\exp(-C\sigma_i), \quad i=1,2,3 \tag{3.17}$$

with A,B and C being constants.

When there is no stress applied, the number of the intact bonds in a unit volume N_0=n. Then, Eqs. (3.16) and (3.17) yield $N_0=nA^3$, and therefore, A=1.

From Eq. (3.17), follows that

$$\varphi(\sigma_i) = \int_{\sigma_i}^{\infty} F(\sigma_{ii})d\sigma_{ii} = (1+B\sigma_i)\exp(-C\sigma_i) \tag{3.18}$$

which yields

$$F(\sigma_{ii}) = (BC\sigma_{ii}+C-B)\exp(-C\sigma_{ii}) \tag{3.19}$$

Since materials have a certain strength, F(0)=0, and thus C=B, which results in

$$F(\sigma_{ii}) = B^2\sigma_{ii}\exp(-B\sigma_{ii}) \tag{3.20}$$

It is easy to see that Eq. (3.20) satisfies the normalization condition.

The mathematical expectation of the bond-opening stress is denoted σ_*. Therefore, using Eq. (3.20), we obtain

$$\sigma_* = \int_0^{\infty} \sigma_{ii}F(\sigma_{ii})d\sigma_{ii} = \int_0^{\infty} B^2\sigma_{ii}^2\exp(-B\sigma_{ii})d\sigma_{ii} \tag{3.21}$$

which yields $B=2/\sigma_*$. Then, the probability density function of bond rapture under stretching in the i-th direction is given by

$$F(\sigma_{ii}) = \frac{4}{\sigma_*^2}\sigma_{ii}\exp(-2\sigma_{ii}/\sigma_*) \tag{3.22}$$

3.3.2.C. Mat Plasticity as Bond Rupture Process

Assume that all bonds behave as Hookean elastic solids until they rupture. We aim to show below that the macroscopic nanofiber mat plasticity can result from rupture of individual bonds in the mat under uniaxial stretching.

Fibers in the mat experience different stretching from the overall macroscopic axial stretching imposed on the sample ε. Indeed, for an inclined fiber the strain ε_i is given by

$$\varepsilon_i = \varepsilon \cos^2(\varphi) \tag{3.23}$$

According to Eq. (3.22), if an initially unloaded bond was stretched to a certain stress σ, its probability to stay intact P_{intact} is

$$P_{intact} = \left(1 + \frac{2\sigma}{\sigma_*}\right) \exp\left(-\frac{2\sigma}{\sigma_*}\right) \tag{3.24}$$

Then, it is easy to see that the longitudinal stress in the mat is given by the following expression

$$\sigma_{xx} = E_m \int_0^{2\pi} \varepsilon_i(\varphi) \cos^2 \varphi P_{intact} f_{or}(\varphi, \varepsilon) d\varphi \tag{3.25}$$

where E_m is proportional to Young's modulus.

Substituting Eqs. (3.8), (3.23) and (3.26) into Eq. (3.25), and accounting for the fact that for an individual Hookean bond according to Eq. (3.23) $\sigma = E_f \varepsilon \cos^2\varphi$ with E_f being the characteristic Young's modulus, we arrive at Eq. (3.2) of the main text.

3.4. Conclusion

The experiments conducted in this work showed that the novel monolithic and core-shell soy protein-containing nanofiber mats recently introduced by this group possess sufficiently high tensile strength for their applications as nonwovens. Their Young's moduli are close to those of pure nylon 6 nanofiber mats, albeit the yield stress and specific strain energy of the latter is higher. The effects of such forming parameters as winding velocity, as well as of the straining history on tensile strength of soy protein-containing nanofiber mats are also elucidated. It is shown that the traditional phenomenological and a novel micromechanical models (the latter is introduced in the present work) can successfully describe stress-strain curves of soy protein-containing nanofiber mats in the elastic and plastic zones. These models are still incapable of describing the catastrophic rupture of such nanofiber mats at high values of tensile strain.

4. Effect of Cross-linking on Tensile Characteristics of Solution-Blown Soy Protein Nanofiber Mats: I- Chemical Cross-linking

4.1. Experimental

4.1.1. Materials

Materials used in this work are as follows. Soy protein isolate [PRO-FAM 955 (SP 955)] was provided by ADM Specialty Food Ingredients. Polyamide-6 (nylon-6) (M_w=65.2 kDa) was obtained from BASF. Formic acid (grade >95%), formaldehyde 37 wt% solution in water, A.C.S. reagent, glyoxal solution (Bioreagent ~40% in H_2O, 8.8 M), zinc sulfate solution 0.1 mol/l in water, and sodium borohydride were purchased from Sigma-Aldrich. All materials were used as received without any further treatment and/or purification.

4.1.2. Blend Solution Preparation

Blends of SPI 955/nylon 6 (40/60 and 50/50 wt/wt %) in formic acid were prepared as described in (Sinha-Ray et al., 2011; Khansari et al., 2012). In brief, to prepare a blend of 40/60 wt/wt % soy protein/nylon 6, 1.0 g of soy protein was added to 9.5 g of formic acid and the solution was stirred on a hotplate at 75 °C for 24 h. Then, 1.5 g of nylon 6 was added to the solution and left on a 75 °C hotplate for a day. A homogeneous solution was then ready for solution blowing process. Similarly, to prepare a solution of 50/50 wt/wt% soy protein/nylon 6 blend, 1.5 g of soy protein 955 was mixed with 9.5 g formic

acid for 24 h on a hotplate at 75 °C. Next, 1.5 g of nylon 6 was mixed with the soy protein solution for 24 h at the same temperature. In order to produce core-shell nanofibers, core and shell solutions were prepared separately. Shell solution was 20 wt % nylon 6 in formic acid which was left on a hotplate at 75 °C for a day to stir properly. Core solution was prepared as described in (Sinha-Ray et al., 2011; Khansari et al., 2012). Namely, 1.3 g of SPI 955 was mixed with 8.7 g of formic acid for a day on a hotplate at 75 °C. Adding 1.0 g of nylon 6 to the solution and mixing for another day at the same temperature was the final step to prepare core solution. For solution blowing of pure nylon 6, 20 wt% solutions in formic acid were used.

4.1.3. Solution Blowing of Soy Protein Nanofiber Mats

To prepare soy-protein-based monolithic nanofiber mats and pure nylon 6 nanofiber mats, solution blowing (Sinha-Ray et al., 2011; Khansari et al., 2012) was employed. Solutions were supplied through a 13G needle. While exiting the needle, solutions were exposed to a high speed co-flowing turbulent air jet with the upstream pressure of about 2.0 bar and velocity of about 150-200 m/s issued from a co-annular nozzle. Solution blowing procedure was implemented at room temperature and humidity. As humidity (20-30 %) in the present case was by 20-30 % lower than that in (Khansari et al., 2012), solvent evaporated faster after a solution jet was exiting the needle. Therefore, the needle-to-collector distance was reduced to 15-19 cm. Consequently, soy protein/nylon 6 monolithic nanofibers with the average diameter of 400-500 nm were formed, which corresponds to the diameter of monolithic soy protein nanofibers in (Khansari et al., 2012). These nanofibers were collected and partly aligned on an aluminum rotating drum

with linear velocity of about 3.0 m/s on the surface. Collected nanofibers formed a mat with a thickness of 0.15-0.40 mm.

Solution co-blowing of core-shell nanofibers is discussed in detail in (Sinha-Ray et al., 2011; Khansari et al., 2012). In brief, the shell solution was supplied into a reservoir which surrounded a 18G needle issuing the core solution. The reservoir was placed on top of a 13G needle. Therefore, the core needle was located co-axially inside the shell needle. Both the core and shell solutions were supplied through the 18G and 13G needles, respectively, each with the throughput of 4 ml/h. A third annular nozzle surrounded the 18G and 13G needles, and air was issued through it coaxially with the core-shell liquid jet with the upstream pressure of about 2.0 bar. The co-blown nanofibers were then collected as described above.

4.1.4. Cross-linking of Soy Protein Nanofiber Mats

For cross-linking, a collected nanofiber mat (50/50 SPI/nylon 6) of a certain thickness was removed from the aluminum drum. The mat was then cut into several pieces and every single piece was weighed carefully. The weighed samples were immersed in a solution with a specified weight percentage of a cross-linker to the nanofiber mat. The weight ratio of cross-linking agents to nanofiber samples was 5, 10, and 20 wt/wt%. This procedure was followed for four different types of cross-linking agents: formaldehyde, glyoxal, zinc sulfate, and sodium borohydride. After adding a cross-linking solution to the samples, open vials were left at room temperature for 24 h to dry out completely. It is emphasized that only samples prepared from the same batch were used for cross-linking at different concentrations to avoid variability between

samples prepared from different batches. All the resulting cross-linked nanofiber mats were subjected to uniaxial tensile tests to measure the mechanical properties similarly to (Khansari et al., 2012). In addition, solubility tests were done using samples after rapture in tensile tests, which allowed us to link solubility in water with known mechanical properties.

It is emphasized that treating fiber mats above 50 wt/wt % cross-linker weight ratio to nanofiber mat, led to visible macroscopic cracks in the samples. Therefore, cross-linking experiments were conducted only with 5, 10, and 20 wt/wt % ratios, except the case of heat treatment discussed below where also 50 wt/wt % ratio was used. The above-mentioned cracking is illustrated in Fig. 4.1 where a soy protein/nylon 6 (50/50 wt/wt %) nanofiber mat treated with 80 wt/wt% is shown. Only the cracked sample treated with glyoxal is shown, since the formaldehyde-, zinc sulfate-, and sodium borohydride- treated samples cracked similarly.

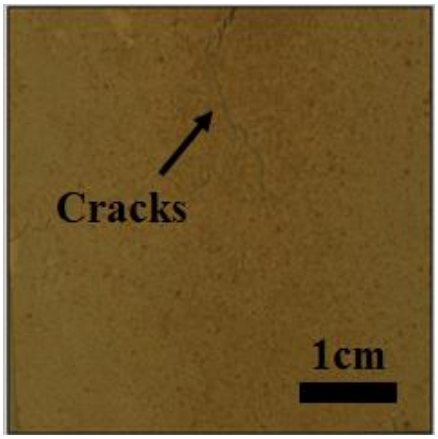

Figure 4.1. Soy protein/nylon 6 (50/50 wt/wt %) nanofiber mat cross-linked at 80 wt/wt% glyoxal/nanofiber mat ratio. Macroscopic cracks are visible in the sample.

4.1.5. Heat Treatment of Cross-linked Soy Protein/Nylon 6 Nanofiber Mats

In a different set of experiments, soy protein/nylon 6 (40/60 wt/wt %) monolithic nanofibers were cross-linked with the following three of the above-mentioned cross-linking agents: formaldehyde, glyoxal, and zinc sulfate. For each bonding agent, cross-linking procedure in this case was conducted with four different cross-linker weight ratios to nanofiber mat: 1, 5, 10, and 50 wt/wt %. For each cross-linker concentration, one half of nanofiber samples from a batch were heat treated after being chemically cross-linked. The second half from the same batch which were not heat treated, were used for control. Thermal treatment was conducted as follows. After being exposed to a chemical cross-linker with a specified concentration for 24 h, the samples were left at 80 ^{o}C for 20 min on a glass-light on a hotplate. Then, mechanical properties of the heat treated cross-linked samples were compared with the control (non-heat-treated) samples from the same batch. As a result, effect of heat treatment on different covalent and ionic bonds in cross-linked samples was elucidated.

4.1.6. Tensile Tests of Cross-linked Nanofiber Mats

Cross-linked soy protein/nylon 6 (40/60 and 50/50 wt/wt %) nanofiber mats were cut into rectangular shapes as described in (Khansari et al., 2012). In brief, rectangular nanofiber mats which were 6-15 mm wide and 20-35 mm long underwent uniaxial stretching test using Instron machine (model 5294) with 100 N capacity on pneumatic grips. The rate of stretching was kept at 1.0 mm/min for all the experiments. As a result, stress-strain behavior and mechanical properties such as Young's modulus, yield stress and maximum strain and stress at rupture (E, Y and $\varepsilon_{rupture}$,$\sigma_{xx,rupture}$, respectively) were

measured following (Khansari et al., 2012), and the effect of different chemical cross-linking agents was investigated. For control, stress-strain curves of chemically-bonded nanofiber mats were compared to those of the corresponding non-cross-linked samples. As mentioned in (Khansari et al., 2012), optical observations of solution-blown soy protein/nylon 6 nanofiber mats demonstrate that they possess a layered structure and only 50% of a mat cross-section is filled with nanofibers. Therefore, tensile stress applied to each sample by Instron machine is only supported by a 50% cross-sectional area, which was taken into account while calculating mechanical properties.

4.1.7. Solubility Tests of Soy Protein Nanofiber Mats

Nanofiber samples (soy protein/nylon 6 50/50 wt/wt%) were put inside an enclosure made of a metal grid and immersed in de-ionized water for 24 h at room temperature. Water was constantly stirred. After the immersion, the samples withdrawn and left at room temperature for 24 h to dry out completely. Each sample was weighed before immersion and in two days after the complete drying to determine the percentage of lost weight L as

$$L=\left(1-\frac{W_2}{W_1}\right)100\% \qquad (4.1)$$

where W_1 is the sample weight before immersion, and W_2 is the weight after immersion and drying.

4.1.8. Theoretical Model

Mechanical properties of soy protein/nylon 6 monolithic and core-shell nanofibers were measured and characterized using the phenomenological model described in (Khansari et al., 2012). For a planar strip which undergoes uniaxial tensile test the stress-strain dependence is given by

$$\sigma_{xx} = \sqrt{\frac{8}{3}} Y \tanh\left(\sqrt{\frac{2}{3}} \frac{E}{Y} \varepsilon\right) \tag{4.2}$$

where σ_{xx} is tensile stress and ε is tensile strain, E is Young's modulus and Y is the yield stress. This model was used in (Khansari et al., 2012) to predict the elastic and plastic behavior of soy/nylon 6 nanofiber mats up to the rupture point.

4.2. Experimental Results and Discussion

4.2.1. Cross-linking of Soy Protein with Aldehydes and Ionic Salts

Cross-linking of soy protein with aldehydes is an example of a carbonyl-amine reaction. A detailed description of the reaction mechanism can be found in (Fraonkel-Conrat et al., 1948; Nayudamma et al., 1961; Quiocho et al., 1966; Bedino, 2003). In brief, chemical cross-linking can be explained as follows. In the seminal work (Fraonkel-Conrat et al., 1948) it was shown that in a wide range of pH, cross-linking starts between amino group of one amino acid with primary amide and/or guanidyl group to the other one under the action of aldehyde. In soy protein isolates used in the present work the absence of aspargine and glutamine (Pro-Fam 955 Data Sheet) implies that guanidyl groups are the potential source of cross-linking via methylene bridging. Soy protein

isolate 955 used in the present work contains a very reactive lysine amino acid [~6.3% of the entire protein content (Pro-Fam 955 Data Sheet)], which acts as the most preferential site for cross-linking due to its conformational freedom and external surface availability because of the steric effect. It is emphasized that in addition to methylene bridging, sulfhydryl groups also participate in sulfide linkage as it was found in (Consden et al., 1946). Note that the reaction kinetics reveal that complete cross-linking occurs in a time frame of 24 h (Nayudamma et al., 1961). That is why during cross-linking the samples were left in cross-linker solution for 24 h to facilitate complete inter- and intra- fiber cross-linking. The covalent bonds thus formed restrict protein macromolecule mobility and rotation, which facilitates an increase in Young's modulus and fiber strength. A reduced flexibility of thus cross-linked protein chains makes nanofiber mats more brittle and results in reduction of strain at rupture point, $\varepsilon_{rupture}$.

Cross-linking of soy protein nanofiber mats with $ZnSO_4$ relies on metal chelation and ionic bonding. Soy protein isolates contain many polar amino acids. The addition of $ZnSO_4$ forms stable ionic bonds with these polar amino acids. In addition, Zn^{2+} forms chelating complexes with soy protein (Berg et al., 1996; Zhang et al., 2001), which is expected to increase strength of nanofiber mats.

Sodium borohydride ($NaBH_4$) is a very strong reducing agent. Whenever protein molecules come in contact with it, the labile disulfide group containing polar amino acid (cystine) is attacked, which results in sulfhydryl-disulfide exchange. This, in turn, results in opening up of the inter- and intra-molecular disulfide bonds, which are readily oxidized by air and cross-linked across the chain (Wall, 1971).

4.2.2. SEM Images of Cross-Linked Nanofiber Mats

All observations were done by Hitachi S-3000N variable pressure SEM and JEOL 6320F scanning microscope after sputter coating a 8 nm layer of Pd-Pt onto samples.

SEM images of a cross-linked sample with 20 wt% of the cross-linkers are shown in Fig. 4.2. In particular, Figs. 4.2a-d show SEM images of the samples treated with formaldehyde, glyoxal, zinc sulfate and sodium borohydride, respectively. It can be seen that for the organic cross-linkers, formaldehyde (Fig. 4.2a) and glyoxal (Fig. 4.2b), nanofiber morphology does not change and there is no deposit or film formed. These observations show that reaction between nanofiber mats and the organic cross-linkers were completed. However, for the ionic cross-linker, zinc sulfate, (Fig. 4.2c) there are visible deposits of zinc sulfate on nanofibers, which shows that an excessive cross-linker was left. For $NaBH_4$ (Fig. 4.2d), it is seen that there are some sharp crystalline features visible on nanofibers (shown by arrows), which means that a higher than 20 wt% mass ratio of the ionic cross-linker would be definitely too much. It was found that when the mass ratio of zinc sulfate was decreased to 10 wt%, there was no more deposits on nanofibers anymore (Fig. 4.3a). However, for $NaBH_4$ it was found that even at 10 wt% mass ratio, some nanofibers with fewer sharp features were still visible (Fig. 4.3b). Only when the mass ratio of $NaBH_4$ was reduced to 5 wt% these features practically disappeared (Fig. 4.3c). To resolve the chemical nature of these sharp structures, the elemental analysis was done on a nanofiber mat treated with 10 wt% $NaBH_4$. Two different places were used: the smooth part, and the rough patches (shown by two arrows in Fig. 4.3b). In these experiments Hitachi S-3000N variable pressure SEM was used. It was found that at both places the amount of sodium was comparable (~6-8% of the total

signal in both cases). If the sharp features were only comprised of the excessive $NaBH_4$, the elemental analysis would have shown higher amounts of sodium there compared with the smooth fiber part. Comparable amounts of sodium at both locations clearly show that the reaction is complete. Therefore, these sharp features are most probably remnants of broken pieces caused by handling. This conclusion is supported below by the results of the tensile tests, which show that cross-linking with $NaBH_4$ made nanofiber mats most brittle.

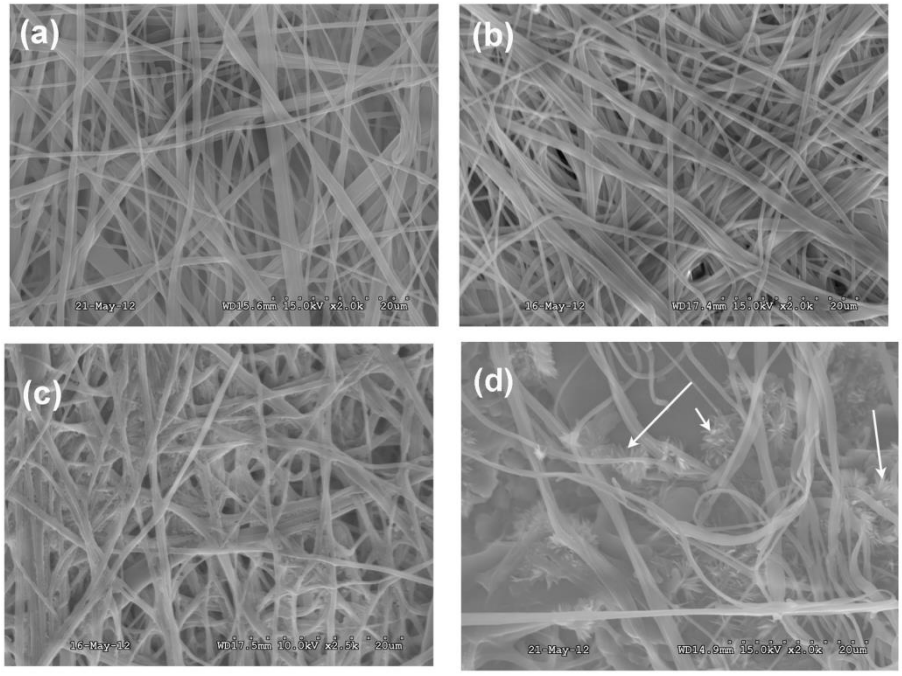

Figure 4.2. SEM images of nanofibers mat treated with 20 wt% of: (a) formaldehyde, (b) glyoxal, (c) zinc sulfate, and (d) $NaBH_4$. Panel (c) shows that there is an excessive zinc sulfate deposited on the mat. Panel (d) shows that there are sharp features formed on the nanofibers mat (shown by arrows).

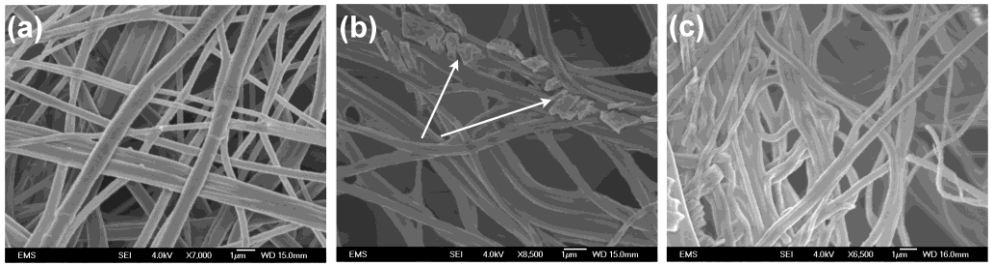

Figure 4.3. SEM images of nanofibers cross-linked with: (a) 10 wt% zinc sulfate, (b) 10 wt% and (c) 5 wt% of $NaBH_4$. In panel (b) arrows point at the sharp features.

4.2.3. Stress-Strain Curves of Cross-linked Soy Protein Nanofiber Mats

Figs. 4.4a-d illustrate the typical stress-strain dependences of soy protein/nylon 6 (50/50 wt/wt %) nanofiber mats after cross-linking in the presence of 5, 10, and 20 wt/wt% of different cross-linkers. It is seen that sodium borohydride and zinc sulfate mostly affected the strength of nanofiber mats, whereas the samples treated with formaldehyde and glyoxal show more plastic behavior than those treated with $NaBH_4$ and $ZnSO_4$. This clearly demonstrates that the ionic agents were more effective in cross-linking in comparison to the aldehydes, which will be discussed in more detail in the following sections.

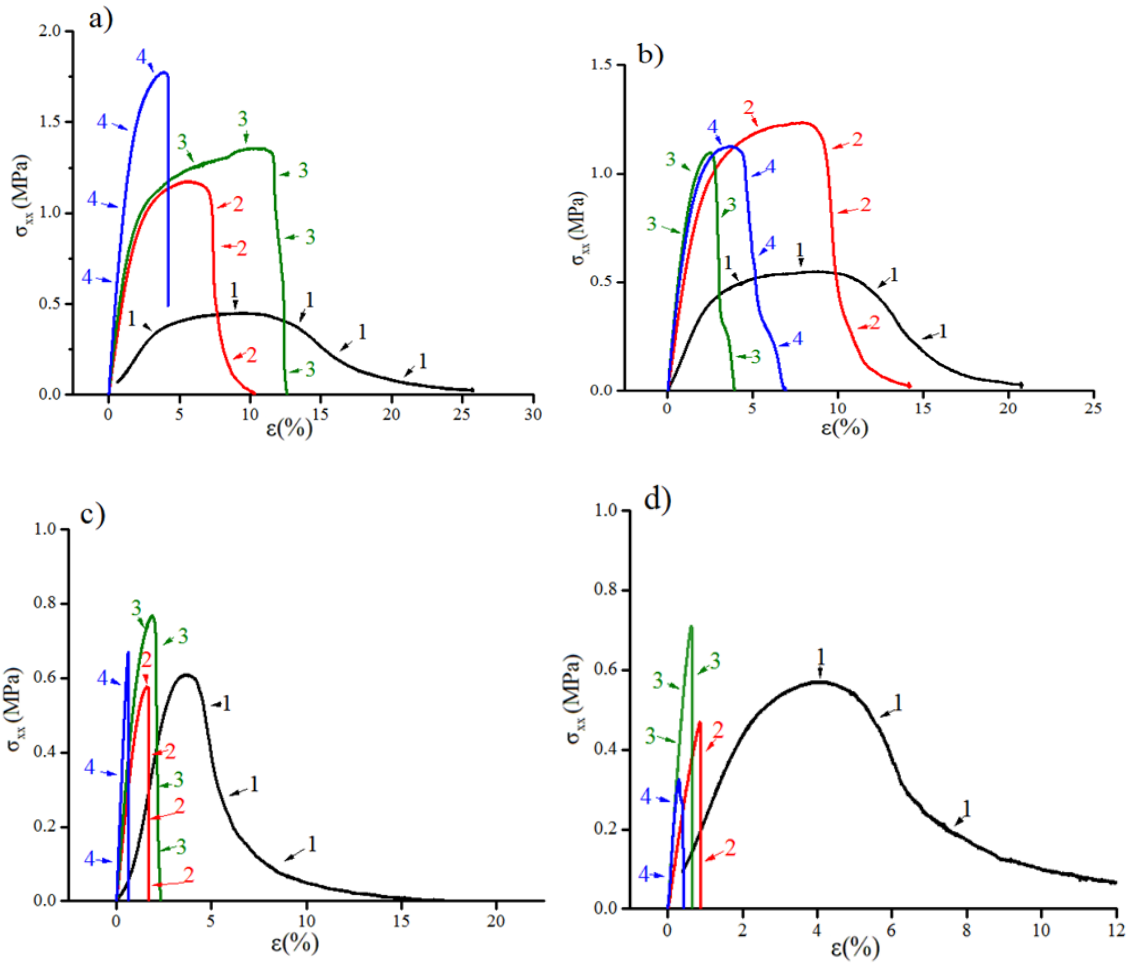

Figure 4.4. Stress-strain behavior of cross-linked soy protein nanofiber mats for different cross-linkers with various concentrations. In all panels, curves 1 show the stress-strain dependence for untreated soy protein nanofibers used for control; curves 2 correspond to 5 wt/wt % cross-linker/nanofiber mat ratio; curves 3 correspond to 10 wt/wt % cross-linker/nanofiber mat ratio, and curves 4 correspond to 20 wt/wt % cross-linker/nanofiber mat ratio. Panel (a) shows stress-strain behavior of soy protein/nylon 6 (50/50 wt/wt%) when formaldehyde was used as a bonding agent. In panel (b) glyoxal was used as a

cross-linking agent. Panel (c) corresponds to zinc-sulfate-treated samples. Panel (d) shows sodium borohydride- treated nanofibers.

4.2.4. Mechanical Properties of Soy Protein Nanofibers Cross-linked Using Formaldehyde

While using formaldehyde as a cross-linker, it was found that an addition of formaldehyde resulted in an increase in Young's modulus of soy protein nanofiber mat and reduction of strain at rupture ($\varepsilon_{rupture}$) compared to the corresponding non-cross-linked samples (Table 4.1 and Fig. 4.5a). The maximum increase in Young's modulus corresponded to the ratio of 20 wt/wt% of cross-linker to nanofiber mat in the cross-linking process. The mechanical properties of formaldehyde-cross-linked samples are listed in Table 4.1. Average Young's modulus of non-cross-linked soy protein/nylon 6 nanofiber mats was measured as 16.51±2.39 MPa, whereas the value of 66.81±16.05 MPa was achieved for the ratio of 20 wt/wt% of formaldehyde to nanofiber mat. In addition, maximum strain at rupture for the non-cross-linked samples is reported as 9.63±2.88%. In the present work the maximum strain at rupture was reduced to 3.47±2.00% for the formaldehyde-cross-linked samples with 20% wt/wt% cross-linker/nanofiber mat ratio. An increase in formaldehyde content in the cross-linking process resulted in a lower strain at rupture, which implies a reduced plasticity of the cross-linked nanofiber mats. Consequently, lower plasticity observed in samples cross-linked with a higher than 20 wt/wt% formaldehyde mass ratio resulted in noticeable ruptures while drying at room temperature. Therefore, tensile tests could not be conducted with these samples. The average Young's modulus of comparable pure nylon

6 solution-blown nanofiber mats is 8.59±0.88 MPa. Therefore, chemically modified soy protein nanofiber mats with formaldehyde used as a cross-linker reveal a higher Young's modulus than for the corresponding pure nylon 6 nanofiber mats.

Table 4.1. Young's modulus, yield stress, and maximum strain and stress at rupture for soy protein/nylon 6 (50/50 wt/wt%) nanofiber mats cross-linked at different formaldehyde, glyoxal, zinc sulfate and sodium borohydride/nanofiber mat mass ratios.

Cross-linking agent	Cross-linking ratio (wt/wt %)	Average thickness of the samples (mm)	Average width of the samples (mm)	Average Young's modulus E (MPa)	Average yield stress Y (MPa)	Average specific strain energy U (MPa)	Average maximum strain at rupture $\varepsilon_{rupture}$(%)
Formaldehyde	0	0.2	7.04	16.51±2.39	0.29±0.11	9.63±2.88	0.38±0.08
	5	0.2	6.85	36.15±15.49	0.52±0.20	4.05±1.71	0.80±0.30
	10	0.2	7.66	57.55±14.25	0.80±0.21	4.79±2.11	1.28±0.35
	20	0.2	8.09	66.81±16.05	0.87±0.22	3.47±2.00	1.18±0.41
Glyoxal	0	0.2	8.36	13.87±6.36	0.37±0.13	7.65±3.26	0.56±0.17
	5	0.2	7.62	54.31±15.77	0.67±0.13	4.39±1.49	1.09±0.21
	10	0.2	7.38	66.95±17.48	0.70±0.15	3.24±1.23	1.14±0.22
	20	0.2	7.23	59.22±17.16	0.67±0.17	3.74±1.50	1.07±0.26
Zinc sulfate	0	0.2	8.84	13.56±5.44	0.53±0.17	4.32±1.54	0.54±0.14
	5	0.2	7.94	37.25±12.45	0.49±0.13	1.96±0.49	0.59±0.17
	10	0.2	6.58	48.82±13.37	0.56±0.16	1.31±0.48	0.62±0.16
	20	0.2	6.35	93.60±15.43	0.73±0.13	0.71±0.32	0.67±0.20
Sodium borohydride	0	0.2	7.12	16.43±4.09	0.39±0.20	3.63±0.61	0.46±0.08
	5	0.2	7.78	84.90±24.36	0.62±0.16	0.82±0.27	0.67±0.13
	10	0.2	8.21	90.88±20.24	0.52±0.14	0.53±0.16	0.53±0.07
	20	0.2	8.09	121.74±8.05	0.73±0.12	0.43±0.09	0.69±0.05

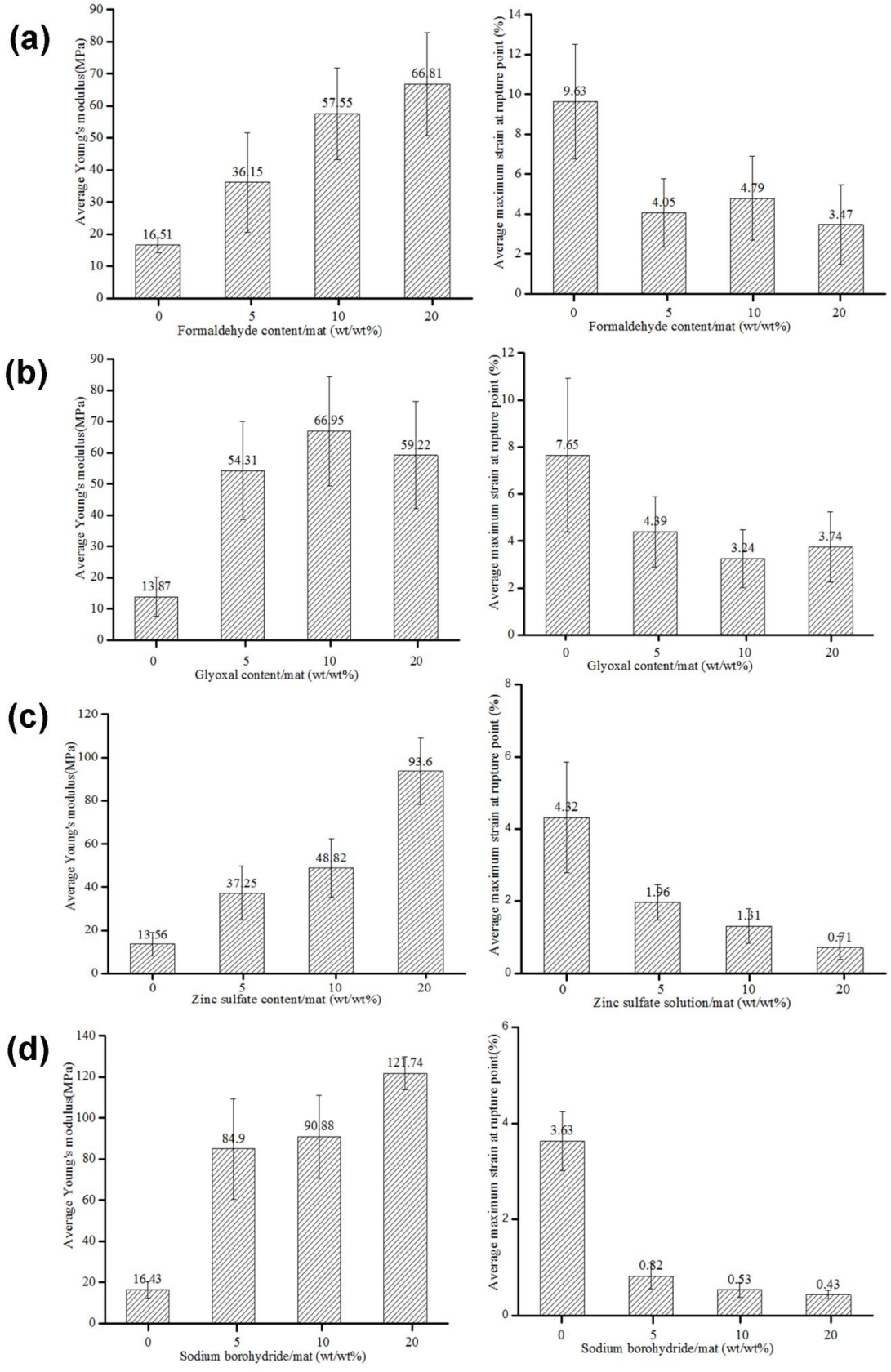
(a)
Average Young's modulus(MPa)
16.51
36.15
57.55
66.81
Formaldehyde content/mat (wt/wt%)
Average maximum strain at rupture point (%)
9.63
4.05
4.79
3.47
Formaldehyde content/mat (wt/wt%)
(b)
Average Young's modulus(MPa)
13.87
54.31
66.95
59.22
Glyoxal content/mat (wt/wt%)
Average maximum strain at rupture point (%)
7.65
4.39
3.24
3.74
Glyoxal content/mat (wt/wt%)
(c)
Average Young's modulus(MPa)
13.56
37.25
48.82
93.6
Zinc sulfate content/mat (wt/wt%)
Average maximum strain at rupture point (%)
4.32
1.96
1.31
0.71
Zinc sulfate solution/mat (wt/wt%)
(d)
Average Young's modulus(MPa)
16.43
84.9
90.88
121.74
Sodium borohydride/mat (wt/wt%)
Average maximum strain at rupture point(%)
3.63
0.82
0.53
0.43
Sodium borohydride/mat (wt/wt%)

Figure 4.5. Average Young's modulus and maximum strain at rupture for the same batch of cross-linked soy protein samples using different concentrations of (a) formaldehyde, (b) glyoxal, (c) zinc sulfate and (d) sodium borohydride as cross-linker is shown. Fiber mats revealed lower plasticity as the cross-linker content increased.

4.2.5. Mechanical Properties of Soy Protein Nanofibers Cross-Linked Using Glyoxal

The effect of glyoxal as a cross-linker is specified in Table 4.1 and Fig. 4.5b. The glyoxal/mat weight ratio in the cross-linking process varied in the range 0-20 wt/wt%. Young's modulus and yield stress increased with glyoxal percentage up to 10 wt/wt%. It can be seen that using glyoxal as a cross-linker led to Young's modulus of soy protein nanofiber mats almost 5 times higher than that of the non-cross-linked samples, which is reported as E=13.87±6.36 MPa (Table 4.1). In the present work, Young's modulus of glyoxal-cross-linked soy protein nanofiber mats reached E=66.95±17.48 MPa for 10 wt/wt% cross-linker/nanofiber mat ratio. The average maximum strain at rupture reported as 7.65±3.26% for the non-cross-linked samples was reduced to 3.24±1.23% for 10 wt/wt% glyoxal/nanofiber mat ratio in the cross-linking process. This result reveals an increased brittleness of nanofibers due to cross-linking with glyoxal. Increasing glyoxal content above 20 wt/wt% in the cross-linking process did not further improve mechanical properties of the samples due to high brittleness. It led to observable cracks in the nanofiber mat structure. These cracks resulted in fragile nanofiber samples.

Comparison of the data for glyoxal cross-linking listed in Table 4.1 with those for the formaldehyde cross-linking in Table 4.1 shows that the former results in higher values

of Young's modulus E than the latter up to the cross-linker mass ratio of 20 wt/wt%. It is emphasized that in the case of formaldehyde, the E value increased monotonically with an increase in the content of formaldehyde. On the contrary, in the case of glyoxal, the E value increased up to 10 wt/wt% of glyoxal and then decreased when the mass ratio increased to 20 wt/wt% of glyoxal. Also, the strain at rupture is lower in the case of glyoxal compared to that of formaldehyde. References (de Carvalho et al., 2000; Rhim et al., 2000;) report comparable to our values of E in solid extruded sheets cross-linked using glyoxal and formaldehyde.

The higher stiffness achieved using glyoxal compared to that with formaldehyde up to 10 wt/wt% can be explained as follows. Both glyoxal (OCHHCO) and formaldehyde (HCHO) have aldehyde groups. However, glyoxal has more available aldehyde groups facilitating more cross-linking sites than formaldehyde, which results in a higher strength of glyoxal-cross-linked nanofiber mats compared to the formaldehyde-treated ones. Note also that nanofiber mats subjected to cross-linking are porous fluffy materials in distinction from the solid extruded sheets cross-linked in (de Carvalho et al., 2000; Rhim et al., 2000). The open porosity of nanofiber mats resulted in an easier cross-linker access and high E values comparable to those of solid sheets in (de Carvalho et al., 2000; Rhim et al., 2000).

Table 4.1 also reveals that Young's modulus E reached the maximum values for the cross-linker/nanomat ratio in the cross-linking process in the range 10-20 wt/wt%. A further increase in the cross-linker content resulted in a decrease of E. One can speculate as in (de Carvalho et al., 2000) an increase in the cross-linker content might have plasticized the samples. However, Table 4.1 show that as the cross-linker/nanomat ratio

increased, the strain at rupture decreased. This shows that the cross-linkers did not plasticize the samples for higher concentrations. The reduction in the value of E at the higher cross-linker mass rations can be attributed to the fact that as the aldehyde content was increased, the number of possible inter- and intra-fiber linkages between protein chains also increased. Therefore, the material became overstretched and micro-cracks appeared. This resulted in an earlier rupture and lowered strength, as revealed experimentally.

4.2.6. Mechanical Properties of Soy Protein Nanofibers Treated Using Zinc Sulfate

Effect of cross-linking with $ZnSO_4$ is shown in Table 4.1. It can be seen that adding zinc sulfate solution to soy protein nanofiber mats resulted in about 7 times increase in the average Young's modulus of samples which were cross-linked at 20 wt/wt% zinc sulfate/nanofiber mat ratio compared to untreated samples. As nanofiber mats became stronger due to the effect of the ionic bonding agent, brittleness of the mats became more considerable. Reduction of the maximum strain at rupture from 4.32±1.54% for non-cross-linked samples to 0.71±0.32% for those cross-linked at 20 wt/wt% zinc sulfate/nanofiber mat ratio clearly shows that. Table 4.1 demonstrates that cross-linking with $ZnSO_4$ has a stronger effect compared to aldehyde compounds. Fig. 4.5c shows the overall trends for soy protein/nylon 6 (50/50 wt/wt %) mats, in particular, in Young's modulus and maximum strain at rupture at different zinc sulfate contents.

4.2.7. Mechanical Properties of Soy Protein Nanofibers Treated Using Sodium Borohydride

Tensile tests were also conducted with soy protein/nylon 6 samples which were cross-linked using sodium borohydride. Table 4.1 demonstrates that the maximum strength for such nanofiber samples was achieved at 20 wt/wt% cross-linker/nanofiber mat ratio. As with the other types of cross-linkers, stronger nanofiber mats were less plastic. Using sodium borohydride resulted in almost 7 times stronger nanofiber mats compared to the untreated ones (cf. Table 4.1 and Fig. 4.5d).

Both zinc sulfate and sodium borohydride had the strongest effect on the soy protein nanofiber strength compared to the same formaldehyde- or glyoxal-to-nanofiber mat ratio. Therefore, stronger protein-protein interactions were achieved in nanofiber mats that were chemically treated with sodium borohydride and zinc sulfate solutions. This implies that ionic bonds formed between polymeric chains in protein structure are stronger than inter-and intra-molecular bonds formed by covalent cross-linking agents.

4.2.8. Effect of Heat Treatment on Cross-linked Soy Protein Nanofiber Mats

Cross-linked soy protein/nylon 6 nanofiber mats were heated up to 80 ^{o}C for 20 min. This was done to reveal the effect of heat treatment on the cross-linked nanofiber mats for different cross-linkers used at different contents. Fig. 4.6 shows the average Young's modulus of soy protein nanofiber samples as a function of cross-linker content for three different agents used for nanofiber treatment: formaldehyde, glyoxal, and zinc sulfate solution. In each case, the average Young's modulus of thermally-treated and untreated cross-linked samples are compared for each cross-linker's content. Fig. 4.6

shows that the average Young's modulus of the heat-treated cross-linked samples is lower compared to Young's modulus of comparable untreated samples.

It was shown in (Zhang et al., 2001; Vaz et al., 2003; Vaz et al., 2005) that heat treatment of chemically non-cross-linked proteins results in stronger inter- and intra-molecular cross-linking mostly between cystine and lysine amino acids owing to the presence of labile disulfide bond, which results in a higher Young's modulus and lower strain at rupture. This effect is, in part, due to the fact that heated samples contain less moisture. Therefore, an inevitable plasticizing effect of water is reduced due to heat treatment, and heat-treated samples reveal a higher Young's modulus and appear to be more brittle. Note also that if non-cross-linked nanofiber mats were subjected to heat treatment, nylon 6 present in the samples would soften and conglutinate nanofibers at certain locations. Such conglutination should result in an increase in strength of the heat-treated non-cross-linked nanofiber mats. However, for the chemically cross-linked samples subjected to heat treatment, the inter- and intra-protein linkages formed by covalent or chelated and ionic bonds break, and by the end of heat treatment, the broken bonds cannot restore themselves completely. For thermally broken bonds it is energetically favorable to form bonds with the nearest possible amino acids instead of the "exotic" linkages formed by the cross-linkers before the heat treatment. This results in an increased flexibility at an expense of the lowered strength in spite of conglutination of nylon-6 in the soy protein nanofiber mats as mentioned before.

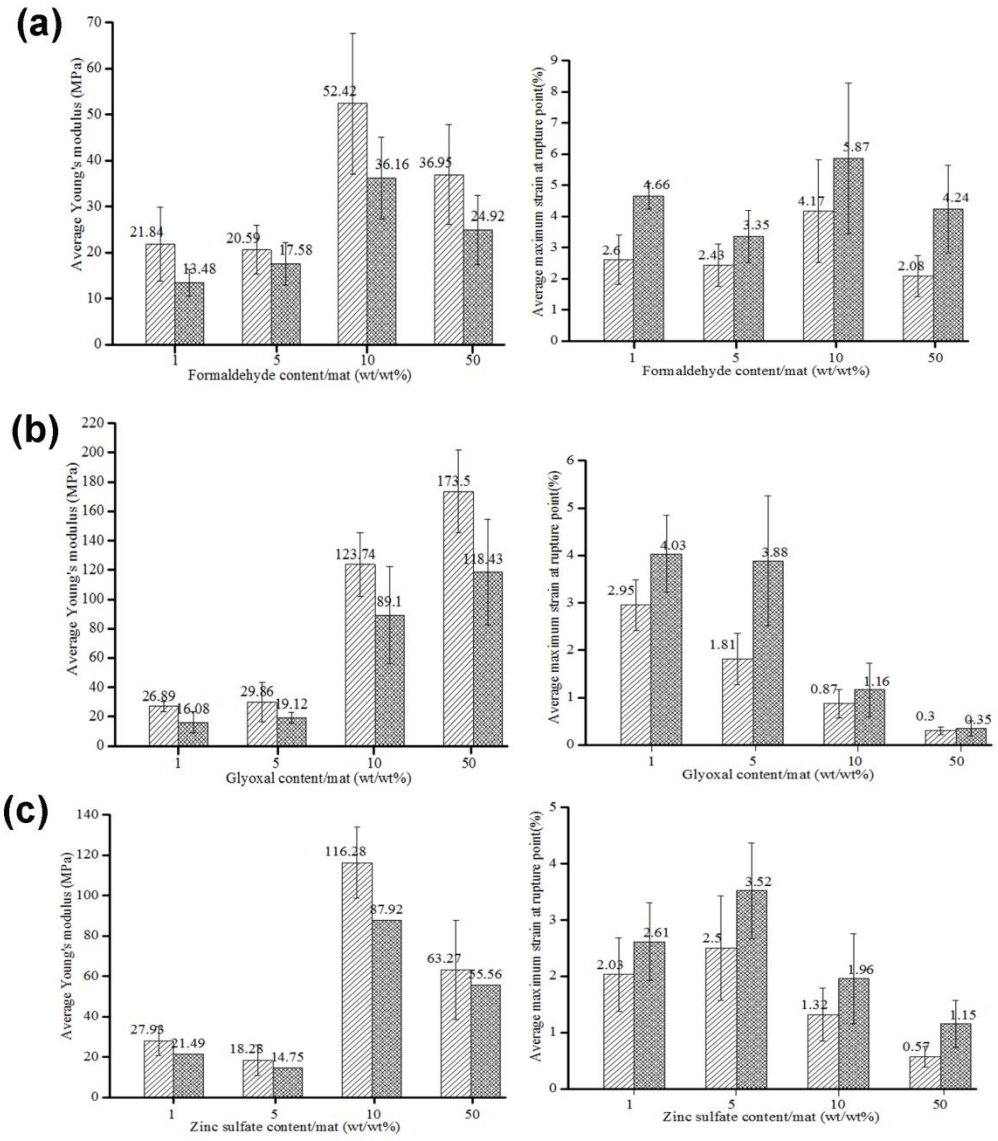

Figure 4.6. Young's modulus and the average maximum strain at rupture for both thermally-treated and untreated soy protein/nylon 6 nanofiber mats (40/60 wt/wt%) which were cross-linked using: (a) formaldehyde, (b) glyoxal, and (c) zinc sulfate solutions. Right columns correspond to the cross-linked nanofiber mats that were heat treated for 20 min at 80 °C on a glass-light left on a hotplate. Left columns illustrate the data for the cross-linked nanofiber sample which were not exposed to any heat treatment. A decrease in the average Young's modulus of heat-treated samples (right columns)

results from the fact that covalent or ionic bonds are destroyed while being heated. In panel (a), maximum brittleness for both thermally treated samples and those which did not undergo heat treatment occurred at 10 wt/wt% formaldehyde/nanofiber mat ratio. In panel (b), as glyoxal percentage in the cross-linking process increased, the sample brittleness increased, which corresponds to the diminished values of $\varepsilon_{rupture}$. However, at those glyoxal concentrations plasticizing effect of heat treatment is small. Panel (c) illustrates the results for the ionically-bonded nanofibers when zinc sulfate solution was used. As zinc sulfate content in the chelation process increases, the samples brittleness increased as well, which results in lower values of $\varepsilon_{rupture}$. Note that plasticizing effect of heat treatment is lower for higher contents of zinc sulfate.

As the amount of cross-linking agent in the cross-linking process increased, nanofiber mats in most cases became more brittle. The heat treatment of the cross-linked samples tends to diminish this effect as is seen in Fig. 4.6. As a result of heat treatment, some cross-linked sites are broken and protein chains recover their mobility, which makes nanofiber mats more plastic. A detailed comparison of the average mechanical properties of heat-treated and non-heat-treated samples which were cross-linked with different agents is presented in Table 4.2.

Table 4.2. Average mechanical properties for formaldehyde-cross-linked soy protein/nylon 6 (40/60 wt/wt %) nanofiber mats. One half of the samples were only cross-linked with formaldehyde. The other half was exposed to heating for 20 min at 80 ^{o}C on a glass-light on a hotplate after cross-linking with formaldehyde, glyoxal, zinc sulfate.

Cross-linking agent	Cross-linking ratio (wt/wt %)	Untreated samples				Thermally-treated samples			
		Average Young's modulus E (MPa)	Average yield stress Y (MPa)	Average maximum strain at rupture $\varepsilon_{rupture}$(%)	Average maximum stress at rupture $\sigma_{xx,rupture}$ (MPa)	Average Young's modulus E (MPa)	Average yield stress Y (MPa)	Average maximum strain at rupture $\varepsilon_{rupture}$(%)	Average maximum stress at rupture $\sigma_{xx,rupture}$ (MPa)
Formaldehyde	1	21.84±8.06	0.31±0.08	2.60±0.79	0.55±0.23	13.48±2.87	0.32±0.04	4.66±0.42	0.50±0.07
	5	20.59±5.28	0.30±0.07	2.43±0.68	0.39±0.07	17.58±4.63	0.33±0.04	3.35±0.84	0.42±0.07
	10	52.42±15.32	0.70±0.13	4.17±1.64	1.10±0.19	36.16±8.91	0.86±0.36	5.87±2.42	1.09±0.15
	50	36.95±10.83	0.39±0.10	2.08±0.66	0.55±0.10	24.92±7.55	0.46±0.11	4.24±1.41	0.69±0.14
Glyoxal	1	26.89±3.41	0.42±0.03	2.95±0.53	0.60±0.04	16.08±7.18	0.52±0.20	4.03±0.81	0.55±0.13
	5	29.86±13.68	0.37±0.07	1.81±0.54	0.43±0.07	19.12±3.65	0.41±0.03	3.88±1.37	0.58±0.07
	10	123.74±21.75	0.84±0.18	0.87±0.38	0.99±0.32	89.10±32.97	1.01±0.17	1.16±0.56	1.04±0.50
	50	173.50±28.12	1.50±0.05	0.30±0.08	0.67±0.21	118.43±36.17	1.17±0.33	0.35±0.16	0.54±0.22
Zinc sulfate	1	27.93±7.20	0.31±0.09	2.03±0.65	0.44±0.12	21.49±6.32	0.38±0.11	2.61±0.69	0.46±0.09
	5	18.28±7.46	0.29±0.09	2.50±0.93	0.36±0.06	14.75±4.00	0.33±0.03	3.52±0.85	0.43±0.07
	10	116.28±17.52	1.10±0.28	1.32±0.47	1.39±0.38	87.92±14.28	0.96±0.11	1.96±0.80	1.28±0.34
	50	63.27±24.46	0.32±0.09	0.57±0.18	0.36±0.13	55.56±17.00	1.39±0.48	1.15±0.42	0.61±0.23

4.2.9. Water Solubility of Soy Protein Nanofiber Mats

Following Eq. (4.1), water solubility of soy protein/nylon 6 (50/50 wt/wt%) nanofiber samples, which were modified with different cross-linking agents, was investigated. Water-solubility test data for monolithic non-cross-linked samples and those monolithic samples that were chemically bonded using various agents are reported in Table 4.3. The table also contains results for core-shell soy protein/nylon 6 nanofiber mats (without any cross-linking). It can be seen that core-shell soy protein/nylon 6

nanofiber samples revealed a significantly lower weight loss in water compared to either cross-linked or non-cross-linked samples. Since soy protein is in the core and protected by nylon 6 in the shell, such core-shell nanofibers possess an enhanced water longevity compared to all monolithic fibers (cross-linked or not). Overall, among the monolithic nanofibers, the cross-linked samples did not show a much different weight loss than the non-cross-linked samples. For comparison, in (Rhim et al., 1998) cast soy protein isolate films were left in a 50 ml beaker for 24 h at 25 °C, which resulted in 28.69±1.1% of material loss.

Table 4.3. Weight loss data for 50/50 wt/wt% soy protein/nylon 6 monolithic nanofiber mats (cross-linked and non-cross-linked) and core-shell nanofiber mats. Samples were left in water for 24 hr at room temperature.

Soy protein/nylon 6 nanofiber samples	**Average weight loss (%)**	**Soy protein/nylon 6 nanofiber samples**	**Average weight loss (%)**
Monolithic non-cross-linked	21.85	Core-shell non-cross-linked	5.28
Monolithic 5 wt/wt% glyoxal cross-linked	19.97	Monolithic 5 wt/wt% zinc sulfate cross-linked	15.48
Monolithic 10 wt/wt% glyoxal cross-linked	21.80	Monolithic 10 wt/wt% zinc sulfate cross-linked	24.60
Monolithic 20 wt/wt% glyoxal cross-linked	17.07	Monolithic 20 wt/wt% zinc sulfate cross-linked	28.29
Monolithic 5 wt/wt% formaldehyde cross-linked	17.05	Monolithic 5 wt/wt% sodium borohydride cross-linked	18.32
Monolithic 10 wt/wt% formaldehyde cross-linked	16.65	Monolithic 10 wt/wt% sodium borohydride cross-linked	17.94
Monolithic 20 wt/wt% formaldehyde cross-linked	23.65	Monolithic 20 wt/wt % sodium borohydride cross-linked	15.51

4.3. Conclusion

The experiments conducted using two covalent cross-linkers (formaldehyde and glyoxal) and two ionic cross-linkers (zinc sulfate and sodium borohydride) showed that for 20 wt/wt % formaldehyde, glyoxal, $ZnSO_4$ and $NaBH_4$ increased nanofiber mat strength almost 3-4, 5, 7 and 7 times respectively showing that ionic bonding in soy protein structure results in the highest Young's modulus compared to the aldehyde-treated fibers. Heat treatment mostly plasticizes the cross-linked nanofiber mats. In the experiments on mass loss in water, it was shown that the best longevity is achieved with core-shell nanofiber mats where soy protein is located in the core.

5. Effect of Cross-linking on Tensile Characteristics of Solution-Blown Soy Protein Nanofiber Mats: II- Thermal and Wet Cross-linking

5.1. Experimental

5.1.1. Materials

The following materials were used in the present work: protein isolate PRO-FAM 955 (SP 955) from ADM Specialty Food Ingredients, polyamide-6 (nylon-6) from BASF (M_w=65.2 KDa), formic acid grade >95%, from Sigma- Aldrich. All the materials were used as received without any further processing.

5.1.2. Solution Preparation

Soy protein/nylon 6 (40/60 wt/wt %) solution in formic acid was prepared as described in (Khansari et al., 2012). In brief, 1.0 g SPI 955 was first mixed with 9.5 g formic acid and left on a hotplate at 75 ^{o}C for 24 h for stirring. Next, 1.5 g nylon 6 was mixed with the blend and left on a hotplate at 75 ^{o}C for 24 h to homogenize properly.

5.1.3. Soy Protein/Nylon 6 (40/60 wt/wt %) Nanofiber Mat Preparation

Blend of soy protein and nylon 6 in formic acid was blown to produce soy protein/nylon 6 nanofibers with the average diameter of 300-500 nm similarly to (Khansari et al., 2012). The general description of the set-up and procedures are

discussed in (Sinha-Ray et al., 2011; Khansari et al., 2012). In this particular experiment, solution blowing was conducted as follows. A 13G needle made of stainless steel was used to supply the solution. This needle was embedded inside an annular nozzle through which air was pumped with an upstream pressure of about 2.0 bar. The solution flow rate was kept at 5 ml/h. The exposure of polymer solution at the needle exit to a high speed air jet results in stretching and flapping of the solution jet, which ultimately thins to produce a continuous nanofiber forming nonwoven laydown. A rotating drum covered with aluminum foil was used in this case in order to collect nanofibers and partially align them in the winding direction. Nanofiber alignment and collection on rotating drum was discussed in detail in (Khansari et al., 2012). Note that solution blowing was done at room temperature ($25^{o}C$) and humidity (20-30%). Collected nanofibers on the drum could be easily removed and handled for further characterization or processing. In particular, the solution blown nanofiber mat was cut into rectangular pieces with average width of about 1.0 cm and length of about 2.5 to 3.0 cm. Nanofiber mat thickness was governed by the duration of the solution-blowing experiment, i.e. roughly, by the deposition time. Our previous observations (Khansari et al., 2012) show that only about 50% of the mat thickness is comprised of soy protein/nylon 6 nanofibers. The other 50% is the cumulative gaps between the collected layers of nanofibers. This fact is accounted for when calculating the stress acting in the mat cross-section in tensile tests.

5.1.4. SEM Observation of Cross-linked Nanofiber Mats

All observations were done by Hitachi S-3000N variable-pressure SEM scanning microscope after sputter coating a 8 nm layer of Pd-Pt onto samples.

5.1.5. Tensile Tests of Soy Protein/Nylon 6 (40/60 wt/wt %) Nanofiber Mats

Tensile tests were conducted using an Instron machine (model 5942) which had capacity of 100 N on the grips. The two grips clamped the sample, with the lower grip kept at its initial position and the upper one stretching the sample with a specified cross-head speed. In the present work, soy protein/nylon 6 nanofiber samples with rectangular shape underwent tension at the stretching rate of 0.1 mm/min. The applied load and strain were recorded at small time intervals. As a result, stress-strain curves for nanofiber mat samples were obtained.

5.2. Results and Discussion

5.2.1. Thermal Bonding

In the experiments described in this section, rectangular pieces of nanofiber mats were ironed for 1 min at $55^{o}C$. As a result, a uniform pressure at elevated temperature was applied to the whole mat. The method led to partial conglutination and cross-linking of nanofibers at the intersection points. After such treatment, nanofiber mats were left at room temperature for 15 min to cool.

The rectangular samples were used in tensile tests in order to reveal their stress-strain characteristics. Fig. 5.1 compares stress-strain curves for samples of soy protein/nylon 6 (40/60 wt/wt %) nanofiber mats which underwent the bonding process described above with those which did not (taken from the same batch of samples). It is clearly seen that thermal bonding increases Young's modulus, the yield stress and tensile stress of soy-protein-containing nanofiber mats. The corresponding average data are

combined in Fig. 5.2, for Young's modulus E, the yield stress Y, and the specific strain energy $U = \int_0^{\varepsilon} \sigma_{xx} d\varepsilon$. The cumulative data for all the measured parameters is presented in Table 5.1. The average Young's modulus of non-treated nanofiber mats was found as 12.89±5.34 MPa. The nanofiber mat strength increased to 18.76±5.17 MPa when exposed to post-heat treatment under compression for only 1 min. When exposed to heat treatment, nylon 6 present in the samples softens and forms conglutination points, which result in physical crosslinking of nanofibers and an increase in the average Young's modulus. Also it was observed that samples became more brittle after heat treating. The original average maximum strain at rupture $\varepsilon_{rupture}$ for soy protein nanofiber mats was found as 8.19±1.71 %, whereas the ironing of the samples at $55\,^{o}C$ for 1 min resulted in $\varepsilon_{rupture}$ of 6.86±1.17 %.

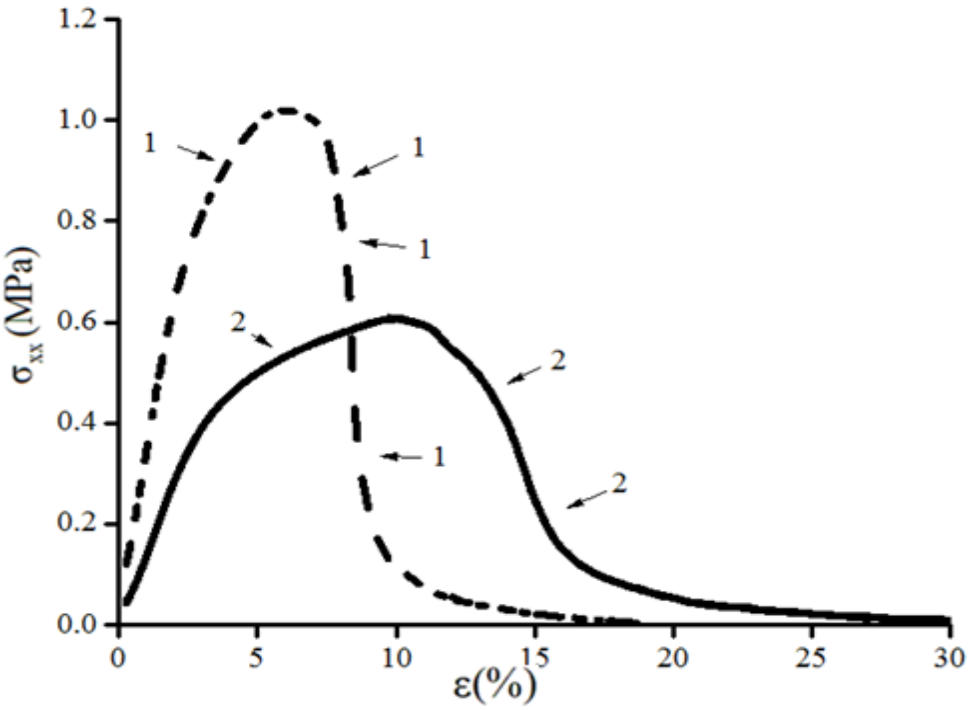

Figure 5.1. Stress-strain curves of soy protein/nylon 6 (40/60 wt/wt %) nanofiber mats for thermally bonded and non-bonded samples. Curve 1-thermally-bonded (at 55 °C under compression) nanofiber mat. Curve 2- non-bonded nanofiber mat. The normal stress in the stretching direction is denoted σ_{xx}, the tensile strain-ε (%).

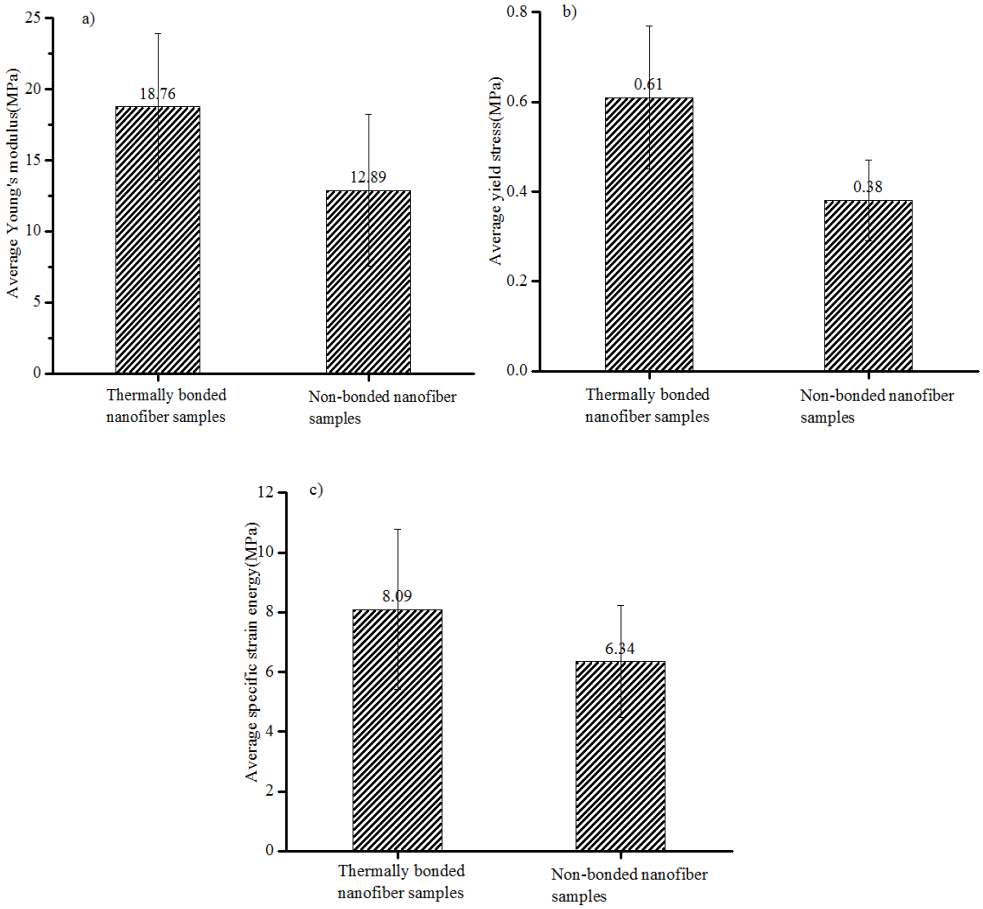

Figure 5.2. Average mechanical properties of thermally bonded soy protein/nylon 6 (40/60 wt/wt %) nanofiber mats in comparison with those of the non-bonded ones. (a) Average Young's modulus, (b) average yield stress, and (c) average specific strain energy. All these three parameters increase when nanofiber samples were exposed to heat treatment.

Table 5.1. Overall mechanical properties of thermally bonded soy protein/nylon 6 (40/60 wt/wt %) nanofibers in comparison with those of the non-bonded ones.

Sample	Average thickness of the samples (mm)	Average width of the samples (mm)	Average Young's modulus E (MPa)	Average yield stress Y (MPa)	Average specific strain energy U (MPa)	Average maximum strain at rupture $\varepsilon_{rupture}$(%)	Average maximum stress at rupture $\sigma_{xx,rupture}$ (MPa)
Thermally-bonded nanofibers	0.22	11.38	18.76±5.17	0.61±0.16	8.09±2.69	6.86±1.17	0.92±0.23
Non-bonded nanofibers	0.22	12.17	12.89±5.34	0.38±0.09	6.34±1.87	8.19±1.71	0.6±0.16

5.2.2. Wet Bonding

In this set of experiments, prior to wet bonding, nanofiber mat samples were submerged in water and immediately taken out. Then, wet samples with the dimensions of about 1 cm in width and 2.5 cm in length were compressed under the mass load of 150 g (i.e. under pressure of 6 kPa) for 24 h at room temperature until they partially dried. After removing the load, these samples were left at room temperature for another day to dry out completely. The dried samples underwent uniaxial tensile test using Instron and their stress-strain curves were measured. As a result, the effect of wet conglutination under a load was evaluated. This effect stems from the inter-fiber conglutination in the wet state at the intersection points. Indeed, soy protein isolate used in the present work is partially soluble in water. In wet state at the intersection points soy protein of different nanofibers merged and forms bonds on drying.

It was found that due to the wet conglutination and the resulting cross-linking effect, the overall mechanical properties of soy-protein-containing nanofiber mats were enhanced. Young's modulus showed an increase of about 65%, which can be attributed to

bonds formed at the wet intersection points. As a result, the specific strain energy U increased by approximately 33%. The average yield stress stayed practically unchanged. However, after wet treating nanofiber mats were also plasticized, as both soy protein isolate and nylon 6 absorb water. That is the reason that the strain at breakup does not decrease although the strength increases. Figs. 5.3, 5.4 and Table 5.2 compare the average mechanical properties of the pre-wetted and wet-conglutinated nanofibers with those of the corresponding untreated samples.

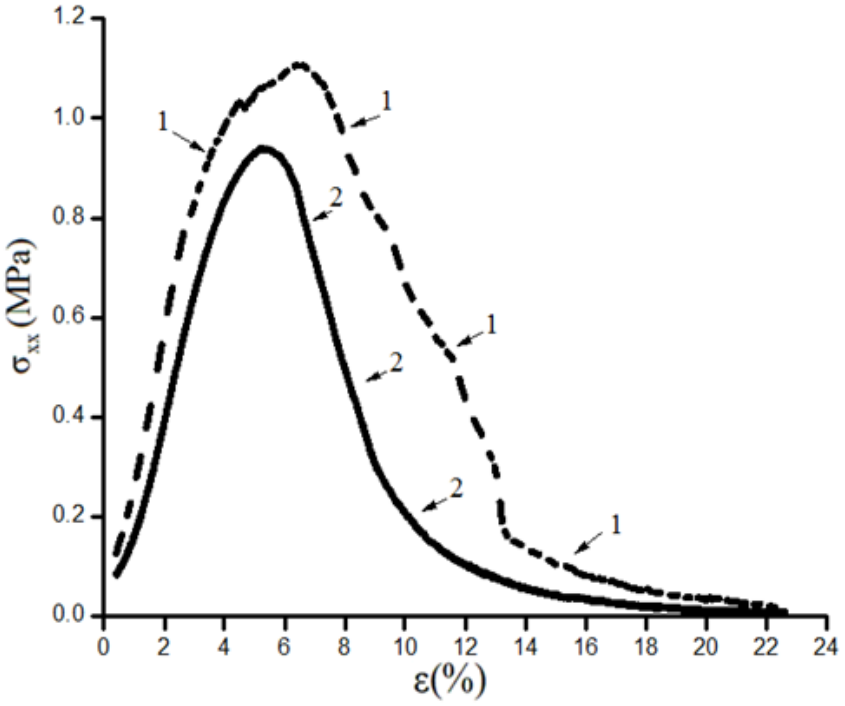

Figure 5.3. Curve 1 shows the stress-strain curve of a pre-wetted, wet-conglutinated nanofiber sample under 150 g load. The stress-strain curve of the corresponding non-treated nanofiber sample from the same batch is shown as curve 2. It can be seen that wet-conglutinated sample reveals a higher Young's modulus and specific strain energy compared to untreated one.

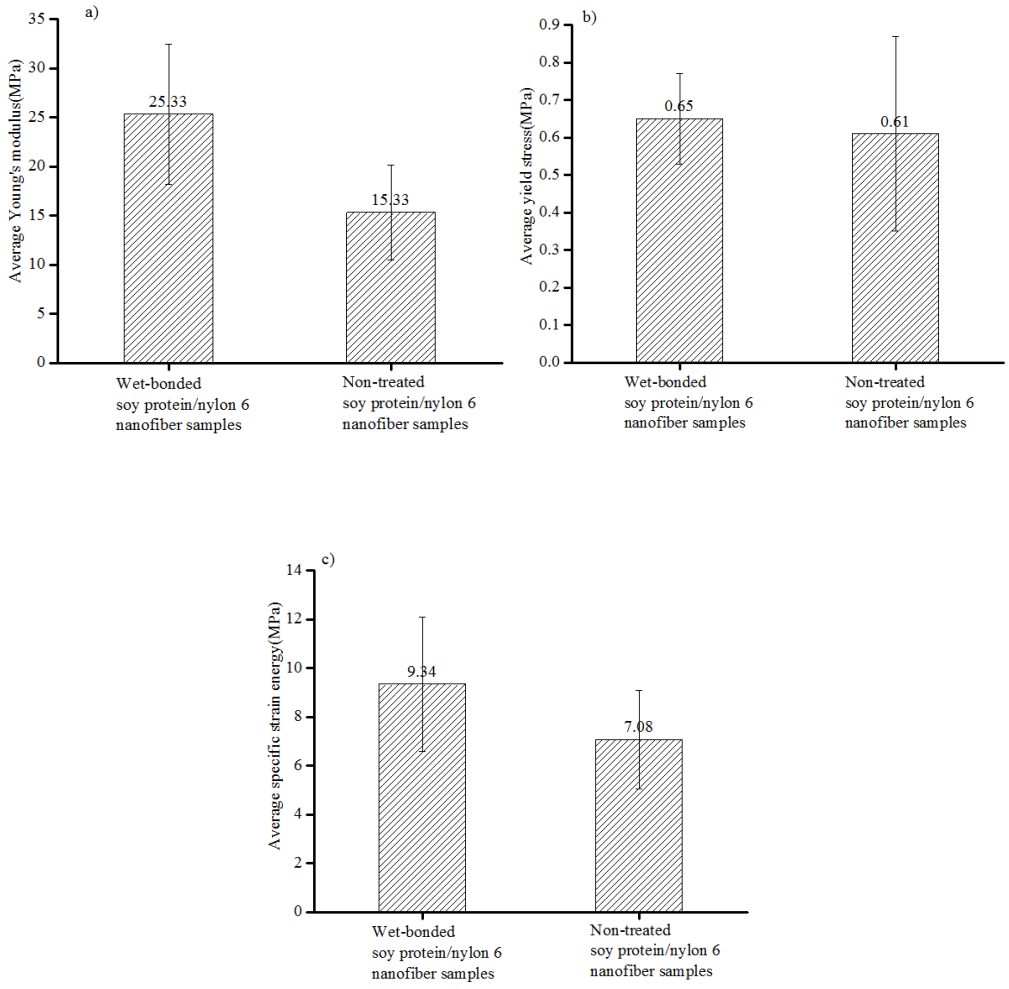

Figure 5.4. The average mechanical properties for pre-wetted, wet-conglutinated soy protein/nylon 6 (40/60 wt/wt %) nanofiber mats in comparison with the non-treated ones. Panel (a) shows the average Young's modulus, panel (b) - the average yield stress, and panel (c) - the average specific strain energy.

.

Table 5.2. Average mechanical properties of pre-wetted, wet-conglutinated soy protein/nylon 6 (40/60 wt/wt %) nanofibers in comparison with the corresponding untreated ones.

Sample	Average thickness of the samples (mm)	Average width of the samples (mm)	Average Young's modulus E (MPa)	Average yield stress Y (MPa)	Average specific strain energy U (MPa)	Average maximum strain at rupture $\varepsilon_{rupture}$(%)	Average maximum stress at rupture $\sigma_{xx,rupture}$ (MPa)
Wet-conglutinated nanofibers	0.16	9.11	25.33±7.15	0.65±0.12	9.34±2.75	7.21±1.62	1.03±0.20
Untreated nanofibers	0.18	8.99	15.33±4.81	0.61±0.26	7.08±2.02	6.31±1.41	0.76±0.20

5.2.3. Fiber Morphology after Wet Conglutination

Fig. 5.5 shows the SEM images of the soy protein/nylon 6 (40/60 wt/wt %) nanofibers after they were pre-wetted and wet-conglutinated under the load of 150 g. The images in Fig. 5.5 demonstrate that after the wet conglutination under load the individual nanofibers keep their individuality.

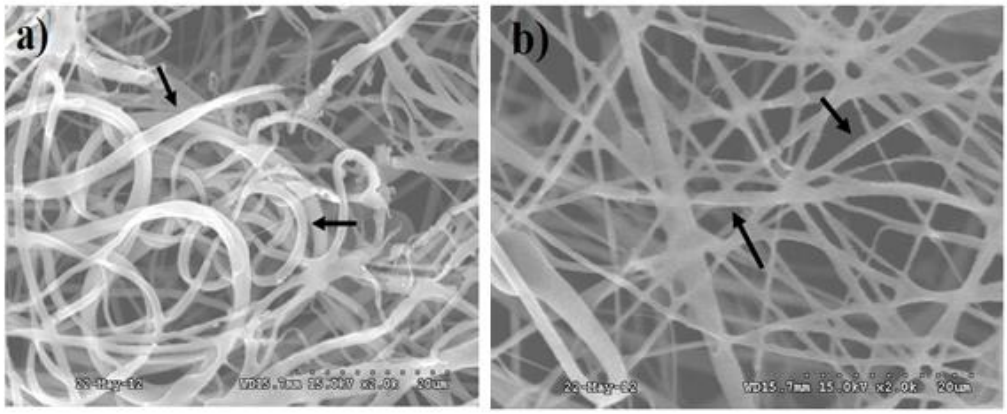

Figure 5.5. SEM secondary electron images of soy protein/nylon 6 nanofibers after pre-wetting and wet conglutination under the load of 150 g. Nanofibers kept their individuality under 6 kPa pressure (as shown by arrows).

5.2.4. Humid Aging Test

The humid aging of soy protein nanofiber mats was explored as follows. Nanofiber samples were left in water at 80 °C for 1 h. After that, the samples were extracted from water and left at room temperature for 24 h to dry out without applying any pressure. Then, the samples were used in tensile tests. This experiment reveals the mechanical properties of soy protein/nylon 6 nanofiber mats after the exposure to severe humidity conditions and elevated temperature. A typical stress-strain curve for humid-aged nanofibers after their immersion in hot water for 1 h is depicted in Fig. 5.6, where the stress-strain curve is compared with the one for the corresponding non-treated sample.

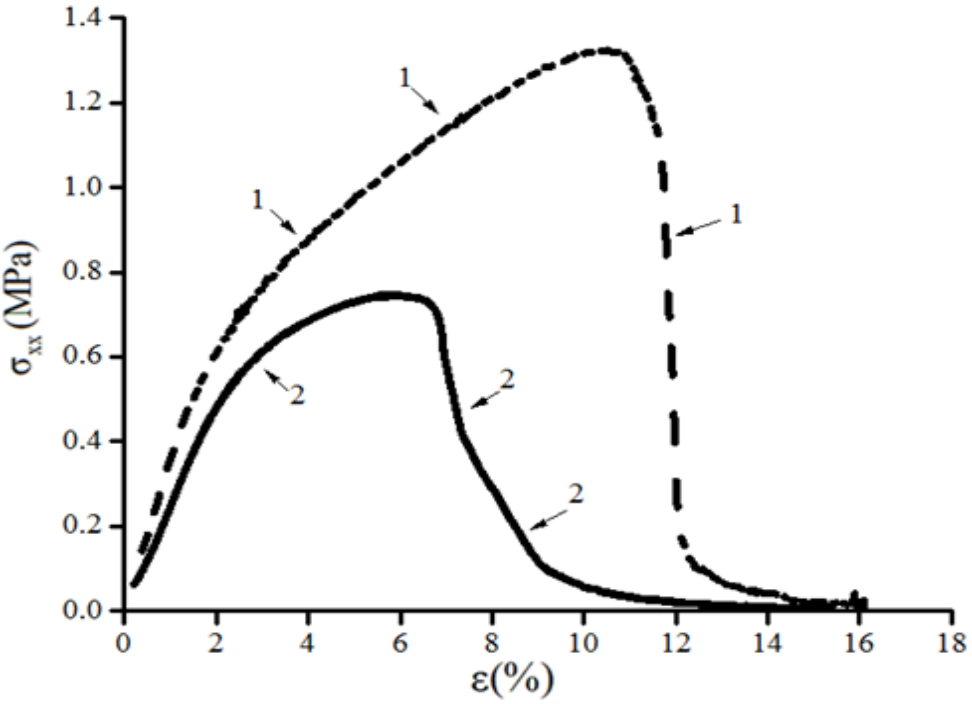

Figure 5.6. Stress-strain curve for a humid-aged (in hot water) soy protein nanofiber sample is shown as curve 1. The stress-strain curve for the corresponding untreated sample is shown as 2. Significantly higher values of Young's modulus and specific strain energy were found for the humid-aged nanofiber samples.

The results obtained for the humid-aged samples demonstrate the effect of wet aging in hot water on soy protein nanofiber mats. An increase of about 16% in Young's modulus and doubled specific strain energy were recorded. On the other hand, the yield stress practically did not change (cf. Fig. 5.7 and Table 5.3). The mechanical properties of the humid-aged nanofiber samples are compared with those for the corresponding untreated samples in Fig. 5.7. In particular, Fig. 5.7c and Table 5.3 illustrate an enhanced plasticity range of humid-aged nanofiber mats. The maximum strain at rupture ($\varepsilon_{rupture}$) is reported as 5.95±1.04 for untreated samples, whereas this parameter increased to 11.49±3.44 for nanofiber mats after the humid-aging experiment. Therefore, it is shown that while soy protein-containing nanofiber mats retained their strength under the conditions of the extreme humidity and temperature, they were also significantly plasticized compared to the original samples.

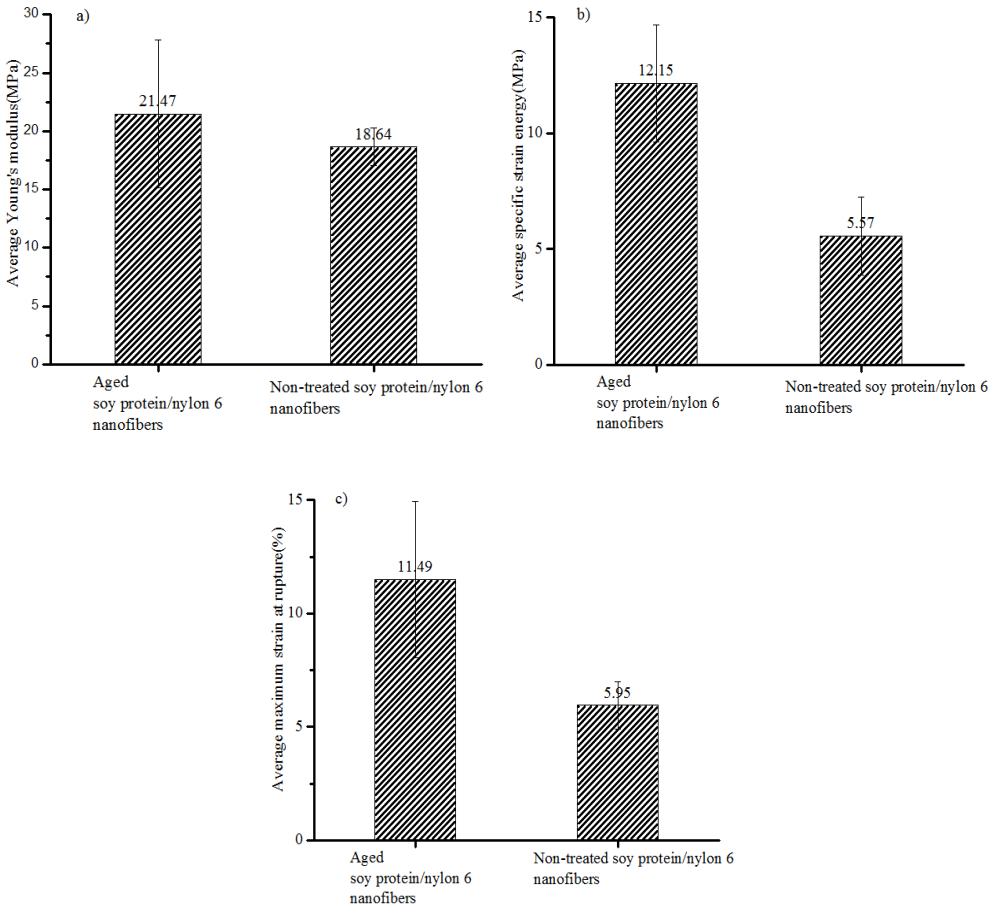

Figure 5.7. (a) Average Young's modulus, (b) average specific strain energy, and (c) average maximum strain at rupture of soy protein/nylon 6 (40/60 wt/wt %) nanofiber mats aged in hot water for 1 h compared to those of the corresponding non-treated samples.

Table 5.3. Average mechanical parameters of soy protein/nylon 6 (40/60 wt/wt %) nanofiber mats aged in hot water ($80\,^{\circ}C$) for 1 h in comparison with the corresponding untreated samples.

Sample	**Average thickness of the samples (mm)**	**Average width of the samples (mm)**	**Average Young's modulus E (MPa)**	**Average yield stress Y (MPa)**	**Average specific strain energy U (MPa)**	**Average maximum strain at rupture $\varepsilon_{rupture}$(%)**	**Average maximum stress at rupture $\sigma_{xx,rupture}$ (MPa)**
Aged nanofibers	0.18	5.06	21.47±6.34	0.44±0.18	12.15±2.52	11.49±3.44	1.09±0.21
Untreated nanofibers	0.17	10.43	18.64±1.61	0.47±0.06	5.57±1.69	5.95±1.04	0.73±0.09

5.3. Conclusion

Solution-blown soy protein/nylon 6 (40/60 wt/wt %) nanofiber mats underwent three different types of post-treatments in order to elucidate possible ways of enhancement of their mechanical properties. These post-treatments include: (i) thermal bonding, (ii) pre-wetting and wet-conglutination, and (iii) humid-aging in hot water. Thermal bonding of nanofibers under compression led to an almost 50% increase in Young's modulus, as well as a slight enhanced brittleness of the samples. Pre-wetting and wet conglutination under a 6 kPa load resulted in samples with Young's modulus of almost 65% higher than for the corresponding non-treated ones. The samples which underwent humid-aging in hot water almost retained their original properties, yet the specific strain energy increased significantly. In this case the much higher maximum strain at rupture of the humid-aged nanofiber mats is indicative of the plasticizing effect of water, and the higher specific strain energy points at a higher nylon 6 content in the aged samples due to soy protein loss at water exposure.

6. Antibacterial Activity of Solution-Blown Soy Protein Nanofiber Mats Decorated with Silver Nanoparticles and Silver Nanoparticles' Leakage in Aqueous Medium

6.1. Experimental

6.1.1. Materials

Materials used in this work are as follows. Soy protein isolate- PRO-FAM 955 (SP 955) was provided by ADM Specialty Food Ingredients. Polyamide-6 (Nylon-6) (M_w=65.2 KDa) was obtained from BASF. Formic acid (grade > 95%), silver nitrate ($AgNO_3$), and sodium borohydride ($NaBH_4$) were purchased from Sigma-Aldrich. *Escherichia coli* (Migula) Castellani and Chalmers (ATCC 25922) were obtained from the American Type Culture Collection (ATCC). Trypticase soy agar and trypticase soy broth were purchased from Cole- Parmer.

6.1.2. Soy Protein Solution Preparation

For solution blowing, 1.0 g SPI was mixed with 9.5 g formic acid and left on a hotplate at 75 °C for 24 h. Next, 1.5 g nylon 6 was mixed with this solution. The mixture was left on the hotplate for another day at the same temperature. For decorating soy protein-containing nanofibers with silver, a 1% $AgNO_3$ solution in de-ionized water was prepared. The solution was sonicated for 30 min to make it homogeneous. Also, a 1% sodium borohydride solution in de-ionized water was prepared by sonicating for 30 min.

6.1.3. Solution Blowing of Soy Protein-Containing Nanofibers

Soy protein isolate/nylon 6 blend in formic acid was solution blown as described in the previous studies (Sinha-Ray et al., 2011; Khansari et al., 2012). In brief, the solution was pumped into a 13G needle that was surrounded by an annular nozzle through which turbulent air jet was issued. The solution flow rate through the needle was kept at 5.0 ml/h during the experiment and the upstream pressure of air was set at 2.0 bar. The polymer solution jet issued from the needle was stretched and bent, and thus thinned, by the surrounding air jet. As a result, nanofibers with average diameter of 300-500 nm were produced. Solution-blown nanofibers were then collected on an aluminum rotating drum with the linear velocity of about 3.0 m/s on the drum surface.

6.1.4 SEM Observation of Silver-Coated Nanofiber Mats

Scanning electron microscopy of silver coated soy based solution blown nanofiber was done using Hitachi S-3000N variable pressure SEM. The samples were coated with 8nm of Pd-Pt before observation.

6.2. Results and Discussion

6.2.1. Silver Nanoparticle-Decorated Soy Protein-Based Nanofiber

Soy protein/nylon 6 nanofibers were decorated with silver nanoparticles as follows. Two different $AgNO_3$ solutions in water were prepared: 4 wt% (to be termed as solution A) and 1 wt% (to be termed as solution B). Collected soy protein-containing nanofibers were immersed in solutions A or B and then left at room temperature for 24 h to dry.

Sample weights were measured before and after immersion and drying. Both sets of samples revealed an increase in their weights since silver ions were deposited onto nanofiber surfaces. The average weight increase after the sample immersion in 1 and 4 wt% $AgNO_3$ solutions is listed in Table 6.1.

Table 6.1. Weight increase of soy protein nanofiber mats after immersion in $AgNO_3$ and drying.

Sample	Average weight increase (%)
Soy protein nanofibers immersed in 1 wt% $AgNO_3$	6.38±2.93
Soy protein nanofibers immersed in 4 wt% $AgNO_3$	45.15±20.60

Then, two different post-treatments of the samples were used. In the first-type of treatment nanofibers soaked in solutions A or B were subjected to a reducing agent solution (1 wt% $NaBH_4$ solution in water). This was done to reduce $AgNO_3$ to silver nanoparticles embedded in nanofibers. After the addition of $NaBH_4$ solution to the nanofibers, the samples were left at room temperature to dry out completely. The post-treated nanofibers thus obtained will be denoted as Ar and Br. The adding of the reducing agent resulted in an additional increase in the sample weight accompanying formation of silver nanoparticles on the nanofiber surfaces, as illustrated in Table 6.2. For control, samples of soy protein nanofiber mats from the same batch which did not undergo treatment with $AgNO_3$ were also immersed in 1 wt% aqueous solution of sodium borohydride solution ($NaBH_4$) and it was found that their weight also increased as shown

in Table 6.2. These results demonstrate that formation of silver nanoparticles is accompanied by deposition of some other materials at the nanofiber surfaces.

Table 6.2. Sample weight after the immersion in 1 wt% $NaBH_4$ solution and drying.

Sample	**Average weight increase after adding reducing agent (%)**
Soy protein nanofibers not decorated with silver	30.43±4.31
1 wt% $AgNO_3$-treated soy protein nanofibers	121.21±29.15
4 wt% $AgNO_3$-treated soy protein nanofibers	115.61±41.51

As the second post-treatment the nanofibers soaked in solution A were heat-treated at a temperature of 120 °C to thermally decompose $AgNO_3$ to the embedded silver nanoparticles. These post-treated samples are denoted as Ah. The SEM images of these three different types of samples obtained using variable pressure Hitachi S-3000N are shown in Fig. 6.1. In particular, Fig. 6.1a shows the SEM image of sample Ar, Fig. 6.4b - sample Br, and Fig. 6.1c - sample Ah. It is seen that sample Ar is completely covered with silver nanoparticles, whereas for sample Br the coverage with silver nanoparticles is less than that of sample Ar. This can be attributed to the fact that sample Ar was prepared using solution A with higher concentration of $AgNO_3$. Fig. 6.1c shows that sample Ah is

covered with silver films rather than silver nanoparticles which cover samples Ar and Br. Note that these differences were also evident from visual observations as a different sample color. Namely, sample Ar was dark brown, sample Br was light brown, and sample Ah was dark yellow.

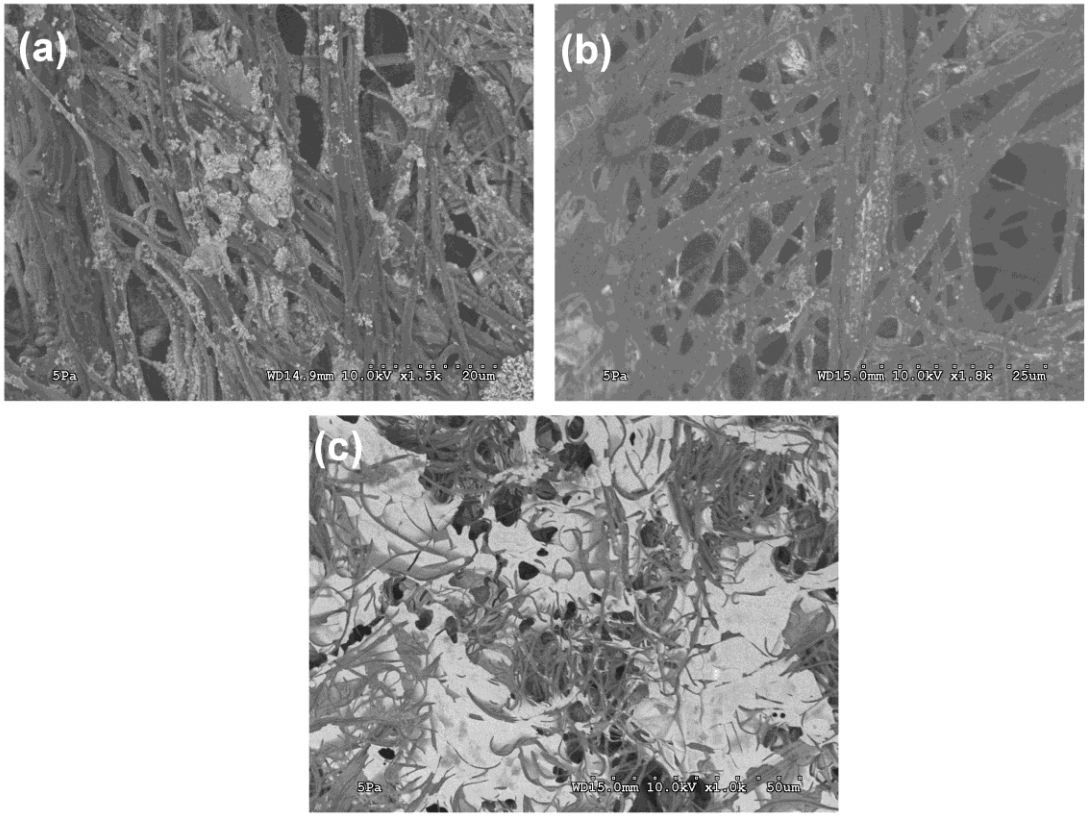

Figure 6.1. SEM backscattered electron images collected under low vacuum (5Pa) conditions for samples of (a) Ar, (b) Br and (c) Ah. It is seen that samples Ar and Br are coated with the embedded silver nanoparticles and their clusters, whereas sample Ah is covered with silver films (silver is visible as light spots in the images). The comparison of panels (a) and (b) shows that the coverage of sample Ar with silver nanoparticles is larger than the coverage of sample Br.

6.2.2. Silver Nanoparticles' Leakage in Aqueous Medium

In order to evaluate silver leaching from soy protein nanofiber mats, samples which were treated with sodium borohydride solution and decorated with silver nanoparticles were immersed in 10 ml of de-ionized water for 24 h. Then they were extracted and left for drying. The control samples without silver nanoparticles but dipped into sodium borohydride solution underwent a similar immersion in water for 24 h and drying. The weight loss of all these samples is listed in Table 6.3.

Table 6.3. Weight loss after immersion in water for 24 h.

sample	**Average weight loss (%)**
Soy protein nanofibers not decorated with silver	34.99±6.52
1 wt% $AgNO_3$-treated soy protein nanofibers	41.72±5.77
4 wt% $AgNO_3$ -treated soy protein nanofibers	40.33±9.74

The difference in the weight loss between silver-decorated and non-decorated nanofibers could be attributed to silver leaching. However, the difference does not exceed the statistical variance, which leads to the conclusion that no measurable silver was detected.

6.3. Conclusion

In this work solution-blown soy protein-based nanofibers were coated with silver nanoparticles. Samples' weight increase after silver coating was also demonstrated. In addition, silver nanoparticles' leakage in aqueous medium was studied. Possible silver leaching was tested, and no reliable evidence of it was found in 24 h. Nanofibers prepared in this work are biocompatible, which allows using them in bandages for wound healing.

7. Protein Tracing in Soy Protein/Nylon 6 Nanofiber Mats Using Coomassie Brilliant Blue G250

7.1. Experimental

7.1.1. Materials

Soy protein isolate [PRO-FAM 781 (SP 781)] was provided by ADM Specialty Food Ingredients. Hydrochloric acid (37 % A.C.S. Reagent), N,N-Dimethylforamide anhydrous 99.8%, poly(ethylene terephthalate) granular and Brilliant Blue G250 were purchased from Sigma-Aldrich. In addition, Poly(acrylonitrile) with average MW=150 kDa was purchased from Polysciences. Inc. All materials were used as received.

7.1.2. Preparation of Dye Solution

Solution of 0.05 wt% Brilliant Blue G-250 was prepared in 10 ml de-ionized water. Then, 2 ml of HCl was added to form highly acidic solution. Final dye concentration was reduced to 0.04% in the acidic condition. The final solution had brownish color. Fig 7.1 shows acidic solution with brownish tint.

Figure 7.1. Coomassie Brilliant Blue G250 acidic solution.

7.1.3. Production of Dye-Protein Complex

Cationic solution of CBB in water and hydrochloric acid was added on top of nanofiber mats which were produced and collected as described in Chapter 3 and (Sinha-Ray et al., 2011; Khansari et al., 2012). Then, the samples were left at room temperature for the dye-protein complex to develop. Protein binding procedure with CCB is fast and occurs in less than two minutes as reported in (Bradford, 1976). The complex is stable until 1 h after formation.

7.2. Experimental Results & Discussion

The Bradford assay's principle is based on formation of complex of Brilliant Blue G250 with protein structure. When protein is added to 'Coomassie Brilliant Blue' solution at low pH level, the dye binds with protein macromolecules and forms dye-protein complex that reveals blue color. This leads to reduction in the number of free ionic forms of the dye in the solution. Blue dye complex has an absorbance wavelength of 595 nm which is used to estimate the amount of protein available in the sample.

It was reported in (Compton, 1985) that CCB at elevated pH levels (above 2) reveals blue color which is due to anionic structure of dye molecules. At pH range of around 1, the greenish color dominates CCB solution in which dye molecules are neutral. Further lowering of pH results in overall positive charge of CCB molecules that brings about red color to be predominant in the solution, with maximum absorbance wavelength of 470 nm. Resonance forms of free ionic CCB are shown in Fig. 7.2 as stated in (Compton, 1985).

Among protein amino acids, arginin which has guanidyl group plays the major role in forming dye-protein complex via electrostatic interactions between NH_3^+ with sulfonic groups of the dye. Anionic form of the dye is not freely present, yet negatively-charged ion resonance is the stable form while interacting with protein.

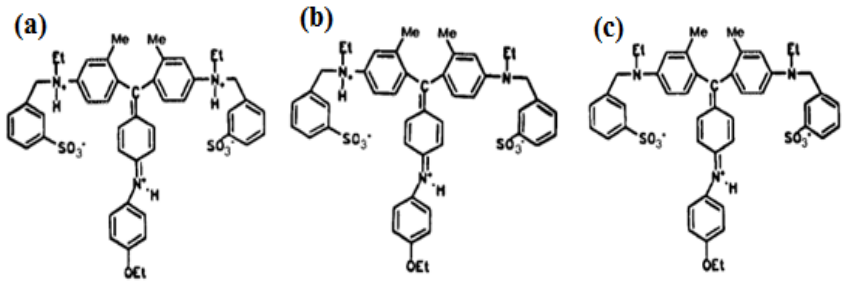

Figure 7.2. Resonance forms of CBB dye. Panel (a) shows red form of the dye where overall charge of the molecule is positive. Zero-charged molecule in panel (b) is indicative of green color, and panel (c) is anionic dye with blue color. (Compton, 1985).

Following the experimental procedure described above, soy protein-based nanofiber mats were stained with CBB acidic solution. Consequently, red solution immediately converted into blue color, which evidently demonstrates presence of soy protein nanofibers as shown in Figs. 7.3. Solution-blown PET nanofiber mat underwent the same staining procedure and the result is illustrated in Fig. 7.4. Red CBB solution was kept intact while being deposited on top of PET nanofibers since there are no protein macromolecules in PET structure.

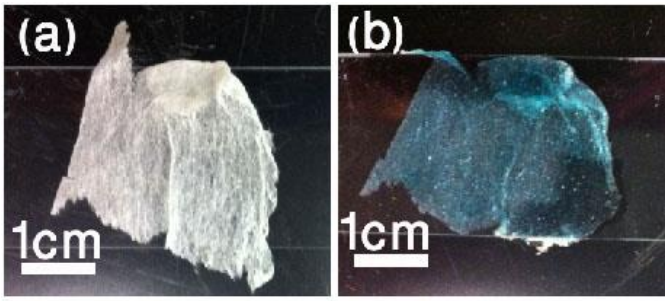

Figure 7.3. Soy protein/nylon 6 (50/50 wt/wt %) nanofiber mats, immersed in acidic CBB solution and left at room temperature. Protein-dye complex which results in anionic form of CBB revealed high-intensity blue color.

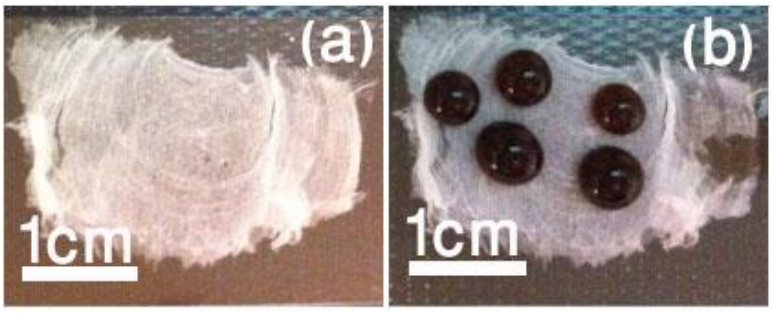

Figure 7.4. Panel (a) shows pure PET nanofiber mat, whereas panel (b) demonstrates acidic CBB solution on top of PET nanofibers. No interaction occurred and the acidic dye solution kept its red color.

The same experiment was conducted on solution-blown soy protein/PAN nanofibers. Blowing soy protein/PAN in DMF solution resulted in beaded PAN nanofibers in which soy protein was deposited on top of nanofibers' surface. Protein tracing in soy protein/PAN nanofiber mat is shown in Fig. 7.5. Red CBB solution turned

in blue only where it was exposed to soy protein as a result of dye-protein complex formation.

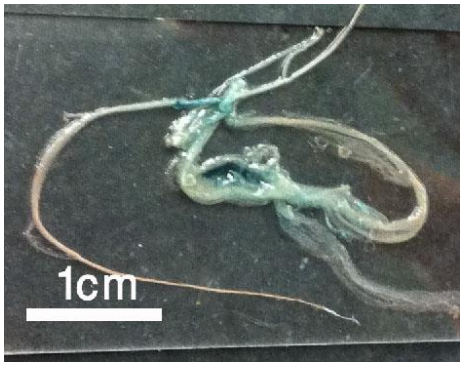

Figure 7.5. Protein staining in soy protein/PAN nanofibers. Due to protein exposure, dye acidic solution turned in blue, while red color remained intact where soy protein was not present.

7.3. Optical Observation of Stained Nanofibers

Solution-blown soy protein/PAN nanofibers are shown in Fig. 7.6.

Figure 7.6. Solution blown soy protein/PAN nanofibers. Soy protein is entrained into PAN nanofibers in the form of beads comprised of the protein molecules.

Using optical microscope Olympus BX-51, images of protein stained with CBB solution are shown in Fig. 7.7 for soy protein/PAN nanofibers. It is clearly seen in Fig. 7.7 that protein beads have turned into blue color due to the dye-protein complex, whereas the remainder stayed intact.

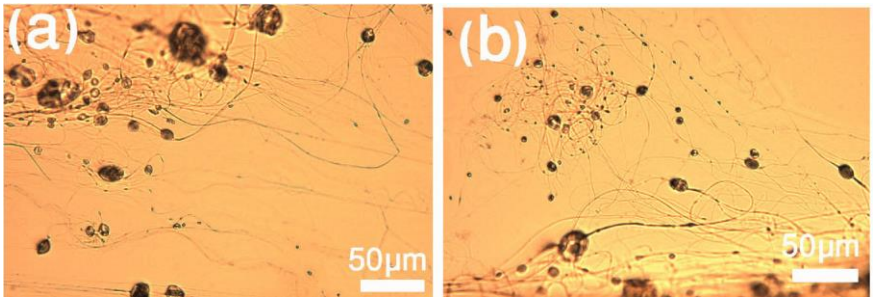

Figure 7.7. PAN nanofibers in which soy protein beads are entrapped into the solution-blown PAN matrix. Soy protein beads have formed electrostatic bonds with CBB molecules and acquired blue color.

7.4. Conclusion

Using modified Bradford test, soy protein was traced in monolithic soy protein/nylon 6 (50/50 wt/wt %) nanofibers. Due to the binding of CCB molecules with proteins, complexes were formed and pH of the solution changed drastically. Acidic solution that had red color was turned in alkali due to complex formation. Higher pH solution revealed blue color which was a clear indication of protein presence inside nanofiber samples.

8. Two-stage Desorption-controlled Release of Fluorescent Dye and Vitamin from Solution-Blown and Electrospun Nanofiber Mats Containing Porogens

8.1. Experimental

8.1.1. Materials

Protein isolate PRO-FAM 955 (SP 955) was received from ADM Specialty Food Ingredients. Polyamide 6 (nylon 6) (M_w=65.2 kDa) was supplied by BASF. Formic acid grade >95%, trifluoroacetic acid, TFA (ReagentPlus 99%), chloroform anhydrous ≥99%, poly(ethylene glycol) with the average molecular weight of 3400 Da, riboflavin ≥98% and Rhodamine B fluorescent dye were purchased from Sigma-Aldrich. Also poly(ethylene oxide) (PEO) with three different average molecular weights (200, 400, and 600 kDa) was purchased from Sigma-Aldrich. Poly(vinyl alcohol), 88 mol% hydrolyzed ,~78 kDa was supplied by Polysciences, Inc. Polyethylene terephthalate (PET) granular was provided by NC State University. All products were utilized without any post-processing and further treatment.

8.1.2. Solution Preparation

As in (Khansari et al., 2012), blend of soy protein/nylon 6 (50/50 wt/wt%) was prepared, with 1.5 g of SP 955 being mixed with 9.5 g of formic acid and stirred on a hotplate at 75 °C for 24 h. After that, 1.5 g of nylon 6 was added to this solution and

stirred on the hotplate for another 24 h at the same temperature. Then, 0.03 g of Rhodamine B was added to the prepared blend, and the vial containing the solution was wrapped with aluminum foil completely in order to prevent its exposure to light. Soy protein/nylon 6 solution containing Rhodamine B was sonicated for 30 min in order to mix the dye in the solution completely.

Also, two blends of soy protein/nylon 6 (50/50 wt/wt %) were produced as described above, and PEG was added to both of them. PEG content was 5 wt/wt % PEG/soy protein and nylon 6 in one blend and 10 wt/wt % PEG/soy protein and nylon 6 in the other one. After adding PEG, the samples were left on the hotplate for 30 more minutes under stirring to mix completely. The last step was to cover the vials with aluminum foil and add 0.03 g of Rhodamine B to each solution. The samples were then sonicated for 30 min to form a homogeneous solution.

Solution of nylon 6 in formic acid was prepared as follows. 2.0 g of nylon 6 was added to 10.0 g of formic acid and left on the hotplate at $75^{o}C$ for a day. After that 0.02 g of Rhodamine B was added to this solution and sonicated for half an hour.

In order to produce core-shell nanofibers, the core and shell solutions were prepared as follows. The core solution consisted of 1.3 g of SP 955 mixed with 8.7 g of formic acid for 24 h at $75^{o}C$. Then, 1.0 g of nylon 6 was mixed with this blend. Finally, 0.023 g of Rhodamine B was added to the core solution and the vial was wrapped with aluminum foil to prevent light exposure. The shell solution was a blend of 20 wt% nylon 6 in formic acid with no Rhodamine B added. In order to examine the effect of PEG as the leachable polymer (porogen) on the drug release kinetics from core/shell nanofibers, two additional shell solutions were prepared. Namely, 20 wt% nylon 6 solution in formic acid was used

as a base. Then, 5 wt % PEG/nylon 6 and 10 wt % PEG/nylon 6 were prepared from it and left on the hotplate at 75 °C for 30 min to mix completely. Note that these two latter solutions were used as a nanofiber PEG-containing shell, whereas the core solutions were prepared as described above.

Also, a solution of soy protein with poly(vinyl alcohol) (PVA) was prepared, with the SP/PVA ratio being 50/50 wt/wt %. First, 0.8 g of soy protein was mixed with 9.5 g of formic acid for a day at 75 °C. Then, 0.8 g of PVA was added to the solution and kept under stirring for another day. After that, 0.04 g of Rhodamine B was finally added to the solution. The blend of SP/PVA with Rhodamine B was left under stirring for 30 min at room temperature fully protected from light.

Solution of 15 wt% PET was prepared by mixing 1.5 g PET with 8.5 g of solvent consisting of 50 wt% TFA and 50 wt% chloroform. The solution was kept at 55 °C on the hotplate for 4 h. Then 0.03 g of Rhodamine B was added to the homogenous solution and sonicated for 30 min to mix properly.

In order to prepare PET/PEG solution, 15 wt% PET solution in TFA/chloroform was prepared as explained above. Next, 0.15 g of PEG was added, and the solution was mixed for 30 min using magnetic stirring at 55 °C on the hotplate. Finally, 0.03 g of Rhodamine B was added and sonicated for half an hour.

Solution of PET/PEG/PEO was prepared by adding 0.15 g PEO to the above-mentioned PET/PEG solution and mixing on the hotplate for 1 h at 55 °C. Three different solutions of this type were prepared with various molecular weights of PEO (i.e. 200, 400, and 600 kDa). In this case, PEG and PEO are used as two different leachable

polymers (porogens). At the end, 0.03 g Rhodamine B was mixed with each solution and left to sonicate for 30 min.

In order to prepare riboflavin-containing solutions, PET-based solutions were prepared as explained above. In each case, instead of Rhodamine B, 0.03 g of riboflavin was mixed and sonicated for 30 min. Note that all the Rhodamine B- and riboflavin-containing solutions were wrapped with aluminum foil to prevent light exposure.

8.1.3. Solution Blowing

Solution blowing was used to produce nanofibers from the above-mentioned solutions, following (Sinha Ray et al., 2010a; Sinha Ray 2011; Khansari et al., 2012). A 13G needle made of stainless steel was used to issue a solution when monolithic nanofibers were formed. At the end of the needle, the solution was entrained by the co-axial high-speed air jet with an upstream pressure of about 30 psi. The solution flow rate was kept at 4.0 ml/h. As a result, a solution jet was formed and stretched and underwent stretching and bending instability due to the air jet surrounding the needle. Consequently, continuous monolithic nanofibers were produced. To form core-shell nanofibers, the core solution was issued through a 18G stainless steel needle, while the shell solution was supplied through a 13G needle, both at 3 ml/h flow rate. The 18G needle issuing the core solution was located co-axially inside the needle which was delivering the shell solution. The core-shell polymer jet was entrained by a co-axial high-speed air stream similarly to forming monolithic fibers. As a result, the core containing soy protein was encapsulated by nylon 6 shell, and core-shell nanofibers were formed. Both monolithic and core-shell nanofibers were produced at room temperature and humidity. They were collected under

reduced light in order to diminish light exposure of dye-containing nanofibers and kept in an enclosure totally protected from light. Nanofibers were collected on a rotating drum covered with an aluminum foil which was kept at a distance of 15-19 cm below the needle.

The collected Rhodamine B-containing monolithic nylon 6 nanofibers are denoted as sample A, monolithic SP/nylon 6 (50/50 wt/wt %) nanofibers- sample B, monolithic SP/PVA (50/50 wt/wt %) - sample C, monolithic SP/nylon 6 (50/50 wt/wt %)+5 wt% PEG nanofibers - sample D, monolithic SP/nylon 6+10 wt% PEG nanofibers - sample E, core/shell SP/nylon 6 nanofibers - sample F, core/shell SP/nylon 6+5 wt% PEG nanofibers - sample G, and core/shell SP/nylon 6+10 wt% PEG nanofibers - sample H. Several representative images of the collected nanofibers containing Rhodamine B are shown in Fig 8.1.

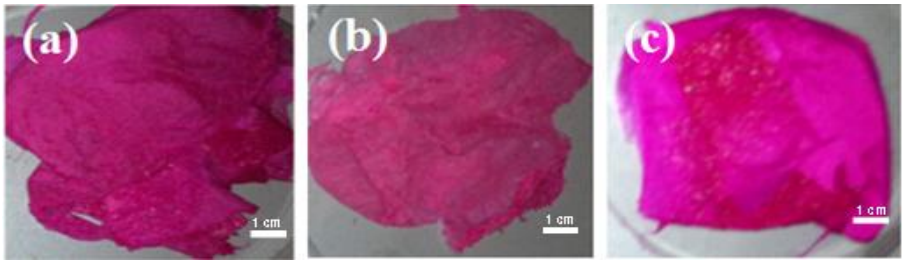

Figure 8.1. Rhodamine B-containing nanofiber mats. Panel (a)- monolithic soy protein/nylon 6 (50/50 wt/wt %) with 1 wt % Rhodamine B. Panel (b)- core/shell soy protein-containing nanofiber mat with 1 wt% dye premixed with the solution and blown into the fiber core. Some dye diffused from the core to the shell when both were still liquid, which explains the pink color of the mat. Panel (c) shows monolithic soy protein/PVA (50/50 wt/wt %) nanofibers with 2.5 wt% Rhodamine B.

8.1.4. Electrospinning

For electrospinning of PET-based solutions, the electric potential difference of 15 kV was applied between the liquid drop at the needle exit and the grounded rotating disc collector. The polymer solution was electrospun from a plastic syringe with an internal diameter of about 25G at the flow rate of 1 mL/h. The fiber mats were collected in darkness to protect the fluorescent materials in the nanofiber mats from degradation. An image of the electrospun PET-based nanofiber mat loaded with Rhodamine B is shown in Fig. 8.2a, and the image of the mat loaded with riboflavin is shown in Fig. 8.2b. For the sake of brevity, the nanofiber mats formed from PET, PET/PEG, PET/PEG/PEO (200 kDa), PET/PEG/PEO (400 kDa) and PET/PEG/PEO (600 kDa) loaded with Rhodamine B are denoted as I1, J1, K1, L1 and M1, respectively. Similarly, nanofiber mats formed from PET, PET/PEG, PET/PEG/PEO (200 kDa), PET/PEG/PEO (400 kDa) and PET/PEG/PEO (600 kDa) loaded with riboflavin are denoted as I2, J2, K2, L2 and M2, respectively.

Figure 8.2. (a) Rhodamine B-containing nanofiber mats I1, J1, K1, L1, and EM1 (from left to right, respectively). (b) Riboflavin- containing nanofiber mats I2, J2, K2, L2, and M2 (from left to right, respectively).

8.1.5. Release Experiments

All nanofiber mats with the embedded Rhodamine B fluorescent dye were cut into rectangular pieces weighing 5-10 mg and put into a glass vial with 5 ml of deionized water inside. The vial was wrapped with aluminum foil to prevent any light exposure of the samples due to sensitivity of the dye to light. In these experiments, dye was released from nanofibers into water, and fluorescence intensity of water was measured periodically to measure the released amount of dye. To do that, 200 µl samples of water with the released dye were periodically extracted from the vial and delivered into a well inside a 96-well micro plate. Four wells were filled with the 200 µl samples simultaneously, and the fluorescence intensity of the dye present in water was measured

using Gemini SpectraMax spectrofluorometer (Molecular Devices) with the excitation wavelength of 553 nm and emission wavelength of 627 nm appropriate for Rhodamine B.

Riboflavin-containing nanofiber mats underwent the release experiments according to the same protocol as described above for Rhodamine B. The only difference was the excitation wavelength of 268 nm and the emission wavelength of 373 nm appropriate for riboflavin.

The average fluorescence intensity corresponding to the four wells was reported as the fluorescence intensity of Rhodamine B or riboflavin released during a certain time. Then, water in the vial was completely replenished. This process was periodically repeated in specified time intervals. The fluorescence intensity is proportional to the released mass in the water sample. Therefore, it was possible to record the mass of released fluorescent material (Rhodamine B or riboflavin) during a certain time interval, and as a result, to measure the cumulative mass released as a function of time. For each type of samples, release experiments were repeated 3 times with nanofiber mat samples cut from the same batch. All the release experiments were conducted at room temperature.

8.1.6. Optical Observations

Scanning electron microscopy (SEM) observations for solution-blown samples were done using Hitachi S-3000N variable pressure SEM. Samples were sputter coated with Pd/Pt up to 10 nm thickness prior to scanning microscopy The as-spun and immersed samples were observed. For electrospun samples, surface morphologies of the nanofibers were observed using Carl Zeiss Evo 40).

8.2. Experimental Results & Discussion

8.2.1. Effect of Immersion of Soy Protein-Based Nanofiber Mats in Water

Weight loss analysis was conducted for the dye-containing soy protein-based nanofiber samples which were immersed in water bath periodically during the dye release experiments. According to (Sinha-Ray et al., 2012), soy protein-based nanofiber mats tend to lose weight in contact with water. Also, for PEG-containing fibers leaching of the porogen (PEG) into water was desired. Note that such host polymer as PVA is also expected to be dissolved in water. After the release process reached its final saturation, the mass loss of the samples was quantified as

$$L=\left(1-\frac{W_2}{W_1}\right)100\% \qquad (8.1)$$

where W_1 is the sample weight before the immersion in water, and W_2 is the sample weight after the completion of the release process and full dry out.

The values of L are reported in Table 8.1 for all the Rhodamine B-containing samples that underwent the release process excluding the pure nylon 6 samples. Since nylon 6 is not soluble in water, almost no weight loss was observed in its samples.

Table 8.1. Average weight loss of the soy protein-based nanofiber samples loaded with Rhodamine B.

Sample	Average weight loss (%)	Sample	Average weight loss (%)
soy protein/nylon 6 50/50 wt/wt %, monolithic nanofibers	11.56±4.41	soy protein core/shell nanofobers	6.41±2.06
soy protein/nylon6+ 5 wt % PEG, monolithic nanofibers	22.00±3.58	soy protein core/shell +5 wt % PEG in shell nanofibers	13.29±2.41
soy protein/nylon 6+ 10 wt% PEG, monolithic nanofibers	35.6±6.39	soy protein core/shell +10 wt % PEG in shell nanofibers	14.47±1.94
soy protein/PVA 50/50 wt/wt % monolithic nanofibers	68.62±9.34		

Table 8.1 shows that the core-shell Rhodamine B-containing samples had the lowest value of the material loss, as the water soluble soy protein in the core was partially sheltered by water-insoluble nylon 6 in the shell. Table 8.1 also shows that PEG-containing samples revealed higher weight loss compared to the monolithic soy protein/nylon 6 nanofibers, which stems from the high solubility of PEG in water. Soy protein/PVA nanofiber mats had the highest weight loss due to high water solubility of PVA in addition to that of soy protein.

SEM images of the nanofiber samples A, B, C, E, F and H before and after the immersion in water are shown in Figs. 8.3a-f, respectively. The images show that the general morphology of the nanofibers does not change after the immersion in water, except for sample C. Fig. 8.3(c2) shows that after the immersion in water, the nanofiber mat C lost its fibrillar structure and turned into an almost solid block, which resulted from

a partial dissolution of the constituent materials (soy protein and PVA). No images for samples D and G before and after the immersion are shown in Fig. 8.3 because they contained the same materials as in the samples E and H, respectively, as well as a larger content of PEG. Therefore, it might be expected that changes in the general morphology of the samples D and G after the immersion in water would be less pronounced than those of the samples E and H in Fig. 8.3.

SEM images of the samples I2, J2, K2, L2 and M2 are shown in Figs. 8.4a-e, respectively. It can be seen that these fibers are larger in comparison to those in Fig. 8.3. For the sake of brevity, SEM images of the samples I1-M1 are not shown.

SEM images of samples I1 (containing Rhodamine B) and I2 (containing riboflavin) after the immersion in water are shown in Fig. 8.5. It is seen that even after the immersion in water there is no visible morphological changes in the sample I1 (Fig. 8.5a) and the fibers stay smooth. On the other hand, there are visible striations on the fibers in sample I2 (Fig. 8.5b). The reason for the appearance of the striations is the following. Since riboflavin is partially soluble in the solvent used to form nanofibers, the blended riboflavin forms striations in the fibers unlike Rhodamine B, which is readily soluble in the solvent. The release of riboflavin makes micro-cracks at the location of the striations, which makes them even more visible as shown in Fig. 8.5b. The presence of the striations also affects the riboflavin release profile as will be shown later. Similar striations were observed in the riboflavin-loaded samples J2-M2. However, the visibility of the striations can be blurred due to the presence of porogens in the nanofibers. For the sake of brevity they are not shown. It is emphasized that in the samples without riboflavin (A, B, C, E, F, H, I1-M1) no striations were observed.

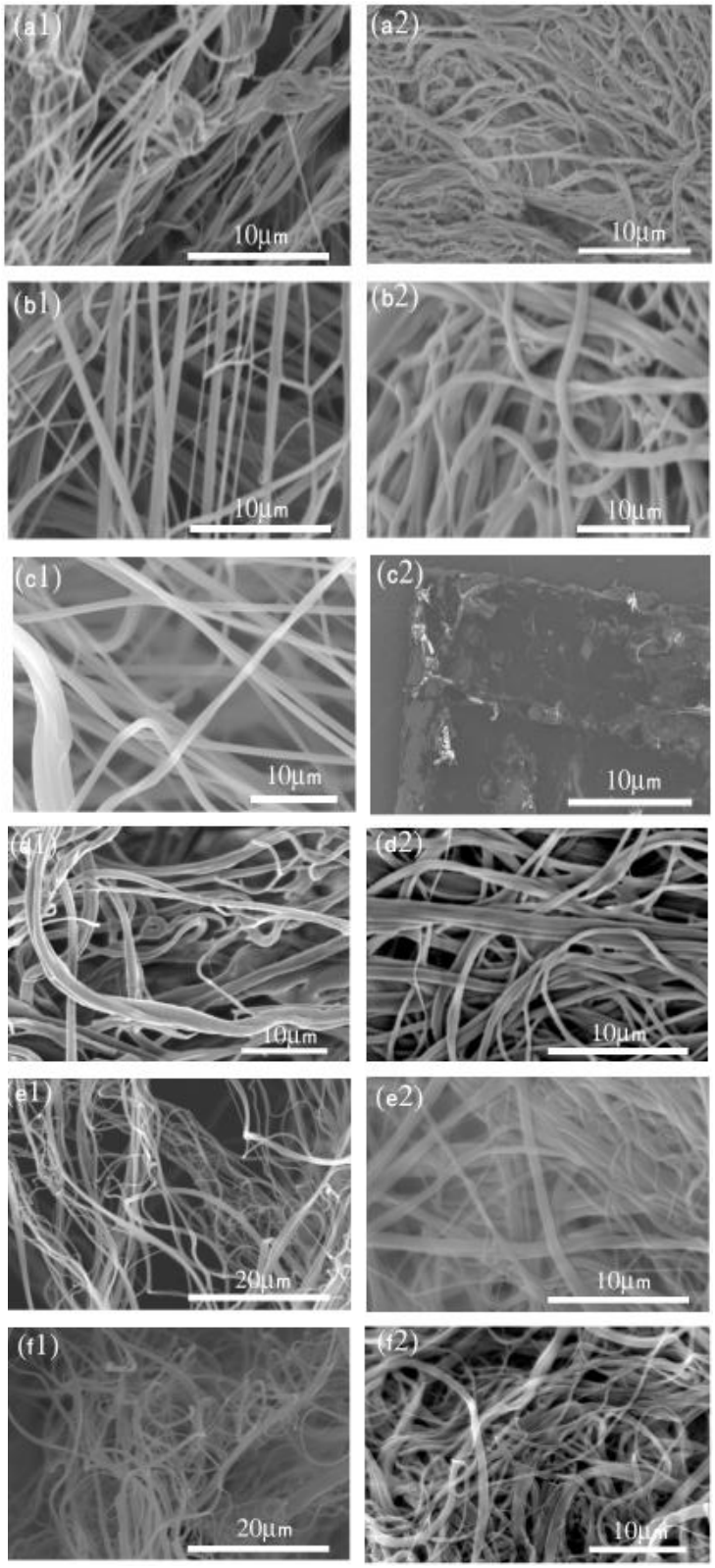
(a1)
10μm
(a2)
10μm
(b1)
10μm
(b2)
10μm
(c1)
10μm
(c2)
10μm
(d1)
10μm
(d2)
10μm
(e1)
20μm
(e2)
10μm
(f1)
20μm
(f2)
10μm

Figure 8.3. SEM images of dye-containing monolithic and core-shell nanofibers mats before and after the immersion in water. Panel (a) shows sample A, (b) - sample B, (c) – sample C, (d) – sample E, (e) – sample F, and (f) – sample H. In all the images, panels 1 depict the dye-containing samples before the immersion in water, whereas panels 2 depict the same samples after the immersion in water after the dye release had reached saturation.

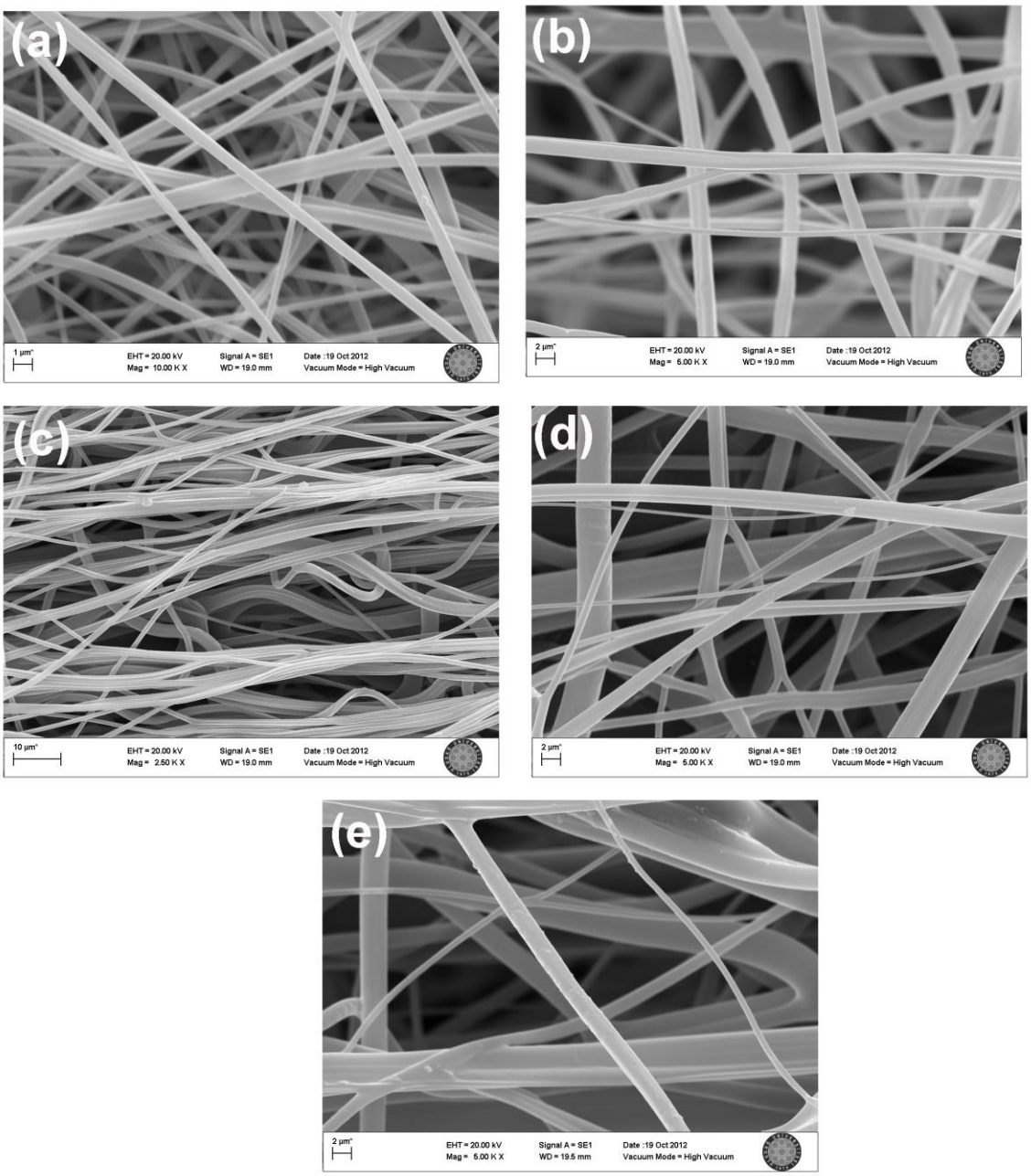

Figure 8.4. SEM images of the electrospun samples I2-M2 are shown in panels (a)-(e), respectively.

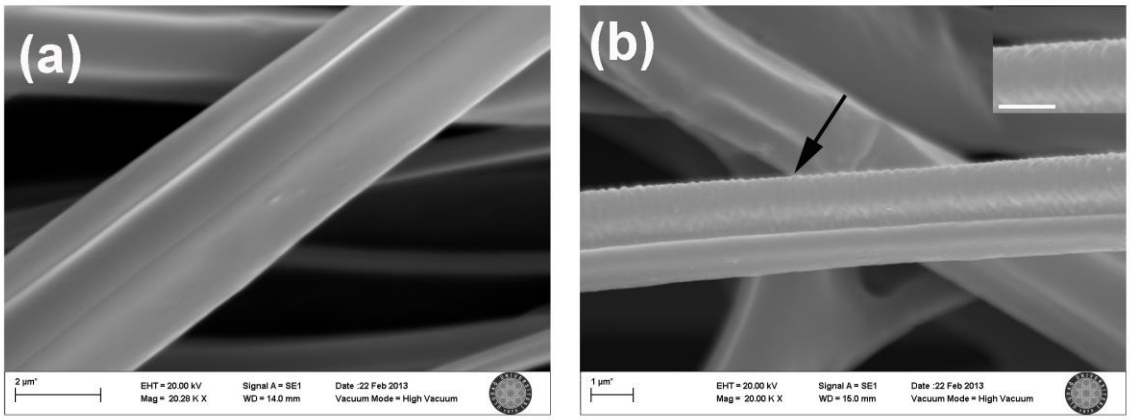

Figure 8.5. SEM images of the electrospun samples I1- panel (a), and I2- panel (b), both after the immersion in water. The arrow in panel (b) points at the striations. A zoomed-in view of the striations is shown in the inset panel (b), with the scale bar in the inset being 1 µm.

8.2.2. Experimental Results

The results of the kinetics of dye release from soy protein-based nanofiber mats are shown in Fig. 8.6. The figure demonstrates that the release process always saturates well below 100 %. For every batch of samples, the release experiments were repeated at least 3 times, and the average release profiles are shown in Fig. 8.6.

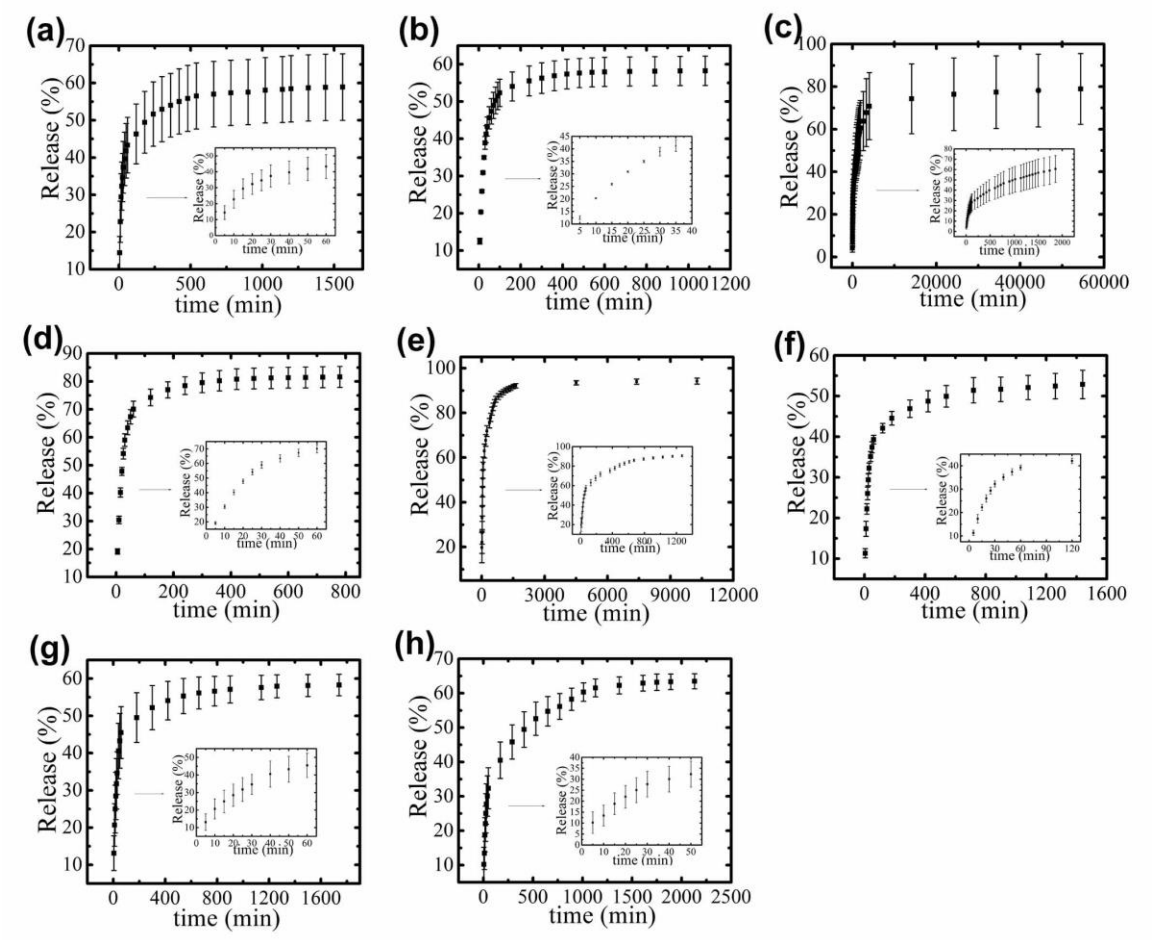

Figure 8.6. Average release profiles from solution-blown Rhodamine B-containing nanofiber mats. Panels (a)-(h) correspond to samples A-H, respectively. It can be seen from the profiles that the release process saturates well below 100%. The insets show the release kinetics at the beginning of the process.

Figs. 8.6a and 8.6b show that the release process for pure nylon 6 nanofiber mats with 1 wt/wt % dye/mat content saturated at a comparable release percentage to the soy protein/nylon 6 (50/50 wt/wt %) fiber mat. For sample A, saturation of the dye release process occurred at 58.93±8.91%, and for sample B – at 60.12±4.17%. Although the release saturation occurred at an almost the same level, the saturation for sample B was

reached at an earlier time in comparison to sample A. This is due to the fact that soy protein contains hydrophilic biopolymeric chains which help to deliver water into the fiber bulk and thus enhance the release process from soy-protein/nylon 6 nanofibers.

In order to enhance the dye release process from the soy protein-containing nanofiber mats, PEG was used as a porogen in the samples with an expectation that due to its faster dissolution in water compared to soy protein, fibers with PEG will rapidly form nanopores after exposure to water. That should facilitate the release process. To demonstrate the effect of PEG, monolithic and core-shell soy protein/nylon 6 nanofibers were seeded with two different amounts of PEG (5 and 10 wt%). In Figs. 8.6d and 8.6e, the release profiles for soy protein/nylon 6 (50/50 wt/wt %) with 5 and 10 wt/wt % PEG nanofibers are shown, respectively. It is seen that a higher content of PEG in the samples resulted in a higher level of the ultimate release saturation for the PEG-containing fiber mats (Fig. 8.6e) compared to the original soy protein/nylon 6 (50/50 wt/wt %) fiber mats (cf. Fig. 8.6b). Monolithic soy protein/nylon 6 nanofiber samples released dye up to 60.12±4.17%. The addition of 5 wt/wt % PEG/mat increased the release level up to 81.59±3.75% for comparable soy protein/nylon 6 nanofiber samples as seen in Fig. 8.6d. For 10 wt/wt % PEG/mat the ultimate release level approached to 94.22±1.33% in Fig. 8.6e. The release process from monolithic soy protein/nylon 6 nanofibers saturated at about 1080 min (Fig. 8.6b), whereas for the comparable samples with 10 wt/wt% PEG, the active release process was much longer and saturated at about 10270 min (Fig. 8.6e).

The release profile for core-shell soy protein/nylon 6 nanofiber mats is illustrated in Fig. 8.6f. In these fibers, the dye-containing core was surrounded by the nylon 6 shell. The lower saturation percentage for the core-shell nanofibers compared to that of soy

protein/nylon 6 (50/50 wt/wt %) nanofibers (cf. Fig. 8.6f with Fig. 8.6b) is easily noticeable. The soy protein/nylon 6 nanofiber samples reached the release saturation at 60.12±4.17%, while for the soy protein/nylon 6 core/shell nanofiber samples the release saturated already at 52.85±3.49%. The nylon 6 shell which is not water soluble hinders the dye release from the core.

Fig. 8.6c illustrates dye release process from soy protein/PVA (50/50) nanofiber mats. As the SEM image (Fig. 8.3c) and Table 8.1 show, dissolution of the soy protein/PVA nanofibers in water is quite significant and is facilitated by the easy solubility of PVA and hydrophilic nature of soy protein. As a result of the fiber material degradation in this case, the release process saturates at 78.32±17.24% over a long period of time.

The presence of PEG in the shell of the core-shell fibers also facilitates dye release. The comparison of Figs. 8.6f, 8.6g and 8.6h demonstrates that a higher content of PEG in the shell (0, 5 and 10 wt%, respectively) facilitates the dye release from the core, increases the saturation level of the release process, and makes it longer. The release from core/shell soy protein/nylon 6 nanofiber mats saturated at 52.85±3.49% (Fig. 8.6f). When 5 wt% PEG was present in the shell, the saturation level increased up to 58.28±2.87% (Fig. 8.6g), and at 10 wt% of PEG – it reached 63.48±2.19% (Fig. 8.6h).

The release kinetics of Rhodamine B from electrospun PET-based nanofiber mats (Samples I1-M1) are illustrated in Fig. 8.7. The dye release from pure PET nanofiber mats saturated at 2.1±0.11% (Fig. 8.7a). The encapsulation of PEG as a porogen in the PET-based nanofibers led to a significant boost in the release of Rhodamine B from the nanofibers. The dye-containing PET/PEG nanofiber mats revealed 30.07±1.03% level of

release saturation (Fig. 8.7b). The encapsulation of an additional porogen (i.e. PEO) in the PET/PEG nanofiber mats resulted in a lower level of the release saturation. PET/PEG/PEO (200 kDa) nanofibers reached the ultimate saturation of 12.50±1.87% (Fig. 8.7c). The addition of the higher molecular weight PEO further reduced the ultimate release saturation value. In particular, the release from the monolithic electrospun PET/PEG/PEO (400 kDa) nanofibers saturated at 3.18±0.21%, and from the PET/PEG/PEO (600 kDa) nanofibers the release saturated at 1.85±0.15% (cf. Figs.8.7d and e, respectively).

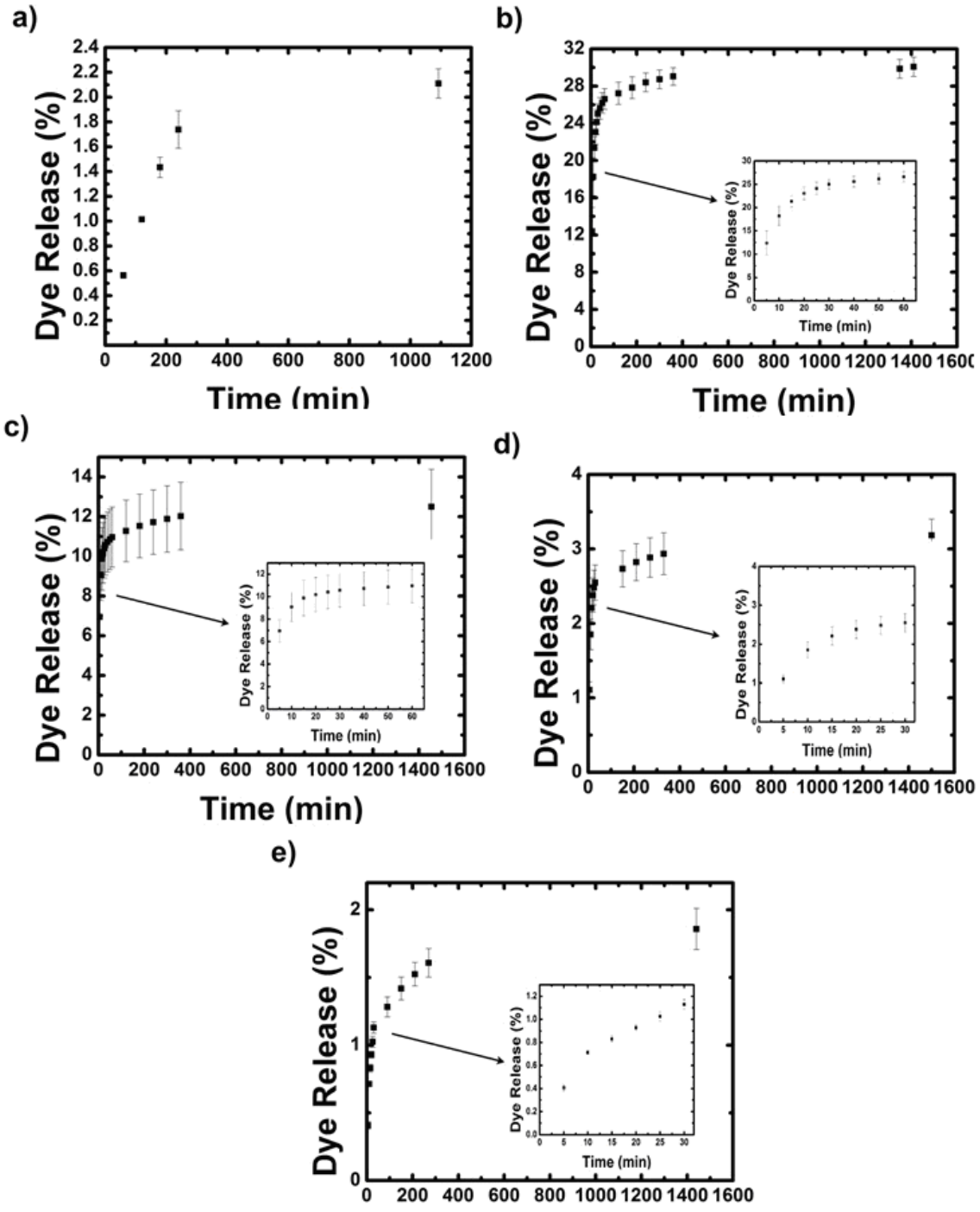

Figure 8.7. Release kinetics of Rhodamine B from electrospun PET-based nanofiber mats. (a) Sample I1, (b) J1, (c) K1, (d) L1, and (e) M1.

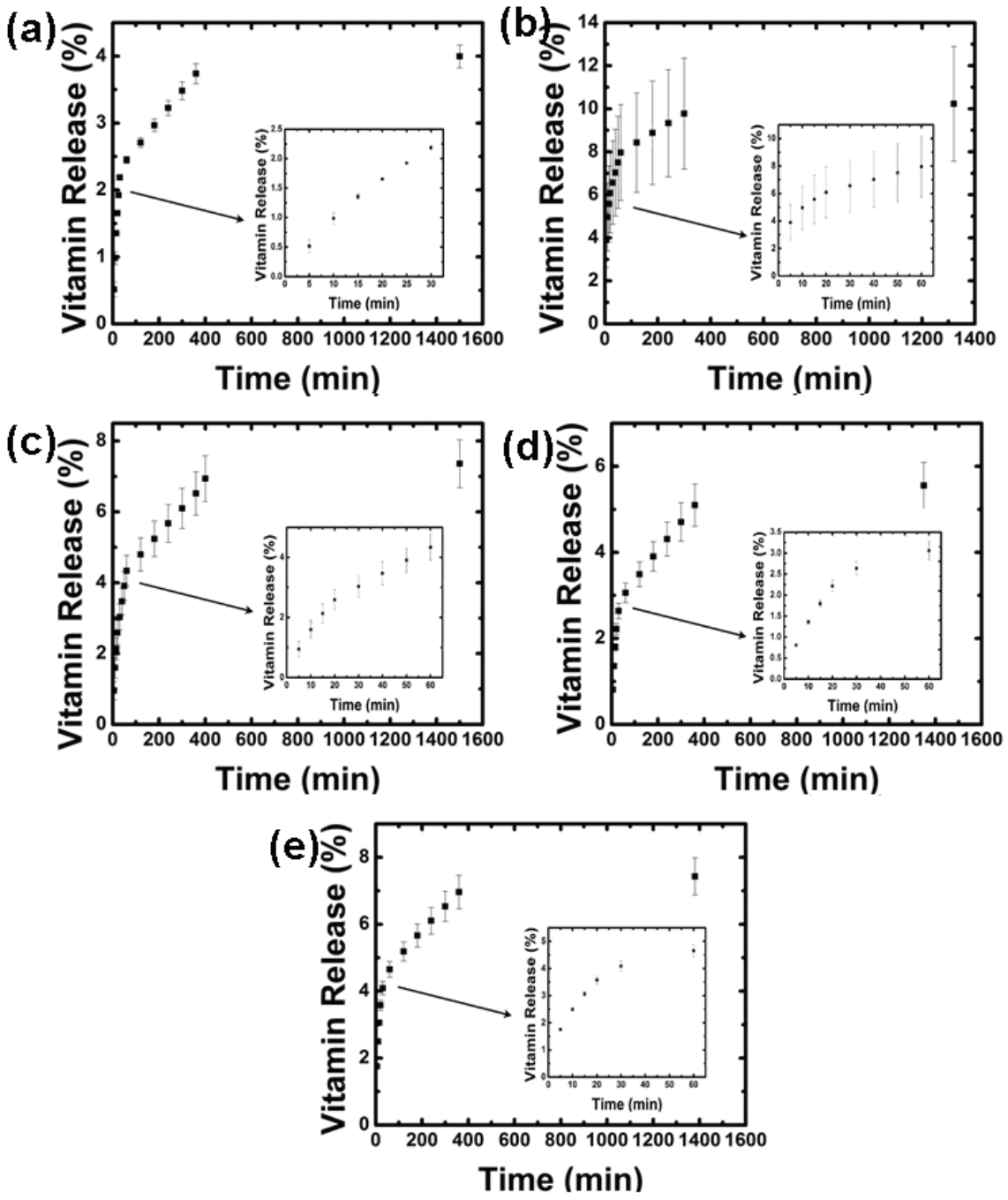

Figure 8.8. Release kinetics of riboflavin from electrospun PET-based nanofiber mats. (a) Sample I2, (b) J2, (c) K2, (d) L2, and (e) M2.

The release kinetics of riboflavin from electrospun PET-based fibers with PEG and PEO encapsulated as porogens is illustrated in Fig. 8.8. Riboflavin-containing nanofiber mats of pure PET revealed saturation of the release process at 3.99±0.16% (Fig. 8.8a). PET/PEG monolithic nanofiber mats loaded with riboflavin revealed release saturation at 10.23±2.66% (Fig. 8.8b). The presence of PEO in addition to PEG was detrimental and reduced the ultimate riboflavin release level to 7.35±0.67% for PET/PEG/PEO (200 kDa), 5.55±0.53% for PET/PEG/PEO (400 kDa), and 7.42±0.55% for PET/PEG/PEO (600 kDa) (Figs. 8.8c-e, respectively).

8.2.3. Theoretical versus Experimental

As reported in (Sinha-Ray et al., 2010c), the maximum solubility of Rhodamine dye in water is of the order of 0.1 wt%. Therefore, the maximum concentration of Rhodamine in water in the present experiments could not exceed 0.00002 wt%, as well as the maximum solubility of dye could not be reached in the release process. Therefore, the saturation of the release process seen in Figs. 8.6,7 cannot be related to the maximum solubility of Rhodamine dye in water, and should be linked to dye desorption from the nanopore surfaces in the individual nanofibers, as shown in (Srikar et al., 2008). A higher resolution SEM images of the individual solution-blown soy protein monolithic and core-shell nanofibers nanofibers in (Sinha-Ray et al., 2011) show that they contain multiple nanopores. The pores perforate the entire nanofiber bulk. Most of the pores in the nanofibrous structure are spread into the bulk from the nanofiber surface. Therefore, when such samples are immersed in water, nanopores are fully exposed to water and the

dye desorption mechanism revealed in (Srikar et al., 2008; Gandhi et al., 2009) is fully responsible for the release saturation seen in Figs. 8.3a-h

According to (Srikar et al., 2008; Gandhi et al., 2009), dye release is a two stage process. First, dye is release by desorption from the nanopore surfaces, which is a relatively slow, limiting stage of the dye/drug release. Then, the released dye is redistributed in water by diffusion, which is a comparatively very fast process. The saturation of the release process well below 100% is a clear manifestation of the fact that the solid state diffusion of dye inside nanofibers in not involved (since diffusion can never stop below 100%, (Srikar et al., 2008; Gandhi et al., 2009)). Accordingly, and the dye embedded in the nanofiber bulk cannot be released at all, and the only dye which is released is the one from the nanopore surfaces exposed to water (Srikar et al., 2008; Gandhi et al., 2009). The same is also true for the release of riboflavin illustrated in Figs. 8.8a-e.

The release kinetics with the desorption-limiting stage is described by the following equation (Srikar et al., 2008; Gandhi et al., 2009)

$$\frac{G_t}{M_{d0}} = \alpha\left[1\text{-}\exp\left(\frac{-\pi^2}{8}\frac{t}{\tau_r}\right)\right] \tag{8.2}$$

where G_t is the amount of dye released by time t; the nanoporosity factor $\alpha = M_{sd0}/\left(M_{sd0}+M_{bd0}\right)$, with M_{sd0} being the initial amount of dye/drug at the nanopore surfaces, and M_{bd0} is the initial amount of dye/drug in the fiber bulk. Correspondingly, $M_{d0} = M_{sd0}+M_{bd0}$ is the total initial amount of dye/drug in the nanofibers. The nanoporosity factor is determined by polymer concentrations and molecular weights in

the blown solutions. In Eq. (8.2) τ_r is characteristic time of the release process, which is determined by the polymer density, as well as the kinetic parameters of desorption, in particular by the pre-exponential k_0 and the activation energy E (Srikar et al., 2008; Gandhi et al., 2009). According to Eq. (8.3), dye release should saturate at the level of $\alpha \times 100\%$.

It is emphasized that the theory of (Srikar et al., 2008; Gandhi et al., 2009) does not account for any dissolution of nanofiber during the release process and the exposition of the newly formed surfaces to the surrounding water. In other words, the original theory does not consider neither the presence of water-soluble PVA, nor PEG (Mark, 1999). Moreover, formally speaking, the theory is applicable only to monolithic, single-polymer nanofibers. Therefore, the theory of (Srikar et al., 2008; Gandhi et al., 2009) is not expected to describe the experimental data for PVA and PEG-containing case, and core-shell fibers, as well it is also not expected to be appropriate for hydrophilic polymers. Fig. 8.9 shows thefit of Eq. (8.2) to the experimental data from the previous section. It clearly demonstrates that the inapplicable theory mostly fails to reproduce the data. The fitting allows determination of the values of the nanoporosity factor and characteristic time, and consequently, the kinetic parameters of the desorption process, albeit in a very rough approximation. These parameters are listed in Table 8.2. It is emphasized that these values are mostly unreliable due to the reasons described above.

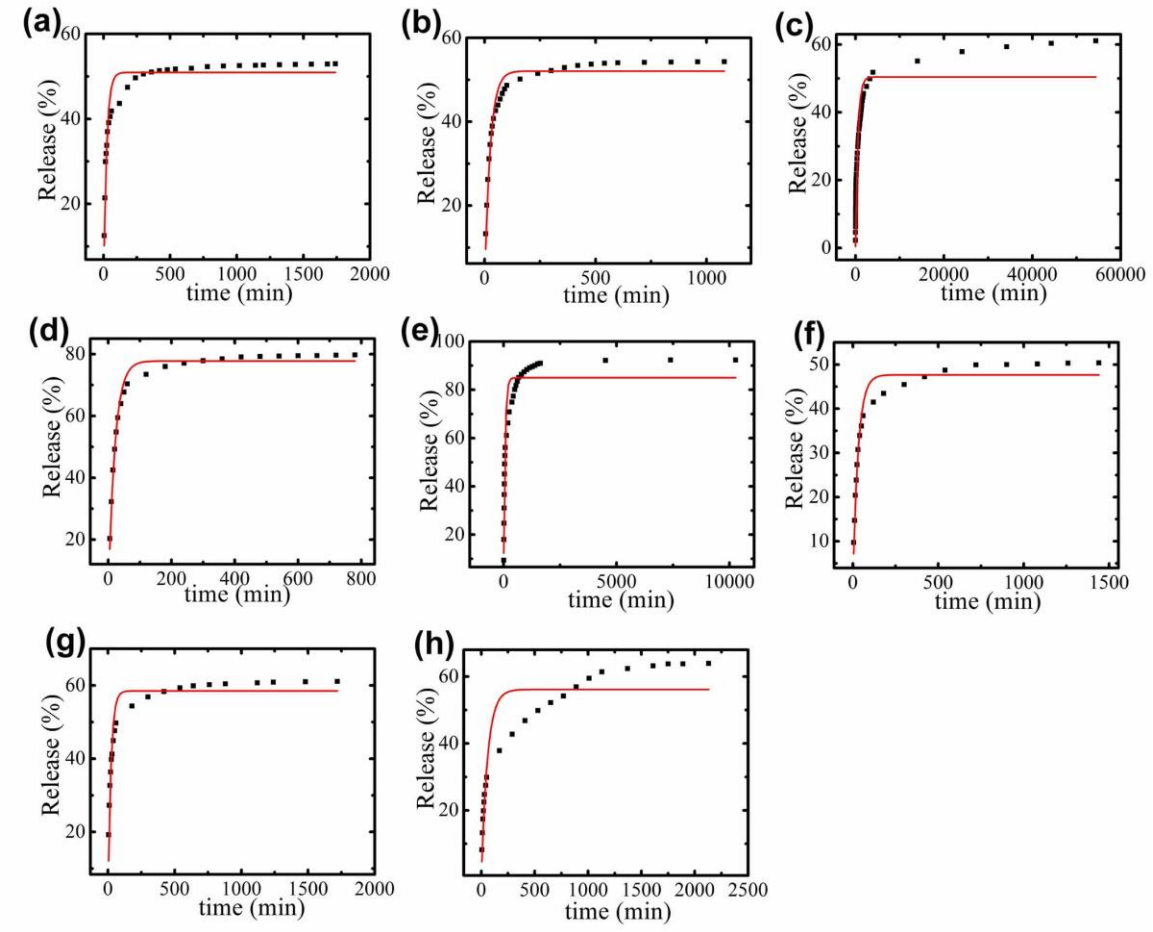

Figure 8.9. Experimental Rhodamine B release profiles versus Eq. (8.2). Panels (a)-(h) correspond to samples A-H from Figs. 8.6a-h. The symbols show the experimental data, and the curves – the best fit of Eq. (8.2).

Table 8.2. Parameters of Eq. (8.2) determined from the fitting in Fig. 8.9. The values of $\alpha(\%)$ shows the ultimate release percentage, $\tau_r(\text{min})$ is the characteristic time, and $E\,(\text{kJ/mol})$ is the desorption enthalpy.

Sample		**Average** $\alpha(\%)$	**Average** $\tau_r(\text{min})$	**Average** $E\,(\text{kJ/mol})$
Monolithic	Nylon 6	55.30±8.42	32.99±5.78	30.37±0.41
	SP/Nylon	58.32±4.49	31.49±2.87	30.28±0.20
	SP/PVA	62.12±11.65	488.34±177.76	36.96±0.95
	SP/Nylon+5%PEG	79.46±3.59	27.71±1.92	29.97±0.17
	SP/Nylon+10%PEG	85.91±0.94	74.58±12.41	32.42±0.43
Core/Shell	SP/Nylon	49.05±2.65	35.44±3.22	30.58±0.23
	SP/Nylon+5%PEG	55.43±3.98	37.12±10.88	30.61±0.66
	SP/Nylon+10%PEG	57.15±2.90	64.58±23.77	31.88±1.07

The comparison in Fig. 8.9a shows that dye release from pure nylon 6 nanofiber mats cannot be described by Eq. (8.2) as well. The latter stems from the following physico-chemical factors. According to (Kawasaki et al., 1962; Inoue et al., 1976), nylon 6 partially swells in water. Water is absorbed in the amorphous regions by reacting with the free amide groups not bonded to the amide groups on the nearby chains, or due to water breaking up the interaction between the chains. As nylon 6 swells in water, new nanopores are either generated or opened up. This factor is not accounted for by the theory in (Srikar et al., 2008; Gandhi et al., 2009) and that is the additional reason that it fails practically in all cases where nylon 6 is present in the fibers. It is emphasized that soy protein isolate is also partially soluble in water as is seen in Table 8.1 (also, cf. PRO-FAM 955 Isolated Soy Protein 066-955 Data Sheet). Therefore, soy-based nanofibers in contact with water dissolve to some extent, which results in generation of new pores-the

phenomenon not accounted for by the theory in (Srikar et al., 2008; Gandhi et al., 2009), as the comparison in Fig. 8.9 confirms.

Similar observations were done regarding the Rhodamine B-containing PET-based nanofiber mats. In particular, Fig. 8.10 shows that the porogens (PEG and PEO) facilitated the release process and resulted in deviations from Eq. (8.2). The fitted rough values of the desorption parameters are listed in Table 8.3.

The release of riboflavin from the PET-based nanofibers follows the same trend (Fig. 8.11 and Table 8.4). It is seen that in this case Eq. 8.2 is even less appropriate for fitting the data for the release kinetics as compared to the previously considered case of Rhodamine B release. This is probably linked to the fact that riboflavin is embedded in striations and develops micro-cracks during its release as was discussed in relation to Fig. 8.5. The development of micro-cracks is effectively identical to riboflavin acting as an additional autocatalytic self-porogen, since it exposes more riboflavin to the surrounding bath during the release process.

Table 8.3. Parameters of Eq. (8.2) determined from the fitting in Fig. 8.10. The values of $\alpha(\%)$ show the ultimate release percentage, $\tau_r(\text{min})$ is the characteristic time, and $E\ (\text{kJ/mol})$ is the desorption enthalpy.

Sample	Average $\alpha(\%)$	Average $\tau_r(\text{min})$	Average $E\ (\text{kJ/mol})$
PET	208.29	2.14	23.59
PET/PEG	27.88	12.8	28.05
PET/PEG/PEO200 kDa	11.28	7.61	26.76
PET/PEG/PEO 400 kDa	2.87	13.25	28.14
PET/PEG/PEO 600 kDa	1.53	25.35	29.76

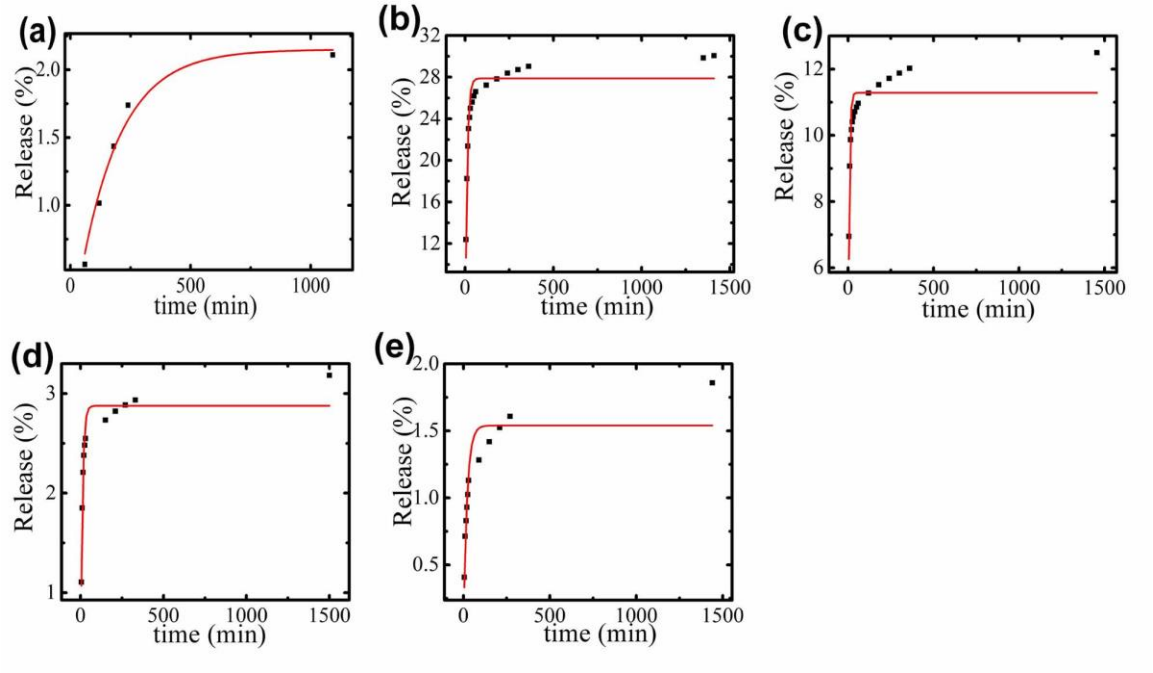

Figure 8.10. Release kinetics of Rhodamine B from samples I1-M1, corresponding to panels (a)-(e) in Fig. 8.7, respectively. The symbols show the experimental data, and the curves – the best fit of Eq. (8.2).

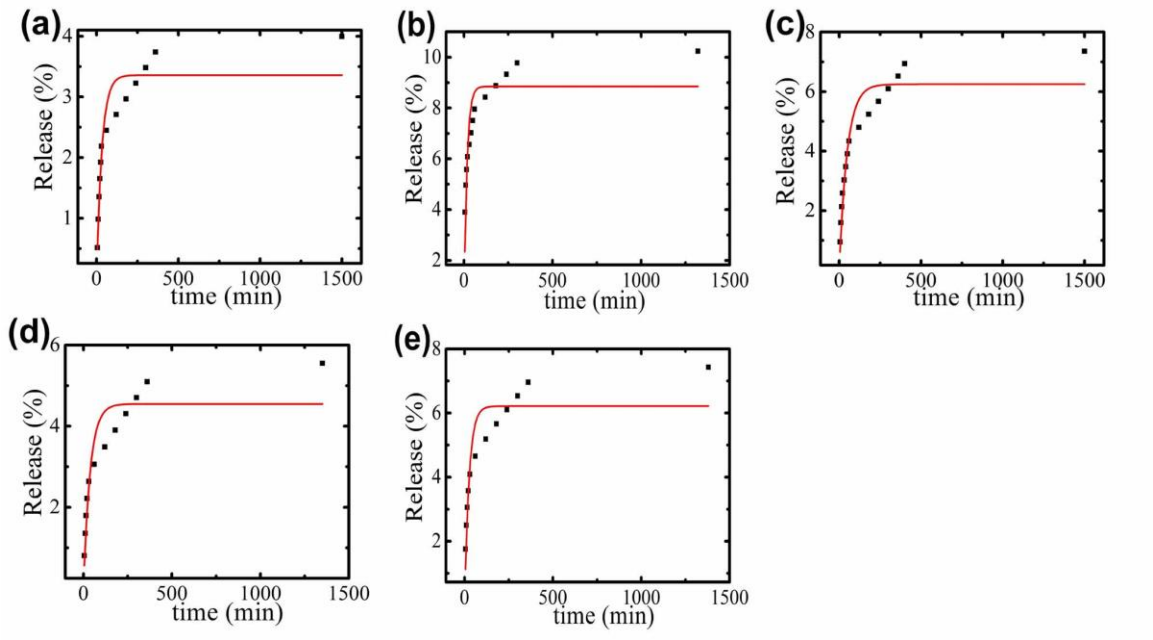

Figure 8.11. Release from riboflavin-loaded nanofiber mats (samples I2-M2), corresponding to panels (a)-(e) in Fig. 8.8, respectively. The symbols show the experimental data, and the curves – the best fit of Eq. (8.2).

Table 8.4. Parameters of (Eq. 8.2) determined from the fitting in Fig. 8.11. The values of $\alpha(\%)$ show the ultimate release percentage, $\tau_r(\text{min})$ is the characteristic time, and $E\,(\text{kJ/mol})$ is the desorption enthalpy for the PET-based nanofiber mats with the embedded riboflavin.

Sample	**Average** $\alpha(\%)$	**Average** $\tau_r(\text{min})$	**Average** $E\ (\text{kJ/mol})$
PET	3.35	39.43	30.86
PET/PEG	8.85	20.08	29.18
PET/PEG/PEO200 kDa	6.24	59.5	31.88
PET/PEG/PEO400 kDa	4.54	46.3	31.26
PET/PEG/PEO600 kDa	6.21	30.71	30.23

The theory of (Srikar et al., 2008), Eq. (8.2), can be amended accounting for the fact that in the present case not only dye is released, but another water-soluble component, soy protein, PVA or PEG are also "released", as well as the riboflavin striations result in micro-cracks and further exposure to the bath medium. Soy protein, PVA and PEG are expected to be "released" much slower than the dye due to a much larger size of their molecules. Micro-cracks in the case of riboflavin release also form in the wake of the leading release process. Then, the additional dye or riboflavin release associated with the opening of the new pores or micro-cracks will proceed with the rate of "release" of the leachable component of the fibers or crack formation. Then, the dye/riboflavin released by time t can be described by the superposition of the two terms dictated by Eq. (8.2), namely by

$$\frac{G_t}{M_{d0}} = \alpha_1\left[1-\exp\left(-\frac{\pi^2}{8}\frac{t}{\tau_{r1}}\right)\right]+\alpha_2\left[1-\exp\left(-\frac{\pi^2}{8}\frac{t}{\tau_{r2}}\right)\right] \tag{8.3}$$

where α_1 and τ_{r1} correspond to dye/riboflavin release from the existing pores, and α_2 and τ_{r2} correspond to the "release" of a leachable component of the fibers or micro-crack formation and thus, to dye/riboflavin release from the surfaces of the newly formed pores/cracks.

According to (Srikar et al., 2008), $\tau_{r1} = L^2/[Dc_{w01}b/\rho_{sd0}]$ where L is the pore length, D is the diffusion coefficient of dye in water, the initial dye/riboflavin concentration in water near the pore surface $c_{w01} = k_{01}\exp(-E_1/RT)\rho_{sd0}/\rho_{sp}$, where k_{01} is the pre-exponential coefficient, E_1 is the desorption enthalpy of dye/riboflavin, R is the universal gas constant, T is the temperature, , ρ_{sd0} is the surface concentration of dye/riboflavin at t=0, and ρ_{sp} is the surface concentration of polymer matrix including the leaching

polymer. Similarly, $\tau_{r2} = L^2/[Dc_{w02}b/\rho_{sl0}]$ where D is the diffusion coefficient of the leaching component in water (for simplicity assumed to be the same as for the dye), the initial concentration of the leachable component in water near the pore surface $c_{w02} = k_{02}\exp(-E_2/RT)\rho_{sl0}/\rho_{spn}$, where k_{02} is the pre-exponential coefficient, E_2 is the desorption enthalpy of the leachable polymer, ρ_{sl0} is the surface concentration of the leachable component at t=0, and ρ_{spn} is the surface concentration of the non-leachable polymer matrix. It can be expected that release of dye by desorption is much easier than release of the leachable component, since the latter has a much higher molecular weight. In the case of riboflavin, the role of the leachable polymer is also associated with riboflavin itself.

Fig. 8.12 compares Eq. (8.3) with the same experimental data on dye release as in Fig. 8.10. It is seen that an almost perfect matching is achieved and the corresponding parameter values are listed in Table 8.5 for all the samples except for sample C in Fig. 8.3c. This soy/PVA nanofiber sample, as shown in Fig. 8.3(c2), lost its fibrillar structure and turned into a solid block owing to the dissolution of the constituents. This effect is not accounted for in the model (8.3) and the agreement is poorer.

Fig. 8.13 compares Eq. (8.3) with the experimental data on dye release from the PET-based nanofibers (samples J1-M1), whereas Fig. 8.14 depicts a similar comparison with the experimental data on riboflavin release from the PET-based nanofibers (samples I2-M2). The corresponding parameter values are listed in Tables 8.6 and 8.7.

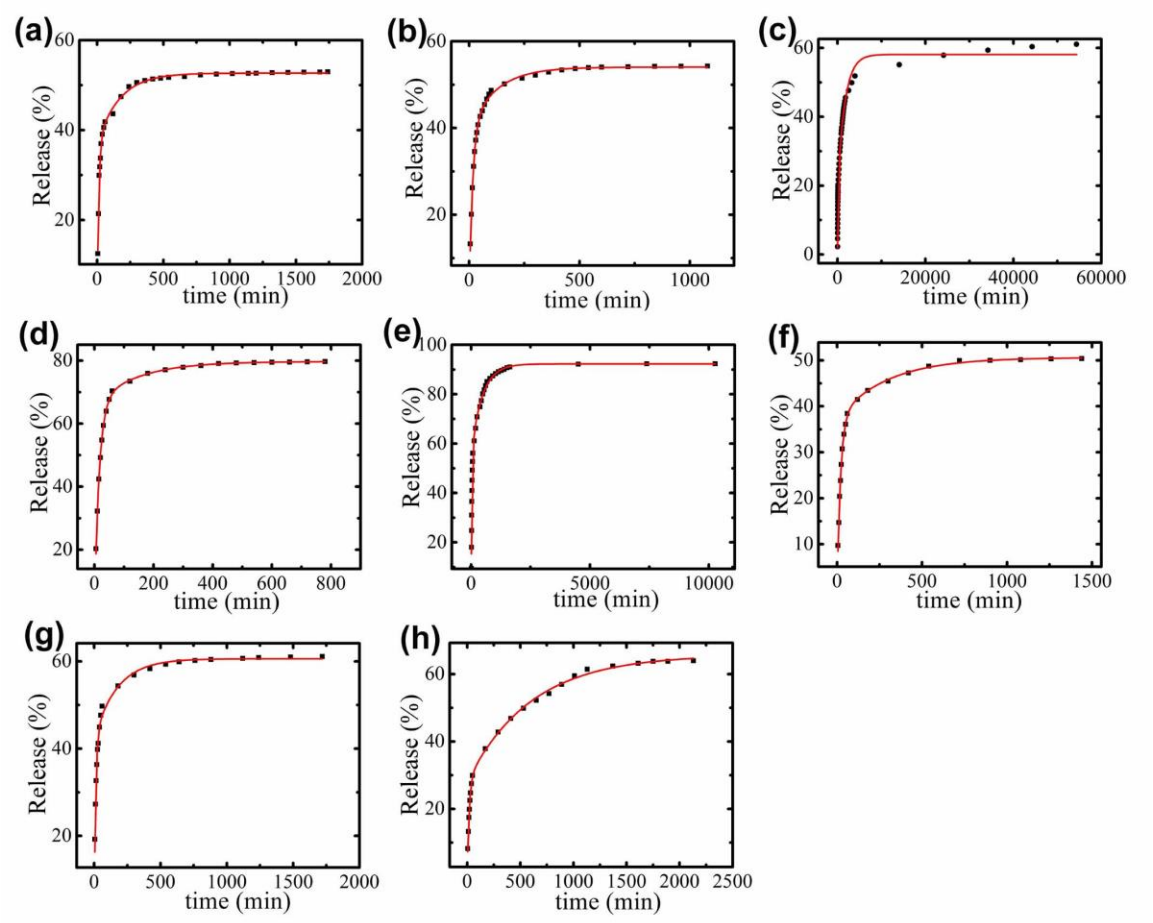

Figure 8.12. Experimental data of the dye (Rhodamine B) release kinetics from soy protein-based nanofiber mat fitted using Eq. (8.3) for samples A-H corresponding to panels (a)-(h), respectively. The symbols show the experimental data, and the curves – the best fit of Eq. (8.3).

Table 8.5. Parameters of eq 3 determined from the fitting in Fig. 8.12 for dye release from soy protein-based nanofiber mats. The values of $\alpha_i(\%)$ show the ultimate release percentages of the dye and porogens, $\tau_{ri}(\text{min})$ - the characteristic times, and E_i (kJ/mol) are the desorption enthalpies.

Sample		Average α_1(%)	Average τ_{r1}(min)	Average α_2(%)	Average τ_{r2}(min)	Average E_1(kJ/mol)	Average E_2(kJ/mol)
Monolithic	**Nylon 6**	**38.21±5.63**	**15.05±2.35**	**20.17±3.72**	**299.15±97.95**	**28.43±0.38**	**35.79±0.6**
	SP/Nylon 6	**49.23±7.22**	**23.40±3.46**	**10.79±3.09**	**199.31±40.66**	**29.53±0.38**	**34.85±0.26**
	SP/Nylon+5%PEG	**66.52±3.84**	**20.55±1.46**	**15.19±1.24**	**191.58±25.17**	**29.23±0.17**	**34.78±0.1**
	SP/Nylon+10%PEG	**56.80±1.63**	**38.37±6.56**	**36.77±1.31**	**490.29±180.73**	**30.75±0.45**	**37.59±0.04**
Core/Shell	**SP/Nylon**	**36.98±0.84**	**20.96±2.71**	**15.66±2.72**	**362.07±14.04**	**29.26±0.31**	**36.39±+0.02**
	SP/Nylon+5%PEG	**38.40±3.98**	**13.67±9.88**	**19.38±1.16**	**396.03±182.93**	**25.13±5.6**	**36.31±1.55**
	SP/Nylon+10%PEG	**30.41±4.34**	**20.20±7.21**	**33.94±3.52**	**607.20±132.24**	**29.00±1.01**	**37.61±0.34**

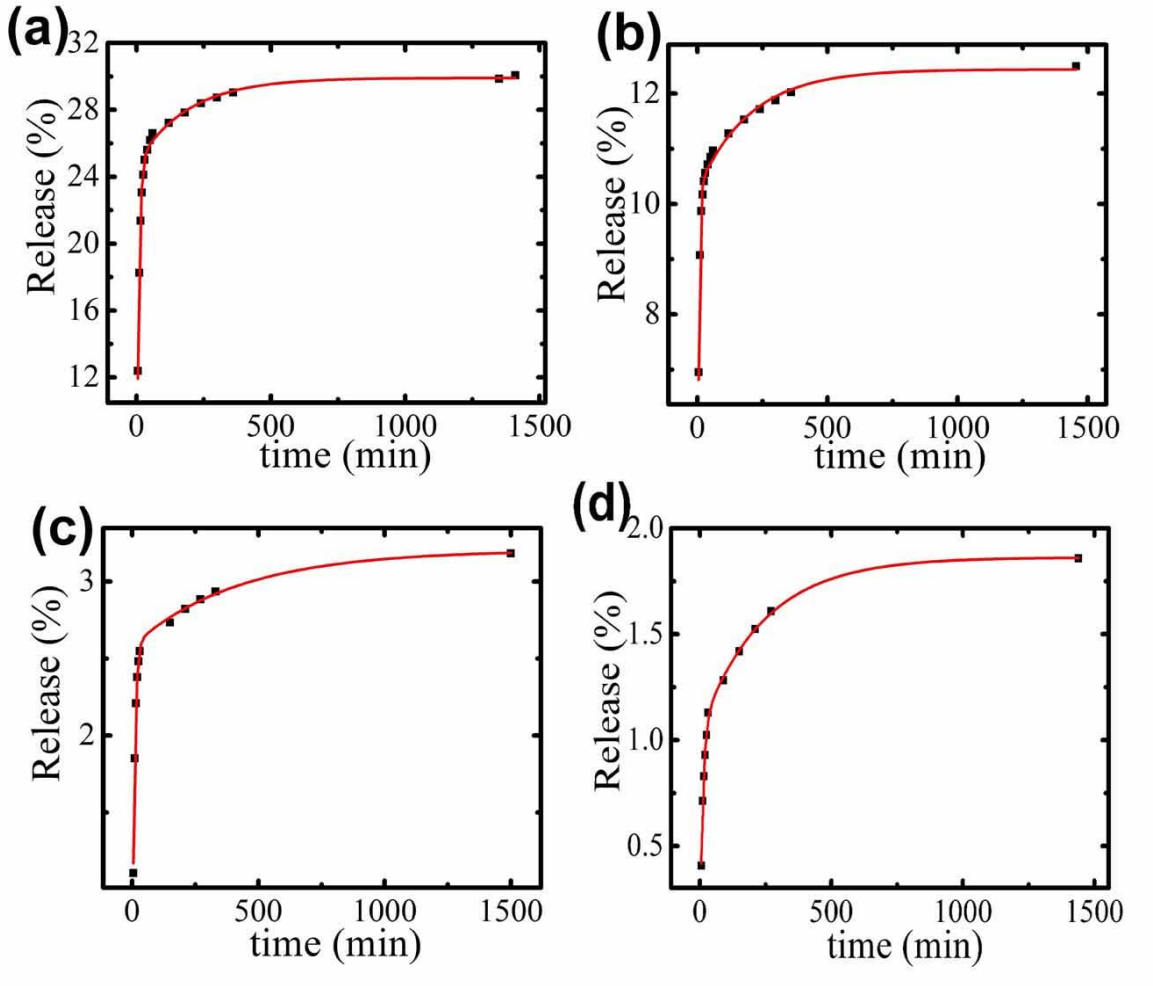

Figure 8.13. Experimental data on dye (Rhodamine B) release profiles from PET-based nanofiber mats fitted using Eq. (8.3) for samples J1-M1 corresponding to panels (a)-(d), respectively. The symbols show the experimental data and the curves – the best fit of Eq. (8.3).

Table 8.6. Parameters of eq 3 determined from the fitting in Fig. 8.13 for dye release from PET-based nanofiber mats. The values of $\alpha_i(\%)$ show the ultimate release percentages of the dye and porogens, $\tau_{ri}(\min)$ - the characteristic times, and E_i (kJ/mol) are the desorption enthalpies.

Sample	Average α_1(%)	Average τ_{r1}(min)	Average α_2(%)	Average τ_{r2}(min)	Average E_1(kJ/mol)	Average E_2(kJ/mol)
PET/PEG	24.77	5.13	9.54	235.96	25.77	35.32
PET/PEG/PEO200 kDa	10.24	2.19	5.71	247.9	23.65	35.44
PET/PEG/PEO400 kDa	2.58	0.62	10.27	519.61	20.50	37.29
PET/PEG/PEO600 kDa	1.04	0.81	12.72	295.06	21.17	35.88

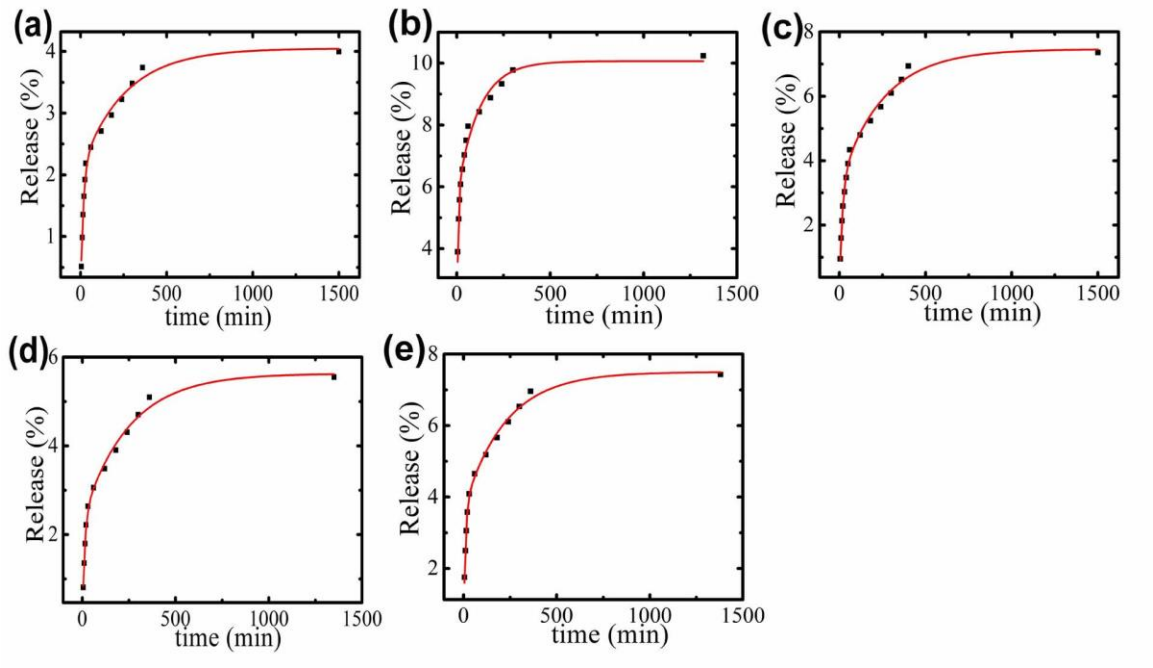

Figure 8.14. Experimental data on the riboflavin release kinetics from the PET-based nanofiber mats fitted using Eq. (8.3) for samples I2-M2 corresponding to panels (a)-(e), respectively. The symbols show the experimental data and the curves – the best fit of Eq. (8.3).

Table 8.7. Parameters of eq 3 determined from the fitting in Fig. 8.14 for the PET-based nanofiber mats releasing riboflavin. The values of $\alpha_i(\%)$ show the ultimate release percentages of riboflavin and porogens, $\tau_{ri}(\text{min})$ - the characteristic times, and E_i (kJ/mol) are the desorption enthalpies.

Sample	Average α_1(%)	Average τ_{r1}(min)	Average α_2(%)	Average τ_{r2}(min)	Average E_1(kJ/mol)	Average E_2(kJ/mol)
PET	2.08	19.05	1.96	315.53	29.04	36.05
PET/PEG	5.7	6.82	4.35	142.78	26.48	34.07
PET/PEG/PEO200 kDa	3.28	21.40	4.18	311.74	29.33	36.02
PET/PEG/PEO400 kDa	2.33	15.14	2.33	303.87	28.47	35.95
PET/PEG/PEO600, kDa	3.66	11.56	3.83	274.46	27.80	35.70

8.3. Conclusion

Water-soluble fluorescent dye Rhodamine B was embedded in solution-blown soy protein/polymer monolithic and core-shell nanofiber mats and the release kinetics from the samples submerged in water was studied experimentally. Similarly, release kinetics of Rhodamine B from PET-based electrospun nanofibers, and release kinetics of the vitamin riboflavin from PET-based electrospun nanofibers was explored. The main finding is that soy protein, PEO, PVA and PEG embedded in nanofibers act as porogens and facilitate development of pores during the dye release process, which affects the release kinetics. In addition, nylon 6 adsorbs water from the bath, which also affects the release kinetics.

Partially-soluble riboflavin embedded in PET-based electrospun nanofibers is not dispersed uniformly but forms striations. During the release process these striations facilitate formation of micro-cracks, which means that riboflavin effectively acts as an autocatalytic self-porogen in addition to the other embedded porogens.

It was shown that the dye release process from nanofiber mats with porogens or self-porogens is associated with the desorption-limited mechanism discovered in (Srikar et al., 2008). Albeit, the release process consists of two stages. At the first one, the dye/vitamin is released from the pre-existing pores, at the second one-from the pores/micro-cracks formed due to leaching or dissolution of the fiber body or generation of micro-crack. The theory of (Srikar et al., 2008) was amended appropriately to account for the two-stage character of the release process.

9. Biopolymer-Based Nanofiber Mats and Their Mechanical Characterization

9.1. Experimental

9.1.1. Materials

Cellulose acetate (M_w=30 KDa), zein, low sulfonate lignin alkali powder (M_w=10 KDa), N,N-Dimethylformamide anhydrous (99.8%), formic acid (grade >95%), dichloromethane anhydrous, DCM (≥99.8%), trifluoroacetic acid, TFA (ReagentPlus 99%), dichloroacetic acid, DCA (ReagentPlus ≥99%), Butvar B-98, and methanol (≥99.8%) A.C.S. Reagent were purchased from Sigma-Aldrich. Polyamide-6 (nylon-6) (M_w=65.2 kDa) was provided by BASF. Polyacrylonitrile, PAN, (M_w=150 KDa) and polyvinyl alcohol, PVA (M_w=78 KDa) were purchased from PolySciences, Inc. Soy protein isolate [PRO-FAM 781 (SP 781)] was provided by ADM Specialty Food Ingredients. Poly ethylene terephthalate, PET granular were provided by NC State University. Silk sericin was obtained from Chagnsha Guanxiang Chemical Trading Co. Finally, bovine serum albumin-Cohn fraction V protease free (BSA) was purchased from LEE Biosolutions. All materials were used without applying any post treatment.

9.1.2. Solution Preparation

Cellulose acetate/PAN solution was prepared by mixing 0.5 g PAN in 9.5 g DMF. The solution was left on a hotplate for 5 h at 60 °C. Then, 0.5 g of cellulose acetate was added to PAN solution and stirred at room temperature for another hour.

Zein solution was prepared in three different contents. In separate vials, 1.0, 2.0, and 3.0 g of zein was mixed with 10.0 g of formic acid and left on a hotplate at 75 °C for 3 h. Then, 1.5 g nylon 6 was added to each solution and left under stirring on the hotplate at the same temperature for 24 h. To produce core-shell zein/nylon 6 nanofibers, solutions were prepared as follows. Core solution consisted of 3.0 g of zein mixed with 13 g of formic acid and left on a hotplate at 75 °C for 3 h. Next, 1.25 g of nylon 6 was added to the core solution and stirred on the hotplate for another day to make it homogeneous. The shell solution was 20 wt % nylon 6 in formic acid.

Soy protein/zein/nylon 6 solution was prepared by adding 0.75 g of SP 781 and 0.75 g of zein to 10 g of formic acid and leaving the solution on a hotplate at 80 °C for 12 h. After that, 1.5 g of nylon 6 was added and the solution was left on a hotplate at 80 °C for stirring for 12 h.

To prepare lignin solutions, 0.5 and 1.5 g of low sulfonate lignin alkali powder were mixed with 9.5 g of formic acid in separate vials and stirred on a hotplate for 24 h at 100 °C. Then, the solutions were filtered using a 1.0 μm GD/X syringe filter. After that, 1.5 g of nylon 6 was added to each filtered solution and they were left on a hotplate at 75 °C to homogenize completely.

Sericin solution was a blend of 1.5 g silk sericin mixed with 9.5 g of formic acid under the same conditions as the zein solution described above. Then, 1.5 g of nylon 6 pellets were added to the solution and left on the hotplate similarly to zein solutions.

To prepare a BSA solution, 10 wt % PVA solution in de-ionized water was prepared by stirring 1.0 g of PVA in 9.0 g of water for 4 h at $80\,^{o}C$. Then, 1.0 g of BSA powder was added to the solution at room temperature and stirred for 10 min.

20 wt% PET solution was prepared by mixing 2.0 g of PET with 8 g of solution comprised of 30 wt% trifluoroacetic acid (TFA), 30 wt% dichloroacetic acid (DCA), and 40 wt% dichloromethane (DCM). The solution was kept at $55\,^{o}C$ on a hotplate for 4 h.

To produce soy protein/PET solution, 0.5 g of SP 781 was mixed with 2.0 g of dichloroacetic acid at high temperature ($100\,^{o}C$). SP solution was then added to 20 wt% solution of pure PET and left at $55\,^{o}C$ for 2 h to become completely homogeneous.

9.1.3. Solution Blowing & Sample Preparation

Solution blowing setup was the same as in the previous works of this group (Sinha-Ray et al., 2010; Sinha-Ray et al., 2011). To form monolithic nanofibers, 13G stainless steel needle was placed coaxially inside an annular nozzle. Solution was pumped into the needle, while air supplied from a high pressure line was issued through the annular nozzle using an upstream regulator. At the needle exit, the solution was exposed to a coaxial high-speed turbulent air jet. The solution jet was stretched and bent due to the aerodynamic forces (Sinha-Ray et al., 2010; Sinha-Ray et al., 2011). To form core-shell nanofibers, 18G stainless steel needle was located coaxially inside the 13G needle in the above-mentioned setup, while the outside coaxial nozzle was still used to issue air jet.

Core solution was issued through the 18G needle, whereas the shell solution was issued from the 13G needle. For both monolithic and core-shell nanofiber blowing, the upstream pressure was kept constant at 2.0 bar and solutions were issued at the rate of 4 ml/h. As a result, monolithic and core-shell nanofibers of 300-500 nm in diameter were formed.

Nanofibers were collected on a rotating drum covered with an aluminum foil, with a linear velocity at the circumference of about 2.9 m/s. The drum was placed 20 cm below the needle exit. As a result, collected nanofibers were partially oriented and pre-stretched in the winding direction. In each case, 5 ml solution was issued from the needle to form nanofiber mat. Collected nanofiber mats were removed from the foil as shown in Fig. 9.1 and cut into rectangular pieces with 5-10 mm width and 15-20 mm length. The thickness of these nanofiber mats was in the range 0.2-0.3 mm. Note that solution-blown BSA/PVA (50/50 wt%) nanofibers were collected on a solid substrate underneath the needle exit as randomly oriented nanofibers, as shown in Fig. 9.1.

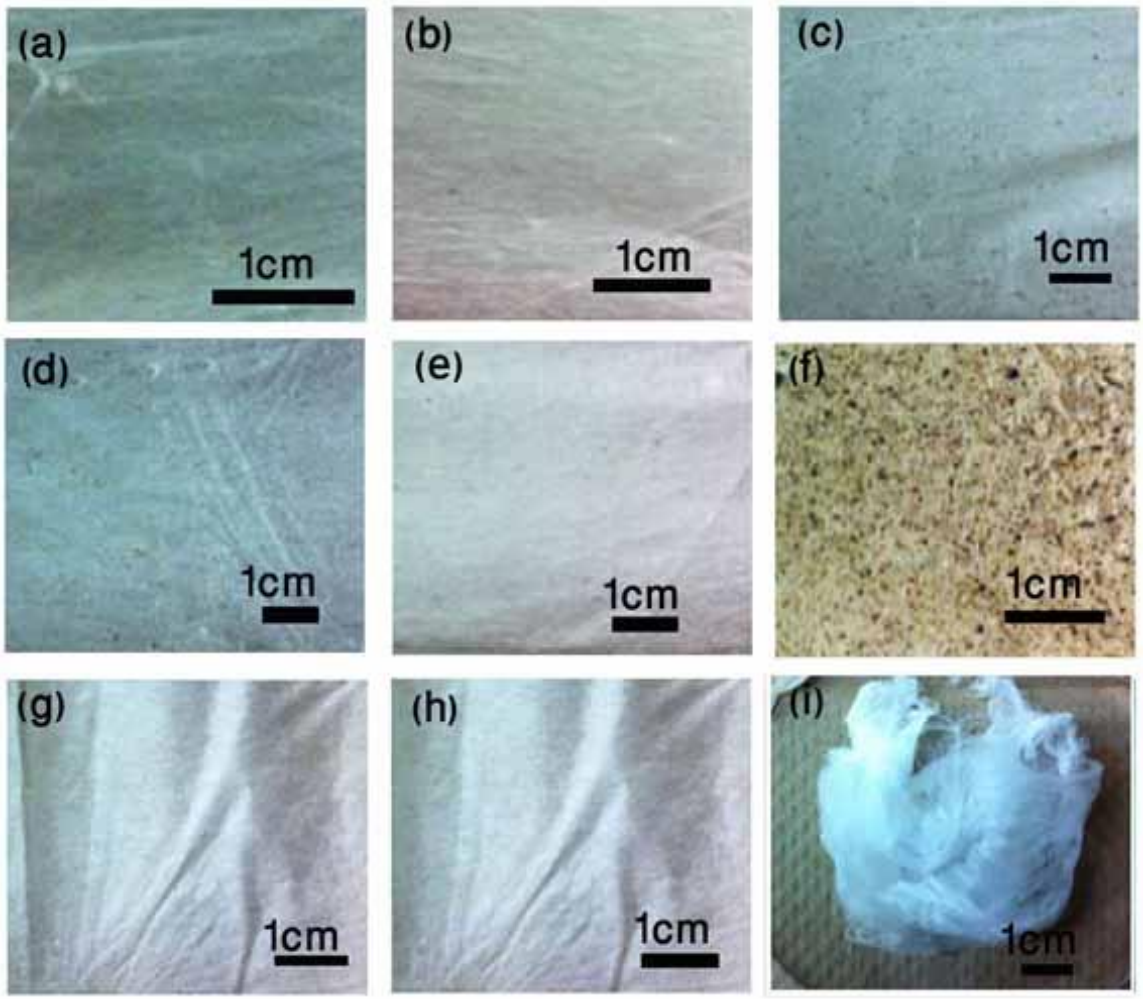

Figure 9.1. Panel (a) shows solution-blown cellulose acetate/PAN (50/50 wt %) nanofiber mat. Panel (b) - cellulose acetate/PAN (30/70 wt %) nanofiber mat. Panel (c) - soy protein/zein/nylon 6(25/25/50 wt %) nanofiber mat. Panel (d) - zein/nylon 6 (57/43 wt %) nanofiber mat. Nanofiber mats in panels (a)-(d) are comprised of monolithic nanofibers. Panel (e) depicts core/shell zein/nylon 6 nanofiber sample, panel (f) - lignin/nylon 6 (50/50 wt %) sample, panel (g) - zein/silk sericin/nylon 6 (25/25/50 wt %) nanofibers, panel (h) silk sericin/nylon 6 (50/50 wt %), and panel (i) BSA/PVA (50/50 wt %) nanofiber samples.

9.1.4. Tensile Tests & Mechanical Characterization

Rectangular nanofiber mat samples underwent uniaxial stretching test similarly to our previous work (Khansari et al., 2012). The experiment was conducted using Instron (model 5942) with cross-head speed of 1.0 mm/min at room temperature and humidity. The stretching continued until total failure of the samples. Stress-strain curves of the samples were measured, as well as the maximum strain and stress at rupture ($\varepsilon_{rupture}, \sigma_{xx,rupture}$, respectively). These features were used to characterize mechanical properties of biopolymer nanofibers using the phenomenological model discussed in (Khansari et al., 2012). As a result, Young's modulus (E) and yield stress (Y) were found from the experimental stress-strain curves. For each specific type of nanofiber sample, 15 rectangular nanofiber mats underwent tensile testing and the average values for the mechanical properties were acquired. It is emphasized that according to the SEM images of soy protein/nylon 6 nanofibers shown in (Khansari et al., 2012), only 50% of the sample thickness is occupied with fibers, which implies that the applied stress is supported by only one half of the samples' thickness, which was accounted for in data processing. For planar strips, stress-strain dependence in the elastic and plastic domain is described by the following equation (Khansari et al., 2012)

$$\sigma_{xx} = \sqrt{\frac{8}{3}} Y \tanh\left(\sqrt{\frac{2}{3}} \frac{E}{Y} \varepsilon\right) \tag{9.1}$$

where σ_{xx} is tensile stress, and ε is tensile strain.

9.1.5. Post-Processing of Solution-Blown Biopolymer Nanofiber Samples

In order to further improve the overall mechanical properties of biopolymer nanofibers, the samples underwent cold and hot drawing before some tensile tests. The samples were stretched up to 1% strain with five equal intervals in between. The samples were kept at each intermediate strain for 5 min. This pre-stretching was conducted at room temperature (cold drawing), as well as at temperatures lower and higher than the glass transition temperature of the host polymer. Drawing of macroscopic nylon and polyethylene fibers has been extensively discussed in (Ziabicki, 1976). It was shown that the optimal drawing temperature is mostly close to the polymer glass transition temperature. In most cases, drawing increases crystallinity of polymer fibers as well as their strength.

9.1.6. Optical Observations

Morphology of biopolymer nanofibers was observed with JEOL JSM-6320F scanning electron microscope under 8 kV accelerating voltage. Samples were sputter-coated by platinum with 8 nm thickness before undergoing observation. Fig. 9.2 shows monolithic and core-shell solution-blown protein nanofibers.

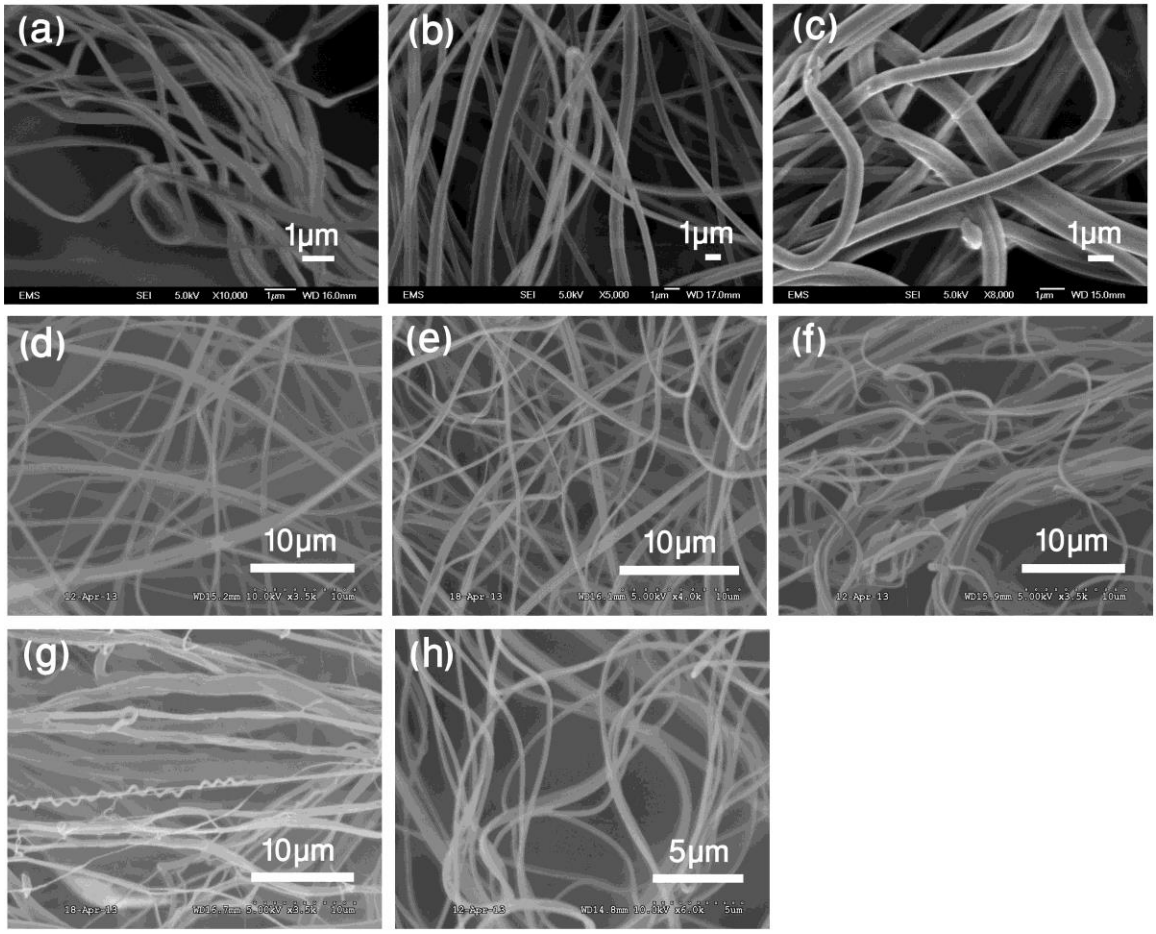

Figure 9.2. SEM micrographs of solution-blown nanofibers. (a) Monolithic cellulose acetate/PAN (50/50 wt/wt%) nanofibers, (b) Monolithic zein/nylon 6 (57/43 wt/wt%) nanofibers, (c)monolithic lignin/nylon 6 (50/50 wt/wt%) nanofibers, (d) monolithic silk sericin/nylon 6 (50/50 wt/wt%), (e) monolithic zein/silk sericin/nylon 6 (25/25/50 wt%), (f) monolithic soy protein/PET (20/80 wt/wt%), (g) monolithic BSA/PVA (50/50 wt/wt%), and (h) core-shell zein/nylon 6 (core: 70 wt% zein) nanofibers..

9.2. Results & Discussion

9.2.1. Mechanical Characterization of Biopolymer Nanofiber Samples

Table 9.1 summarizes the overall mechanical properties of different biopolymer nanofiber mats with various components and contents. The table includes data for both solution-blown monolithic and core-shell nanofiber samples which did not undergo any post-treatment. Following tensile test as discussed above, stress-strain behavior for solution-blown protein-based nanofiber samples are shown in Fig. 9.3.

Table 9.1. Average mechanical properties for biopolymer-containing monolithic and core-shell nanofiber mats with various compositions and contents.

Sample	Content (wt %)	Solvent	Ave. Width (mm)	Ave. Thickness (mm)	Ave. Young's Modulus E; (MPa)	Ave. Yield Stress Y; (MPa)	Max. Strain at Rupture (%)	Max. Stress at Rupture (MPa)
Zein/Nylon	40/60	Formic acid	8.44	0.20	12.53±2.55	0.16±0.07	2.21±0.76	0.19±0.06
Zein/Nylon	57/43	Formic acid	6.47	0.20	3.38±1.69	0.10±0.02	5.56±1.44	0.13±0.02
Zein/Nylon	66/34	Formic acid	7.08	0.20	2.16±0.74	0.04±0.01	4.28±0.92	0.06±0.01
Core-Shell Zein	Core: 70/30	Formic acid	6.44	0.20	6.05±0.69	0.30±0.01	12.22±0.62	0.47±0.03
SP/Zein/Nylon	25/25/50	Formic acid	6.93	0.20	10.90±2.54	0.23±0.04	5.63±2.37	0.35±0.06
Zein/Silk Sericin/Nylon	25/25/50	Formic acid	6.50	0.15	20.46±4.88	0.24±0.05	2.50±0.49	0.35±0.60
Silk Sericin/Nylon	50/50	Formic acid	5.29	0.30	11.02±2.16	0.22±0.06	2.73±0.41	0.28±0.07
Lignin/Nylon	25/75	Formic acid	5.53	0.16	23.39±6.49	0.42±0.08	4.13±1.15	0.61±0.10
Lignin/Nylon	50/50	Formic acid	6.13	0.15	9.78±2.41	0.22±0.02	13.72±3.76	0.38±0.04
SP/PET	20/80	TFA/AC/ DCM	6.55	0.20	28.59±2.63	0.32±0.11	0.88±0.05	0.27±0.04
Cellulose AC/PAN	30/70	DMF	7.90	0.15	3.47±2.67	0.23±0.01	4.50±1.17	0.15±0.05
Pure PET	100	TFA/AC/ DCM	7.56	0.20	28.14±3.24	0.37±0.07	2.28±0.31	0.50±0.008

9.2.3. Discussion

Average Young's modulus of soy protein/nylon 6 (40/60 wt/wt %) nanofiber samples measured in tensile tests was reported in (Khansari et al., 2012) as 19.56±6.48 MPa. Young's modulus of zein/nylon 6 (40/60 wt/wt %) samples, which is 12.53±2.55 MPa, is lower than that of soy protein nanofiber samples containing the same amount of bio-polymer. As zein content increased and nylon 6 content decreased correspondingly in the nanofiber samples, Young's modulus and the average yield stress decreased. At zein content of 66% in the samples, Young's modulus decreased almost tenfold compared to samples with 40% zein content. The average yield stress of zein-containing samples follows the same trend: a four-times decrease occurred in the yield stress for 66% zein-containing samples compared to the samples which contained 40% zein. Although core-shell zein/nylon 6 nanofiber mats contained a higher amount of zein (i.e. 70%), their Young's modulus was found to be higher than that of the monolithic nanofibers containing almost the same amount of zein. The core-shell structure with zein in the core is definitely beneficial, since monolithic zein nanofibers are generally weaker than, for example, soy-protein-containing ones.

For those monolithic nanofibers which were comprised of both zein and soy protein, the average Young's modulus was found to be higher than that of the zein-containing nanofibers and lower than the one reported in (Sinha-Ray et al., 2012) as an average value of Young's modulus for soy protein-nylon 6 (50/50 wt %) nanofiber mats.

Lignin nanofibers revealed lower Young's modulus compared to that of comparable soy protein-containing samples as reported in (Sinha-Ray et al., 2012), yet the strength of lignin/nylon 6 (50/50 wt %) samples is slightly higher than that of the zein-containing

samples with almost the same content percentage. Higher nylon 6 content in the lignin nanofiber mats [lignin/nylon 6 (25/75 wt/wt %)] led to stronger samples with the average Young's modulus of 23.39±6.49 MPa.

Silk protein/nylon 6 (50/50 wt %) samples revealed the average strength close to that of lignin-containing nanofiber mats with the same content.

Solution-blown PET and soy protein/PET nanofiber mats revealed higher Young's moduli compared to solution-blown nylon 6 nanofibers reported in (Khansari et al., 2012), as well as soy protein/nylon 6 samples.

Monolithic cellulose acetate/PAN samples showed lower Young's modulus compared to the other bio-polymer samples with nylon 6 or PET as a synthetic part of the nanofibers.

Sample stress-strain behavior for various protein-based nanofiber mats is shown in Fig. 9.3.

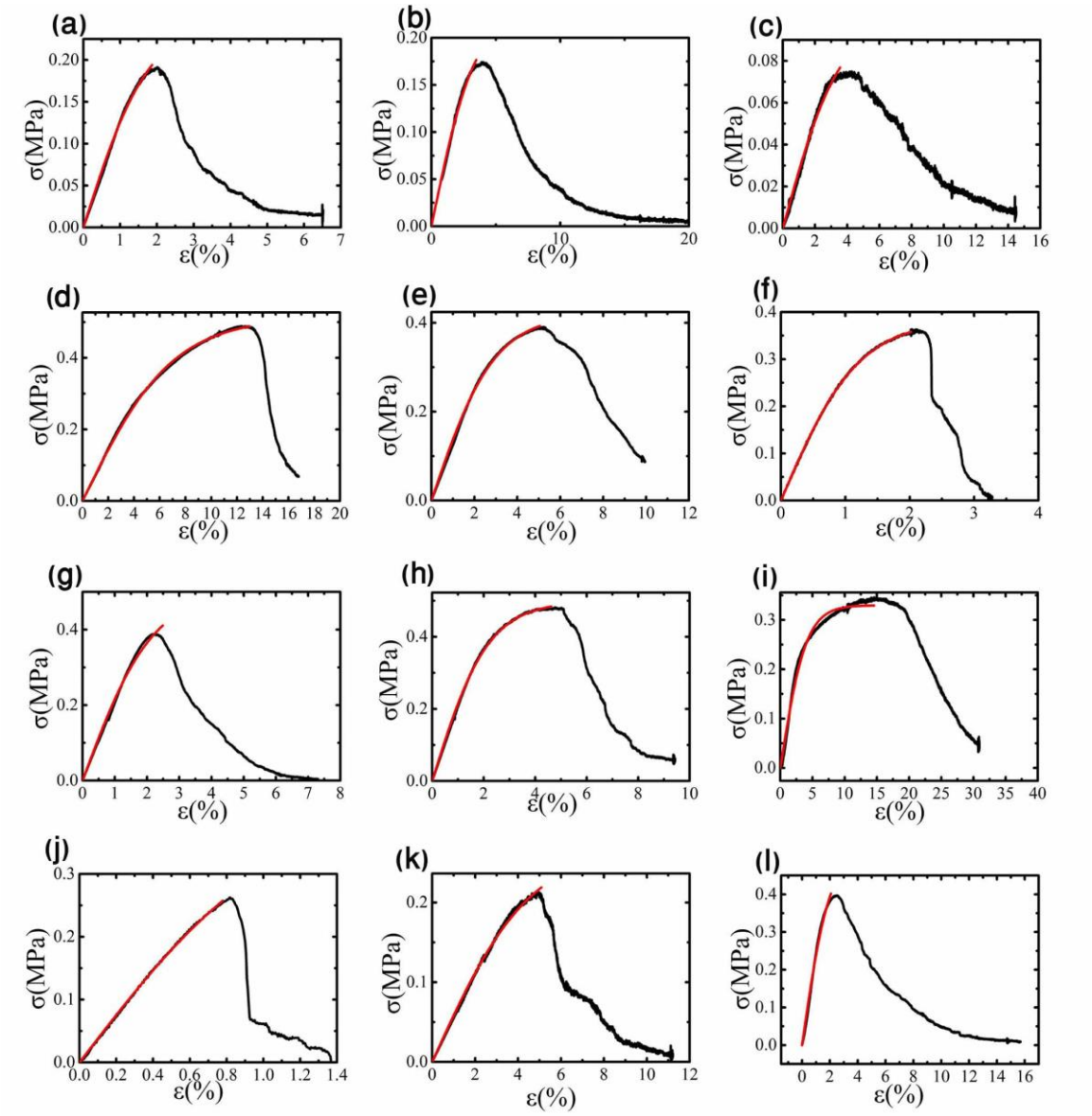

Figure 9.3. Stress-strain behavior for plant-based protein solution blown nanofiber mats for (a) monolithic zein/nylon 6 (40/60 wt%), (b) monolithic zein/nylon 6 (57/43 wt%), (c) monolithic zein/nylon 6 (66/34 wt%), (d) core/shell zein/nylon 6 (70 wt% zein in core), (e) monolithic soy protein/zein/nylon 6 (25/25/50 wt%), (f) monolithic silk sericin/zein/nylon 6 (25/25/50 wt%), (g) monolithic silk sericin/nylon 6 (50/50 wt%), (h) monolithic lignin/nylon 6 (25/75 wt%), (i) monolithic lignin/nylon 6 (50/50 wt%), (j) soy protein/PET (20/80 wt%), (k) monolithic cellulose acetate/PAN (30/70 wt%), (l)

monolithic pure PET samples. In all the panels, black line depicts experimental stress-strain curve whereas red line shows phenomenological model (Eq.1) fitted with the tensile test results.

9.2.4. Cold- and Hot Drawing of Nanofiber Mats

The effect of drawing on soy protein/PET (20/80 wt/wt %) nanofibers is reported in Table 9.2. All these samples were pre-stretched up to 1% strain with five equal intervals in between. Drawing of soy protein/PET nanofiber samples was conducted 45, 55, 80, and 115 $^{\circ}$C (hot drawing). Maximum increase in samples' Young's modulus was observed at 80 $^{\circ}$C: the average Young's modulus was doubled compared to the non-treated samples. Note that glass transition temperature for PET is in the range 76-81°C. The stress-strain behavior for soy/PET nanofiber samples which underwent tensile testing is demonstrated in Fig. 9.4. For control, hot and cold drawn samples were compared with non-treated ones. Also the stress-strain curves were fitted with Eq.1 as described above.

Table 9.3 and Fig. 9.5 compare the results for cold and hot drawing in case of pure solution-blown nylon 6 nanofiber samples. These samples underwent drawing procedure following similar trend as mentioned above and the results are reported in Table 9.3. Note that glass transition temperature for nylon 6 is 47°C, yet drawing post-treatment did not affect the samples' mechanical properties significantly.

Table 9.2. Overall mechanical properties of soy protein/PET (20/80 wt/wt %) nanofiber mats that underwent cold and hot drawing in comparison to non-treated samples.

Sample	Average Width (mm)	Average Thickness (mm)	Average Young's Modulus E; (MPa)	Average Yield Stress Y; (MPa)	Max. Strain at Rupture (%)	Max. Stress at Rupture (MPa)
Non-treated	6.55	0.20	28.59±2.63	0.32±0.11	0.88±0.05	0.27±0.04
Cold Drawn	6.47	0.20	28.96±1.80	0.41±0.09	0.83±0.12	0.25±0.06
Hot Drawn at 45°C	6.77	0.20	30.42±7.3	0.50±0.29	0.88±0.07	0.29±0.04
Hot Drawn at 55°C	5.5	0.20	44.57±10.1	0.27±0.04	0.29±0.06	0.29±0.06
Hot Drawn at 80°C	5.71	0.20	64.05±9.74	0.46±0.16	0.518±0.1	0.37±0.05
Hot Drawn at 115°C	5.26	0.20	55.98±13.23	0.41±0.13	0.28±0.02	0.23±0.06

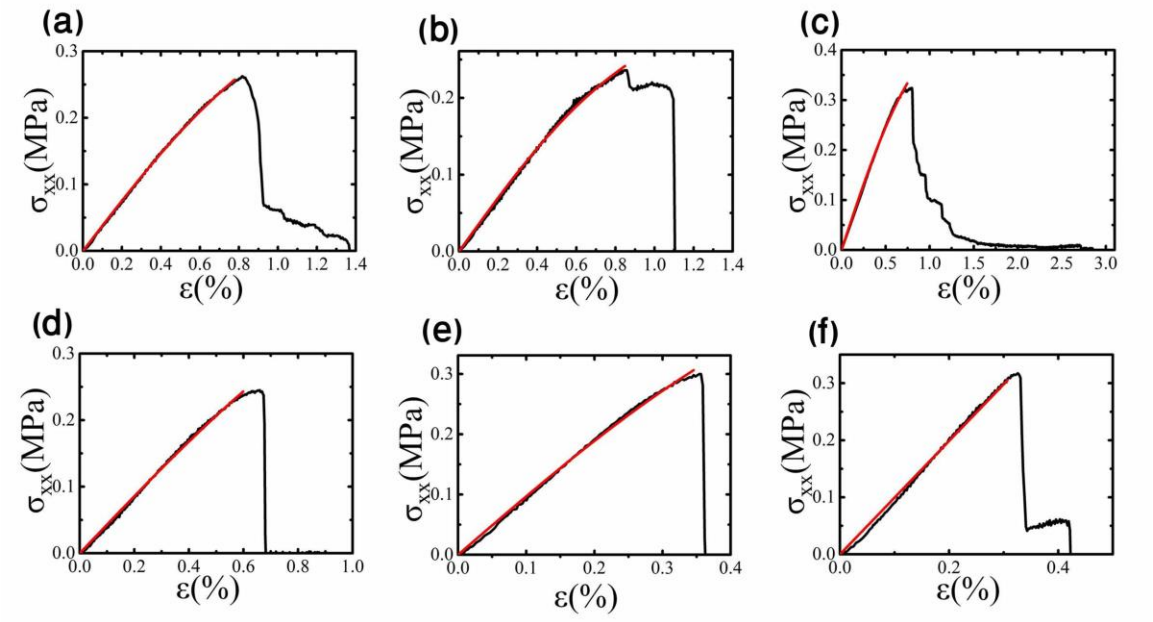

Figure 9.4. Stress-strain curves for soy-PET (20/80 wt%) nanofiber mats which underwent cold and hot drawing process. In all the panels, black curves are representative of experimental data, while black curves show the fitting of Eq.1 to the experiments. Panel (a) shows non-treated samples, panel (b) – cold drawn samples, panel (c) - hot drawn samples at 45°C, panel (d) - hot drawn samples at 55°C, panel (e) - hot drawn samples at 80°C, panel (f) -hot drawn samples at 115°C.

Table 9.3. Average mechanical properties of solution-blown nylon 6 nanofiber mats that were post-treated with cold and hot drawing procedure compared to the samples from the same batch that did not undergo drawing treatment.

Sample	Average Width (mm)	Average Thickness (mm)	Average Young's Modulus E; (MPa)	Average Yield Stress Y; (MPa)	Max. Strain at Rupture (%)	Max. Stress at Rupture (MPa)
Non-treated	9.53	0.20	15.06±2.68	1.4±0.06	14.24±2.27	1.45±0.03
Cold Drawn	7.66	0.20	19.091±1.51	1.38±0.09	12±2.04	1.28±0.06
Hot Drawn at 45°C	7.71	0.20	18.42±5.22	1.27±0.06	11.48±2.33	1.34±0.08
Hot Drawn at 55°C	7.52	0.20	18.97±3.43	1.37±0.10	12.91±2.04	1.45±0.11
Hot Drawn at 80°C	6.92	0.20	15.77±2.58	1.25±0.04	13.03±1.85	1.25±0.05
Hot Drawn at 115°C	7.39	0.20	22.65±3.45	1.40±0.10	10.57±1.81	1.50±0.18

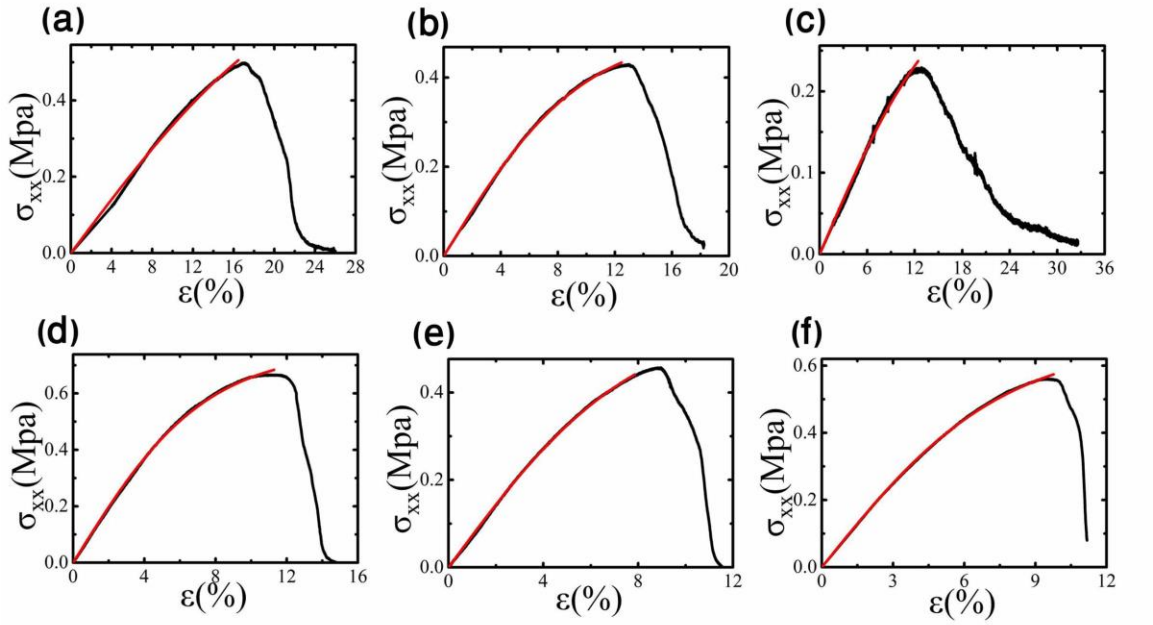

Figure 9.5. Mechanical behavior of pure nylon 6 nanofiber mats under uniaxial elongation experiment. It is shown that cold or hot drawing did not affect stress-strain behavior of nylon 6 samples significantly. In all the panels, black curves show

experimental results and red curves depict the theoretical model (Eq.1) being fitted to the experiments. Panel (a) demonstrates non-treated nylon 6 samples, panel (b) – cold drawn samples, panel (c) hot drawn at 45°C, panel (d) - hot drawn at 55°C, panel (e) - hot drawn at 80°C, panel (f) - hot drawn at 115°C.

9.3. Conclusion

Solution blowing was successfully applied to form nanofiber mats comprised of different plant- and animal-derived proteins. Soy protein, cellulose acetate, zein, silk sericin, lignin, and different blends of them were used to produce monolithic and core-shell plant-protein-derived nanofibers. These bio-polymers were mixed with such synthetic polymers as nylon 6 and PET to enhance their overall mechanical properties. Bovine serum albumin (an animal-derived protein) also underwent solution blowing and was used to form BSA/PVA (50/50 wt%) nanofibers, which are of interest for wound dressing, drug carriers, and other applications due to their biocompatibility and biodegradability. Solution blowing of pure synthetics polymers was also demonstrated in the present work by producing PET nanofibers. Their tensile strength was also measured for control. All the above-mentioned nanofibers were collected as nonwoven mats and their Young's modulus and yield stress were estimated using the phenomenological Prager equation. Forming nanofibers from plant- and animal-derived proteins using solution blowing holds great promise for their industrial application, since these biocompatible and biodegradable nanofibers can be produced at rates incomparably higher than those of electrospinning.

10. CONCLUSION

In this dissertation, proteins extracted from plant and animal tissues were used as raw materials to form polymeric nonwovens. Solution blowing was used as the main method to produce nano-scaled protein-based fibers. Monolithic and core-shell biopolymer nanofibers were produced and collected on a rotating drum with a specified linear velocity at the collector's surface (~ 2.9 m/s). The nanofibers then underwent tensile tests in order to reveal their overall mechanical properties. Young's modulus, yield stress, and maximum stress and strain at rupture point for the samples were measured. Two different theoretical models were developed in this work to describe the stress-strain curves of soy protein-containing nanofiber mats. The phenomenological model was capable of predicting elastic and plastic behavior of biopolymer nanofiber samples up to rupture point. This type of model is rooted in the 'hypo-elastic' model for solids developed by Prager. A novel micromechanical model is based on the fact that rupture of individual bonds in nanofibrous structure leads to plasticity in the nonwoven samples. Therefore, the onset of plasticity is interpreted as an outcome of bond ruptures in the nanofiber samples.

The effect of experimental parameters on the overall mechanical properties of polymeric nanofibers, specifically soy protein-based nanofiber samples, was also investigated. Cross-head speed in the tensile test, the effect of pre-stretching and the winding velocity of the rotating collector are the parameters of interest in the present work. It was shown that a higher stretching rate results in higher resistance of nonwoven samples to the applied stress which leads to a higher Young's modulus of the samples.

Pre-stretching in the elastic region also enhanced mechanical behavior of polymeric samples. Besides, it was shown that there is an optimum winding velocity in order to collect the samples, since the rotating collector helped to align the samples in the winding direction which enhanced strength to the samples.

Mechanical characteristics of soy protein-based nanofiber mats were compared with those of pure nylon 6 samples which were produced and collected similarly. It was shown that the soy protein nanofibers had comparable mechanical properties to those of nylon 6 samples. This comparison implies that soy protein nanofiber mats can be used as an alternative to synthetic products that are currently widely produced in industry.

Although soy protein nanofiber samples revealed comparable mechanical properties with those of synthetic materials, it is of importance to further enhance their mechanical properties in order to actually apply them in construction industry, automobiles, and civil infrastructures. Therefore, in this work cross-linking agents were used as enhancers to form covalent and ionic bonds in the protein fibrous network. Proteins consist of amino acids with side chains that might be polar or charged. Consequently, these materials can undergo chemical treatment to form intra- and intermolecular bonds in the protein structures. This leads to aggregation in protein network and improved tensile characteristics of these types of biodegradable materials. Soy protein-based nanofiber mats were treated with four different crosslinking agents. Formaldehyde and glyoxal were used as covalent crosslinkers, whereas sodium borohydride and zinc sulfate were representative of ionic crosslinkers. It was shown that ionic bonds formed in the protein structure were stronger than covalent bonds. This was inferred by the fact that soy protein nanofiber samples which were treated by ionic crosslinkers revealed significant increase

in the average Young's modulus. The addition of sodium borohydride and zinc sulfate led to the 7-fold increase in the average Young's modulus of solution-blown soy protein nanofibers. Similar samples which were treated by covalent crosslinkers (i.e. formaldehyde and glyoxal) showed only a 5-fold increase in their overall strength.

In addition, the effect of heat treatment on cross-linked soy protein nanofibers was also investigated. Due to the heat exposure, covalent or ionic bonds formed between protein side chains were partly broken which results in a lower strength of the samples.

In order to further apply protein-based samples in industrial applications, it is of importance to investigate their humidity resistance, which was explored in this thesis. Soy protein is intrinsically partly-hydrophilic due to the presence of polar amino acid side chains in its structure. When soy protein samples were immersed in water for 24 h, the loss of material of about 20% was observed for protein-based nanofiber mats. This could be a favorable or an adverse effect based on the type of application defined for the material.

Apart from chemical treatment of protein nanofiber samples, the effect of physical crosslinking on soy protein nanofibers was investigated. Thermal calendaring is a widely-used method in nonwoven industry to enhance the strength of textiles. A modified procedure of thermal calendaring was applied to soy protein samples. They were heat treated under pressure for 1 min. This resulted in about 50% increase in the samples' strength. Wet conglutination was another method to physically bond nanofibers. Soy protein/nylon 6 samples were soaked and left under pressure to dry out. This led to 65% increase in the strength of the samples. In addition, sustainability of samples in extreme humidity and elevated temperature was studied. It was shown that the samples kept their

average strength after 1 h of water immersion at $80^{\circ}C$. Note that samples were plasticized while exposed to water.

The antibacterial effect of biopolymer nanofibers decorated with silver nanoparticles was addressed as well. The effect of silver-coated soy protein-based nanofibers against E. coli was elucidated in the work of former PhD student, Dr.Yiyun Zhang using the samples developed in the present work. Here, in addition, durability of silver-coated nanofiber samples in aqueous medium was investigated and no detectable amounts of silver nanoparticles were leached from soy protein nanofiber surface.

To demonstrate the presence of soy protein in the solution-blown nanofiber mats, one Chapter of the present work is devoted to modification of the Bradford method used to track the protein in the samples.

A part of this thesis aimed at potential applications of soy protein nanofibers in biomedical field. Soy protein monolithic and core-shell nanofibers were produced via 'solution blowing' method and used as carriers for a model drug. Rhodamine B dye was used as the model drug in this case because it can be traced by fluorescence. Soy protein nanofibers were loaded with the dye and immersed in aqueous medium in order to investigate drug release kinetics. In addition, hydrophobic PET-based nanofibers were produced via electrospinning and were loaded with Rhodamine B and riboflavin in separate sets of experiments. Note that riboflavin is fluorescence-sensitive drug model which partly dissolves in aqueous medium. The mechanism of dye/drug release from porous nanofibers' surface was studied and it was shown that desorption from the surface of fibers acts as the limiting stage during the release process. In order to the predict release mechanism, the model developed by (Srikar, et al., 2009) was modified to

account for the presence of porogens (PEG and PEO) used in the present experiments. The modified theory was able to capture major experimental trends.

Finally, the last part of the thesis was an effort to encompass various plant- and animal-based proteins and explore whether they can be converted into nanofibers via Solution Blowing. Cellulose acetate, lignin, zein, and silk sericin were used as plant-based protein, while bovine serum albumin represented animal-based protein. Monolithic and core-shell nanofibers of these protein macromolecules with synthetic materials such as nylon 6 and poly(ethylene terephthalate) were produced. The samples then underwent tensile test to reveal their stress-strain dependences. This is of importance in order to evaluate the strength of various protein-based nanofiber nonwovens under specified conditions. In addition, cold and hot drawing was applied to protein-based and pure synthetic nanofibers in order to improve their overall mechanical characteristics.

CITED LITERATURE

Ahmed, I., Decker, J., Morris, D., **1994**, How much does it take to make a gallon of soydiesel? Report for the National SoyDiesel Development Board, Jefferson, Missouri.

Alemdar, A., Sain, M., **2008**, Isolation and characterization of nanofibers from agricultural residues – wheat straw and soy hulls. Bioresource Technology 99, 1664–1671.

Anderson, J.M., Shive, M.S., **1997**, Biodegradation and biocompatibility of PLA and PLGA microspheres. Advanced Drug Delivery Reviews 28, 5-24.

Andrady, A.L., **2007**, Physical properties of polymers handbook. Chapter 56 (Biodegradability of polymers) 951-964, Springer.

Arana, J., Melian, J.A.H., Rodrıguez, J.M.D., Diaz, O.D., Viera, A., Pena, J.P., Sosa, P.M.M., Jimenez, V.M., **2002**, TiO2-photocatalysis as a tertiary treatment of naturally treated wastewater. Catalysis Today 76, 279-289.

Bedino, J.H., **2003**, Embalming chemistry: Glutaraldehyde versus formaldehyde. Official publication of research & educational department, The Champion Co. 649, 2614-2621.

Bennett, T.P., **1967**, Membrane filtration for determining protein in the presence of interfering substances. Nature 213, 1131-1132.

Berg, J.M., Shi, Y., **1996**, The galvanization of biology: A growing appreciation for the roles of zinc. Science Magazine 271, 1081-1085.

Bhardwaj, N., Kundu, S.C., **2010**, Electrospinning: a fascinating fiber fabrication technique. Biotechnology Advances 28, 325-347.

Bhat, G.S., Jangala, P.K., Spruiell, J.E., **2004**, Thermal bonding of polypropylene nonwovens: effect of bonding variables on the structure and properties of the fabrics. Journal of Applied Polymer Science 92, 3593-3600.

Bhat, G.S., Malkan, S.R., **2002**, Extruded continuous filament nonwovens: advances in scientific aspects. Journal of Applied Polymer Science 83, 572-585.

Bhatkhande, D.S., Pangarkar, V.G., Beenackers, A.A., **2001**, Photocatalytic degradation for environmental applications – a review. Journal of Chemical Technology and Biotechnology 77, 102-116.

Bhatnagar, A., Sain, M., **2005**, Processing of cellulose nanofiber-reinforced composites. Journal of Reinforced Plastics & Composites 24, 1259-1268.

Boland, E.D., Telemeco, T.A., Simpson, D.G., Wnek, G.E., Bowlin, G.L., **2004a**, Utilizing acid pretreatment and electrospinning to improve biocompatibility of poly(glycolic acid) for tissue engineering. Journal of Biomedical Materials Research Part B: Applied Biomaterials 71B, 144–152.

Boland, E.D., Matthews, J.A., Pawlowski, K.J. Simpson, D.G., Wnek, G.E., Bowlin, G.L., **2004b**, Electrospinning collagen and elastin: preliminary vascular tissue engineering. Frontiers in Bioscience 9, 1422-1432.

Bradford, M.M., **1976**, A rapid and sensitive method for the quantitation of microgram quantities of protein utilizing the principle of protein-dye binding. Analytical Biochemistry 72, 248-254.

Braun, J.L., Holtman, K.M., Kadla, J.F., **2005**, Lignin-based carbon fibers: Oxidative thermostabilization of kraft lignin. Carbon 43, 385–394.

Burgess, D.J., Davis, S.S., Tomlinson, E., **1987**, Potential use of albumin microspheres as a drug delivery systems. I. Preparation and in vitro release of steroids. Internationa Journal of Pharmaceutics 39, 129–136.

Cancedda, R., Dozin, B., Giannoni, P., Quarto, R., **2003**, Tissue engineering and cell therapy of cartilage and bone. Matrix Biology 22, 81-91.

Caplan, A.I., **2000**, Tissue engineering designs for the future: new logics, old molecules. Tissue Engineering 6, 1-8.

Chabba, S., Matthews, G.F., Netravali, A.N., **2005**, 'Green' composites using cross-linked soy flour and flax yarns. Green Chemistry 7, 576-581.

Chandra, R., Rustgi, R., **1998**, Biodegradable Polymers. Progress in Polymer Science 23, 1273–1335.

Charis, M.N., Cheng, H.S., Aleksandra, A.D., Ng, A.M.C., Fredrick, C.C.L., Chan, W.K.J., **2011**, Multicomponent antimicrobial transparent polymer coatings. Journal of Applied Polymer Science 122, 1572-1578.

Chen, G., Liu, H., **2008**, Electrospun cellulose nanofiber reinforced soybean protein isolate composite film. Journal of Applied Polymer Science 110, 641-646.

Cho, D., Nnadi, O., Netravali, A., Joo, Y.L., **2010**, Electrospun hybrid soy protein/PVA fibers. Macromolecular Materials and Engineering 295, 763-773.

Cho, S.Y., Rhee, C., **2002**, Sorption characteristics of soy protein films and their relation to mechanical properties. Lebensm.-Wiss. u.-Technol. 35, 151-157.

Ciannamea, E.M., Stefani, P.M., Ruseckaite, R.A., **2010**, Medium-density

particleboards from modified rice husks and soybean protein concentrate-based adhesives. Bioresource Technology 101, 818–825.

Compton, S.J., Jones, C.G., **1985**, Mechanism of dye response and interference in the Bradford protein assay. Analytical Biochemistry 151, 369-374.

Consden, R., Gordon, A.H., Martin, A.P., **1946**, The identification of amino-acid derived from cystine in chemically modified wool. Biochemical Journal 40, 580-584.

Cui, W., Zhou, Y., Chang, J., **2010**, Electrospun nanofibrous materials for tissue engineering and drug delivery. Science and Technology of Advanced Materials 11, 014108-014119.

Curry, S., Brick, P., Franks, N.P., **1999**, Fatty acid binding to human serum albumin: new insights from crystallographic studies. Biochimica et Biophysica Acta 1441, 131-140.

de Carvalho, R.A., Grosso, C.R.F., **2006**, Properties of chemically modified gelatin films. Brazilian Journal of Chemical Engineering 23, 45-53.

Dewanjee, M.K., Gross, D.R., Zhai, P., Lanzo, S., Shim, H., Park, K., Schaeffer, D.J., Twardock, A.R., **1999**, Thrombogenicity of polyethylene oxide-bonded Dacron sewing ring in a mechanical heart valve. The Journal of Heart Valve Disease 8, 324–

330.

Doshi, J., Reneker, D.H., **1995**, Electrospinning process and applications of electrospun fibers. Journal of Electrostatics 35, 151-160.

Dror, Y., Ziv, T., Makarov, V., Wolf, H., Admon, A., Zussman, E., **2008**, Nanofibers made of globular proteins. Biomacromolecules 9, 2749-2754.

Duzyer S., Hockenberger A., Zussman E., **2011**, Characterization of solvent-spun polyester nanofibers. Journal of Applied Polymer Science 120, 759-769.

Fang, J., Niu, H., Lin, T., Wang, X., **2008**, Applications of electrospun nanofibers. Chines Science Bulletin 53, 2265-2286.

Fedorova, N., Verenich, S., Pourdeyhimi, B., **2007**, Strength optimization of thermally bonded spunbonded nonwovens. Journal of Engineered Fibers and Fabrics 2, 38-48.

Filatov, Y., Budyka, A., Kirichenko, V., **2007**, Electrospinning of micro- and nanofibers: fundamentals and applications in separation and filtration processes. Begell House Inc., New York.

Flemming, R.G., Murphy, C.J., Abrams, G.A., Goodman, S.L., Nealey, P.F., **1999**, Effects of synthetic micro- and nano-structured surfaces on cell behavior. Biomaterials

20, 573-588.

Formhals, A., **1939**, Richard Schreiber-Gastell, assignee of forty-five one hundredths. Method and apparatus for spinning. United States patent US 2160962.

Formhals, A., **1940**, Richard Schreiber-Gastell, assignee of forty-five one hundredths. Artificial thread and method of producing same. United States patent US 2187306.

Formhals, A., **1943**, Richard Schreiber-Gastell and Formhals, A., assignees. Process and apparatus for preparing artificial threads. United States patent US 1975504.

Formhals, A., **1943**, Production of artificial fibers from fiber forming liquids. United States patent US 2323025.

Formhals, A., **1944**, Method and apparatus for spinning. United States patent US 2349950.

Fraonkel-Conrat, H., Olcoh, H.S., **1948**, The reaction of formaldehyde with proteins. V. cross-linking between amino and primary amide or guanidyl groups. Journal of the American Chemical Society 70, 2673-2684.

Frey, M.W., **2008**, Electrospinning cellulose and cellulose derivatives. Polymer Reviews 48, 378–391.

Friess, W., **1998**, Collagen-Biomaterial for drug delivery. European Journal of Pharmaceutics and Biopharmaceutics 45, 113-136.

Fuhrmann, G., Rothstein, A., **1968**, The mechanism of the partial inhibition of fermentation in yeast by nickel ions. Biochimica et Biophysica Acta (BBA) Biomembranes 163, 331-338.

Fujishima, A., Rao, T.N., Tryk, D.A., **2000**, Titanium dioxide photocatalysis, Journal of Photochemistry and Photobiology C: Photochemistry Reviews 1, 1-21.

Fujishima, A., Zhangb, X., Tryk, D.A., **2008**, TiO2 photocatalysis and related surface phenomena. Surface Science Reports 63, 515-582.

Fung, L.K., Saltzman, W.M., **1997**, Polymeric implants for cancer chemotherapy. Advanced Drug Delivery Reviews 26, 209-230.

Gandhi, M., Srikar, R., Yarin, A.L., Megaridis, C.M., Gemeinhart, R.A., **2009**, Mechanistic examination of protein release from polymer nanofibers. Molecular Pharmeceutics 24, 965-974.

Gassan, J., Bledzki, A.K., **1997**, Effect of cyclic moisture absorption desorption on the mechanical properties of silanized jute-epoxy composites. Composites Part A 28A, 1001-1005.

Gassan, J., Bledzki, A.K., **1999**, Effect of cyclic moisture absorption desorption on the mechanical properties of silanized jute-epoxy composites. Polymer Composites 20, 604-611.

Gennadios, A., Brandenburg, A.H., Weller C.L., Testin, R.F., **1993**, Effect of PH on properties of wheat gluten and soy protein isolate films. Journal of Agricultural and Food Chemistry 41, 1835-1839.

Gennadios, A., Ghorpade, V.M., Weller, C.L., Hanna, M.A., **1996**, Heat curing of soy protein films. American Society of Agricultural Engineers 39, 575-579.

Geraghty, D., Peifer, M.A., Rubenstein, I., Messing, J., **1981**, The primary structure of a plant storage protein: zein. Nucleic Acid Research 9, 5163-5174.

Gianazza , E., Viglienghi, V., Righetti, P.G., Salamini, F., Soave, C., **1977**, Amino acid composition of zein molecular components. Phytochemistry 16, 315-317.

Gilding, D.K., Reed, A.M., **1979**, Biodegradable polymers for use in surgery polyglycolic/poly (lactic acid) homo and copolymers. Polymer 20, 1459–1464.

Gombotz, W.R., Pettit, D.K., **1995**, Biodegradable polymers for protein and peptide drug delivery. Bioconjugate Chemistry 6, 332-351.

Grassman, W., Hannig, K., **1950**, A simple process for analysis of serum proteins and other protein mixtures. Naturwissenschaft 37, 496-497.

Green, A.E., **1956**, Hypo-elasticity and plasticity. Proceedings of the Royal Society of London. Series A, Mathematical and Physical 234, 46-59.

Haarstrick, A., Kut, O.M., Heinzle, E., **1996**, TiO2-assisted degradation of environmentally relevant organic compounds in wastewater using a novel fluidized bed photoreactor. Environmental Science and Technology 30, 817-824.

Han, S.O., Youk, J.H., Min, K.D., Kang, Y.O., Park, W.H., **2008**, Electrospining of cellulose acetate nanofibers using a mixed solvent of acetic acid/water: Effects of solvent composition on the fiber diameter. Materials Letter 62, 759-762.

Huang-Lee, L.L.H., Cheung, D.T., Nimni, M.E., **1990**, Biomedical changes and cytotoxicity associated with the degradation of polymeric glutaraldehyde derived crosslinks. Journal of Biomedical Materials Research 24, 1185-1201.

Huang, Z., Maness, P.C., Blake, D.M., Wolfrum, E.J., Smolinski, S.L., Jacoby, W.A., **2000**, Bactericidal mode of titanium dioxide photocatalysis. Journal of Photochemistry and Photobiology A: Chemistry 130, 163-170.

Huang, J., Zhang, L., Chen, F., **2003a**, Effects of lignin as a filler on properties of soy protein plastics. I. lignosulfonate. Journal of Applied Polymer Science 88, 3284–3290.

Huang, Z.M., Zhang, Y.Z., Kotaki, M., Ramakrishna, S., **2003b**, A review on polymer nanofibers by electrospinning and their applications in nanocomposites. Composites Science and Technology 63, 2223-2253.

Inoue, K., Hoshino, S., **1976**, Swelling of nylon 6 film due to water sorption. Journal of Polymer Science: Polymer Physics Edition 14, 1513-1526.

Jin, H.J., Chen, J., Karageorgiou, V., Altman, G.H., Kaplan, D.L., **2004**, Human bone marrow stromal cell responses on electrospun silk fibroin mats. Biomaterials 25, 1039-1047.

Jin, H.J., Fridrikh, S.V., Rutledge, G.C., Kaplan, D.L., **2002**, Electrospinning Bombyx mori silk with poly(ethylene oxide). Biomacromolecules 3, 1233-1239.

Kabra, K., Chaudhary, R., Sawhney, R.L., **2004**, Treatment of hazardous organic and inorganic compounds through aqueous-phase photocatalysis: A review. Industrial and Engineering Chemistry Research 43, 7683-7696.

Kadla, J.F., Kubo, S., Venditti, R.A., Gilbert, R.D., Compere, A.L., Griffith, W., **2002**, Lignin-based carbon fibers for composite fiber applications. Carbon 40, 2913–2920.

Kalapathy, U., Hettiarachchy, N.S., Myers, D., Hanna, M.A., **1995**, Alkali modification of soy protein and their adhesive properties on woods. Journal of American Oil Chemists' Society 72, 507–510.

Kamide, K., **2005**, Cellulose and cellulose derivatives, Elsevier B.V.

Kanjanapongkul, K., Wongsasulak, S., Yoovidhya, T., **2010**, Prediction of clogging time during electrospinning of zein solution: Scaling analysis and experimental verification. Chemical Engineering Science 65, 5217-5225.

Kaplan, D.L., **1998**, Biopolymers from renewable resources. Berlin, Springer.

Karck, M., Forgione, L., Haverich, A., **1993**, The efficacy of controlled antibiotic release: for prevention of polyethyleneterephthalate-(Dacron) related infection in cardiovascular surgery. Clinical Materials 13, 149-154.

Karki, B., Maurer, D., Kim, T.H., Jung, S., **2011**, Comparison and optimization of enzymatic saccharification of soybean fibers recovered from aqueous extractions. Bioresource Technology 102, 1228-1233.

Katz, A.K., Glusker, J.P., Beebe, S.A., Bock, C.W., **1996**, Calcium ion coordination: a comparison with that of beryllium, magnesium, and zinc. Journal of the American

Chemical Society 118, 5752-5763.

Kawasaki, K., Sekita, Y., Kanou, K., **1962**, The extension of nylon 6 as a function of the extent and nature of sorbed water. Journal of Colloid Science 17, 865-871.

Kawata, K., Osawa, M., Okabe, S., **2009**, In vitro toxicity of silver nanoparticles at noncytotoxic doses to HepG2 human hepatoma cells. Environmental Science and Technology 43, 6046-6051.

Kenawy, E.R., Bowlin, G.L., Mansfield, K., Layman, J., Simpson, D.G., Sanders, E.H., Wnek, G.E., **2002**, Release of tetracycline hydrochloride from electrospun poly(ethylene-co-vinylacetate), poly(lactic acid), and a blend. Journal of Controlled Release 81, 57-64.

Khadka, D.B., Haynie, D.T., **2012**, Protein- and peptide-based electrospun nanofibers in medical biomaterials. Nanomedicine: Nanotechnology, Biology, and Medicine 8, 1242–1262.

Khansari, S., Sinha-Ray, S., Yarin, A.L., Pourdeyhimi, B., **2012**, Stress-strain dependence for soy-protein nanofiber mats. Journal of Applied Physics 111, 044906 (1-13).

Ki, C.S., Gang, E.H., Um, I.C., Park, Y.H., **2007**, Nanofibrous membrane of wool

keratose/silk fibroin blend for heavy metal ion adsorption, Journal of Membrane Science 302, 20–26.

Kidoaki, S., Kwon, K., Matsuda, T., **2005**, Mesoscopic spatial designs of nano- and microfiber meshes for tissue-engineering matrix and scaffold based on newly devised multilayering and mixing electrospinning techniques. Biomaterials 26, 37-46.

Kim C., Jeong, Y., Ngoc, B.T.N., Yang, K.S., kojima, M., Kim, Y.A., Endo, M., Lee, A.Y., **2007**, Synthesis and characterization of porous carbon nanofibers with hollow cores through the thermal treatment of electrospun copolymeric nanofiber webs. Small Nano Micro 3, 91-95.

Kint, D., Munoz-Guerra, S., **1999**, A review on the potential biodegradability of poly(ethylene terephthalate). Polymer International 48, 346-352.

Klabunde, K.J., **2001**, Nanoscale materials in chemistry. Wiley, New York.

Klass, D.L., **1998**, Biomass for Renewable Energy, Fuels, and Chemicals. Academic Press: New York.

Krassig, H., **1993**, Cellulose: Structure, accessibility and reactivity, CRC Press.

Kumar, R., Choudhary, V., Mishra, S., Varma, I.K., Mattiason, B., **2002**, Adhesives

and plastics based on soy protein products. Industrial Crops and Products 16, 155–172.

Kumar, R., Munstedt, H., **2005**, Silver ion release from antimicrobial polyamide/silver composites. Biomaterials 26, 2081-2088.

Kwon Seo, Dong., Jeun, J.P., Bin Kim, H., Hyun Kang, P., **2011**, Preparation and characterization of the carbon nanofiber mat produced from electrospun PAN/lignin precursors by electron beam irradiation. Reviews on Advanced Materials Science 28, 31-34.

Langer, R., Peppas, N.A., **2003**, Advances in biomaterials, drug delivery, and bionanotechnology. AIChe Journal, Bioengineering, food, and natural products 49, 2990-3006.

Laurencin, C.T., Ambrosio, A.M.A, Borden, M.D., Cooper J.A., **1999**, Tissue engineering: orthopedic applications. Annual Review of Biomedical Engineering 01, 19-46.

Leach, K.J., Mathiowitz, E.(ed.), **1999**, Encyclopedia of controlled drug delivery. Wiley, New York 1, 119–142.

Lee, Y.S., Livingston, A.T., **2011**, Electrospun nanofibrous materials for neural tissue

engineering. Polymers 3, 413-426.

Lewis, D.H., **1990**, Controlled release of bioactive agents from lactide/glycolide polymers. In: Chasin, M., Langer, R.(eds.) Biodegradable polymers as drug delivery systems. Marcel Dekker, New York, 1–8.

Li, W.J., Danielson, K.G., Alexander, P.G., Tuan, R.S., **2003**, Biological response of chondrocytes cultured in three dimensional nanofibrous poly(ε-caprolactone) scaffolds. Journal of Biomedical Materials Research Part A 67A, 1105-1114.

Li, W.J., Tuli, R., Huang, X., Laquerriere, P., Tuan, R.S., **2005a**, Multilineage differentiation of human mesenchymal stem cells in a three-dimensional nanofibrous scaffold. Biomaterials 26, 5158-5166.

Li, W.J., Tuli, R., Okafor, C., Derfoul, A., Danielson, K.G., Hall, D.J., Tuan, R.S., **2005b**, A three-dimensional nanofibrous scaffold for cartilage tissue engineering using human mesenchymal stem cells. Biomaterials 26, 599-906.

Li, C., Vepari, C., Jin, H.J., Kim, H.J., Kaplan, D.L., **2006**, Electrospun silk-BMP-2 scaffolds for bone tissue engineering. Biomaterials 27, 3115-3124.

Liao, I.C., Chew, S.Y., Leong, K.W., **2006**, Aligned core-shell nanofibers delivering bioactive proteins. Nanomedicine 1, 465-471.

Librovich, V.B., Yarin, A.L., **1982**, Effect of mechanical stresses on the combustion velocity of the mixed solid fuels. Combustion, Explosion and Shock Waves 18, 547-551.

Librovich, V. B., Yarin, A. L., **1988**, Problems of the mechanical strength in the combustion theory. Archivum Combustionis 8, 79-99.

Liu, K.S., **1997**, Soybeans: chemistry, technology, and utilization. New York, Chapman & Hall.

Liu, D., Chen, H., Chang, P.R., Wu, Q., Li, K., Guan, L, **2010**, Biomimetic soy protein nanocomposites with calcium carbonate crystalline arrays for use as wood adhesive. Bioresource Technology 101, 6235-6241.

Liu, T., Gu, S.Y., Zhang, Y.H., Ren, J., **2012**, Fabrication and characterization of carbon nanofibers with a multiple tubular porous structure via electrospinning. Journal of Polymer Research 19, 1-6.

Liu, H., Hsieh, Y.L., **2002**, Ultrafine fibrous cellulose membranes from electrospinning of cellulose acetate. Journal of Polymer Science: Part B Polymer Physics 40, 2119-2129.

Liu, X., Mai, P.X., **2004**, Polymeric scaffolds for bone tissue engineering. Annuals of Biomedical Engineering 32, 477-486.

Lu, S.Y., Wu, D., Wang, Q.L. Yan, J., Buekens, A.G., Cen, K.F., **2011**, Photocatalytic decomposition on nano-TiO2: Destruction of chloroaromatic compounds. Chemosphere 82, 1215-1224.

Ma, Z., Kotaki, M., Ramakrishna, S., **2005a**, Electrospun cellulose nanofiber as affinity membrane. Journal of Membrane Science 265, 115-123.

Ma, Z., Kotaki, M., Inai, R., Ramakrishna, S., **2005b**, Potential of nanofiber matrix as tissue engineering scaffolds. Tissue Engineering 11, 101-109.

Ma Z., Kotaki M., Yong T., Wei H., Ramakrishna S., **2005c**, Surface engineering of electrospun polyethylene terephthalate (PET) nanofibers towards development of a new material for blood vessel engineering. Biomaterials 26, 2527-2536.

Mahonty, A.K., Misra, M., Hinrichsen, G., **2000**, Biofibres, biodegradable polymers and biocomposites: An overview. Macromolecular Materials & Engineering 276/277, 1–24.

Maneerung, T., Tokura, S., Rujiravanit, R., **2008**, Impregnation of silver nanoparticles into bacterial cellulose for antimicrobial wound dressing, Carbohydrate Polymers 72,

43-51.

Mark, J.E., **1999**, Polymer Data Handbook. Oxford University Press.

Martina, M., Hutmacher, D.W., **2007**, Biodegradable polymers applied in tissue engineering research: a review. Polymer International 56, 145-157.

Matthews, J.A., Wnek, G.E., Simpson, D.G., Bowlin, G.L., **2002**, Electrospinning of collagen nanofibers. Biomacromolecules 3, 232-238.

McCullen, S.D., Ramaswamy, S., Clarke, L.I., Gorga, R.E., **2009**, Nanofibrous composites for tissue engineering applications. Wiley Interdisciplinary Reviews: Nanomedicine and Nanobiotechnoly 1, 369-390.

McCullagh, C., Robertson, J.M.C., Bahnemann, D.W., Robertson, P.K.J., **2007**, The application of TiO2 photocatalysis for disinfection of water contaminated with pathogenic micro-organisms: a review. Research on Chemical Intermediates 33, 359-375.

Michielsen, S., Pourdeyhimi, B., Desai P., **2006**, Review of thermally point-bonded nonwovens: Materials, processes, and properties. Journal of Applied Polymer Science 99, 2489-2496.

Min, K.D., Park, W.H., **2008**, Controlling size and distribution of silver nanoparticles generated in inorganic silica nanofibers using poly(vinyl pyrrolidone). Macromolecular Research 16, 626-630.

Miyoshi, T., Toyohara, K., Minematsu, H., **2005**, Preparation of ultrafine fibrous zein membranes via electrospinning. Polymer International 54, 1187-1190.

Mo, X., Sun, X.S., Wang, Y., **1999**, Effects of molding temperature and pressure on properties of soy protein polymers. Journal of Applied Polymer Science 73, 2595–2602.

Moroni, L., Licht, M., Boer, J., Wijn, J., Blitterswijk, C., **2006**, Fiber diameter and texture of electrospun PEOT/PBT scaffolds influence human mesenchymal stem cell proliferation and morphology, and the release of incorporated compounds. Biomaterials 27, 4911-4922.

Murata-Kamiya, N., Kamiya, H., Kaji, H., Kasai, H., **1997**, Mutational specificity of glyoxal, a product of DNA oxidation, in the lacI gene of wild-type Escherichia coli W3110. Mutation Research 377, 255-262.

Narasimhan, B., **2001**, Mathematical models describing polymer dissolution: consequences for drug delivery. Advanced drug delivery reviews 48, 195-210.

Nayudamma, Y., Joseph, K.T., Bose, S.M., **1961**, Studies on the interaction of collagen with dialdehyde starch. American Leather Chemists' Association Journal 5, 548-567.

Ochuma, I.J., Osibo, O.O., Fishwick, R.P., Pollington, S., Wagland, A., Wood, J., Winterbottom, J.M., **2007**, Three-phase photocatalysis using suspended titania and titania supported on a reticulated foam monolith for water purification. Catalysis Today 128, 100-107.

Ollis, D.F., **2003**, Integrating Photocatalysis and Membrane Technologies for Water Treatment. Annals New York Academy of Sciences 984, 65-84.

O'Sullivan , A.C., **1997**, Cellulose: the structure slowly unravels. Cellulose 4, 173-207.

Otaigbe, J.U., Adams, D.O., **1997**, Bioabsorbable soy protein plastic composites: effect of polyphosphate fillers on water absorption and mechanical properties. Journal of Environmental Polymer Degradation 5, 199- 208.

Padamwar, M.N., Pawar, A.P., **2004**, Silk sericin and its applications: a review. Journal of Scientific & Industrial Research 63, 323-329.

Paetau, I., Chen, C.Z., Jane, J.L., **1994a**, Biodegradable plastic made from soybean

products. 1. Effect of preparation and processing on mechanical properties and water. Industrial & Engineering Chemistry Research 33, 1821-1827.

Paetau, I., Chen, C.Z., Jane, J.L., **1994b**, Biodegradable plastics made from soybean products. I. Effects of crosslinking and cellulose incorporation on mechanical properties and water absorption. Journal of Environmental Polymer Degradation 2, 211–217.

Paul, G.M., Krinski, T.L., **1983**, Heat coagulable paper composition with a soy protein adhesive binder. US Patent 4,421,564.

Pchat-Bohatier, C., Sanchez, J., Gontard, N., **2006**, Influence of relative humidity on carbon dioxide sorption in wheat gluten films. Journal of Food Engineering 77, 983-991.

Pekakis, P.A., Xekoukoulotakis, N.P., Mantzavinos, D., **2006**, Treatment of textile dyehouse wastewater by TiO2 photocatalysis. Water Research 40, 1276-1286.

Peng, B.L., Dhar, N., Liu, H.L., Tam, K.C., **2011**, Chemistry and applications of nanocrystalline cellulose and its derivatives: a nanotechnology perspective. The Canadian Journal of Chemical Engineering 9999, 1-16.

Peters, Jr. T., **1996**, All About Albumin: Biochemistry, Genetics, and Medical

Applications. Academic Press.

Pham, Q.P., Sharma, U., Mikos, A.G., **2006**, Electrospinning of polymeric nanofibers for tissue engineering applications, a review. Tissue Engineering 12, 1197-1211.

Phiriyawirut, M., Rodchanacheewa, N., Nensiri, N., Supaphol, P., **2008**, Morphology of electrospun mats of soy protein isolate and its blend. Advanced Materials Research 55-57, 733-736.

Pillai, Z.S., Kamat, P.V., **2004**, What factors control the size and shape of silver nanoparticles in the citrate ion reduction method? The Journal of Physical Chemistry 108, 945-951.

Poole, A. J., Church, J. S., Huson, M. G., **2009**, Environmentally sustainable fibers from regenerated protein. Biomacromolecules 10, 1-8.

Prager, W., **1938**, On isotropic materials with continuous transition from elastic to plastic state. Proc. 5th Int. Congr. Appl. Mech., Cambridge, Mass. 234.

Prager, W., **1942**, Fundamental theorems of a new mathematical theory of plasticity. Duke Mathematical Journal 9, 228-233.

Price, R.L., Gutwein, L.G., Kaledin, L., Tepper, F., Webster, T.J., **2003**, Osteoblast

function on nanophase alumina materials: Influence of chemistry, phase, and topography. Journal of Biomedical Materials Research Part A 67A, 1284-1293.

PRO-FAM 955 Isolated Soy Protein 066-955 Data Sheet, ADM Specialty Products-Oilseeds.

Qi, D., Kang, X., Chen, L., Zhang, Y., Wei, H., Gu, Z., **2008**, Electrospun polymer nanofibers as a solid-phase extraction sorbent for the determination of trace pollutants in environmental water. Analytical and Bioanalytical Chemistry 390, 929-939.

Qin, X.-H., Wang, S.Y, **2006**, Filtration properties of electrospinning nanofibers. Journal of Applied Polymer Science 102, 1285-1290.

Quiocho, F.A., Richards, F.M., **1966**, The Enzymic behavior of carboxypeptidase-A in the solid state. Biochemistry 5, 4062-4076.

Radetic, M., Illic, V., Vodnik, V., Dimitrijevic, S., Jovancic, P., Saponjic, Z., Nedeljkovic, J.M., **2008**, Antibacterial effect of silver nanoparticles deposited on corona-treated polyester and polyamide fabrics. Polymers for Advanced Technologies 19, 1816-1821.

Ramires P.A., Mirenghi L., Romano A.R., Palumbo F., Nicolardi G., **2000,** Plasma-treated PET surfaces improve the biocompatibility of human endothelial cells. Journal

of Biomedical Materials Research 51, 535-539.

Ratner, B.D., Hoffman, A.S., Schoen, F.J., Lemons, J.E., **2012**, Biomaterials Science: An Introduction to Materials in Medicine. Academic Press.

Reneker, D.H., Yarin, A.L., Zussman, E., Xu, H., **2006**, Electrospinning of nanofibers from polymer solutions and melts. Advances in Applied Mechanics. 41, 43-197.

Reneker, D.H., Yarin, A.L., **2008**, Electrospinning jets and polymer nanofibers. Polymer 49, 2387-2425.

Rhim, J.W., Gennadios, A., Handa, A., Weller, C.L., Hanna, M.A., **2000**, Solubility, tensile, and color properties of modified soy protein isolate films. Journal of Agricultural and Food Chemistry 48, 4937-4941.

Rhim, J.W., Gennadios, A., Weller, C.L., Cezeirat, C., Hanna, M.A., **1998**, Soy protein isolate–dialdehyde starch films. Industrial Crops & Products 8, 195-203.

Rhim, J.W., Ng, P.K.W., **2007**, Natural biopolymer-based nanocomposite films for packaging applications. Critical Reviews in Food Science and Nutrition 47, 411-433.

Robinson, J.R., Lee, V.H., **1987**, Influence of drug properties and routes of drug administration on the design of sustained and controlled release systems. In:

Robinson, J.R., Lee, V.H.L. (eds.), Controlled drug delivery: fundamentals and applications, 2nd edn. Marcel Dekker, New York, 3–94.

Roduner, E., **2006**, Size matters: why nanomaterials are different. Chemical Society Reviews 35, 583–592.

Rosso, F., Marino, G., Giordano, A., Barbarisi, M., Parmeggiani, D., Barbarisi, A., **2005**, Smart Materials as Scaffolds for Tissue Engineering. Journal of Cellular Physiology 203, 465-470.

Rubin, M.B., Yarin, A.L., **1993**, Journal of Non-Newtonian Fluid Mechanics 50, 79-88. Corrigendum: Journal of Non-Newtonian Fluid Mechanics **1995**, 57, 321.

Ruppert, G., Bauer, R., Heisler, G., **1994**, UV-O3, UV-H2O2, UV-TiO2 and the photo-fenton reaction comparison of advanced oxidation processes for wastewater treatment. Chemosphere 28, 1447-1454.

Schiffman, J.D., Schauer, C.L., **2008**, A Review: electrospinning of biopolymer nanofibers and their Applications. Polymer Reviews 48, 317-352.

Sell, S.A., McClure, M.J., Garg, K., Wolfe, P.S., Bowlin, G.L., **2009**, Electrospinning of collagen/biopolymers for regenerative medicine and cardiovascular tissue engineering. Advanced Drug Delivery Reviews 61, 1007-1019.

Sessa, D.J., Willett, J.L.(Eds.), **1998**, Paradigm for successful utilization of renewable resources, AOCS Press, Champaign, IL.

Sharma, B., Elisseeff, J.H., **2004**, Engineering structurally organized cartilage and bone tissues. Annuals of Biomedical Engineering 32, 148-159.

Shih, F.F., **1994**, Interaction of soy isolate with polysaccharide and its effect on film properties. Journal of American Oil Chemists' Society 71, 1281–1285.

Shimao, M., **2001**, Biodegradation of plastics. Current Opinion in Biotechnology 12, 242-247.

Shukla, R., Cheryan, M., **2001**, Zein: the industrial protein from corn. Industrial Crops and Products 13, 171–192.

Sileikaite, A., Prosycevas, I., Puiso, J., Juraitis, A., Guobiene, A., **2006**, Analysis of silver nanoparticles produced by chemical reduction of silver salt solution. Materials Science 12, 287-291.

Sill, T.J., von Recum, H.A., **2008**, Electrospinning: applications in drug delivery and tissue engineering. Biomaterials 29, 1989-2006.

Sinha-Ray, S., Khansari, S., Yarin, A.L., Pourdeyhimi, B., **2012**, Effect of chemical and physical cross-linking on tensile characteristics of solution-blown soy protein nanofiber mats. Industrial and Engineering Chemistry Research. 51, 15109-15121.

Sinha-Ray, S., Yarin, A.L., Pourdeyhimi, B., **2010a**, The production of 100/400 nm inner/outer diameter carbon tubes by solution blowing and carbonization of core–shell nanofibers. Carbon 48, 3575-3578.

Sinha-Ray, S., Yarin, A.L., Pourdeyhimi, B.J., **2010b**, Meltblowing: I-basic physical mechanisms and threadline model. Journal of Applied Physics 108, 034912-12.

Sinha- Ray, S., Zhang, Y., Placke, D., Megaridis, C.M., Yarin, A.L., **2010c**, Resins with "Nano-Raisins". Langmuir 26, 10243-10249.

Sinha-Ray, S., Zhang, Y., Yarin, A.L., Davis, S., Pourdeyhimi, B., **2011**, Solution blowing of soy protein fibers. Biomacromolecules 12, 2357-2363.

Slawson, R.M., Van Dyke, M.I., Lee, H., Trevors, J.T., **1992**, Germanium and silver resistance, accumulation, and toxicity in microorganisms. Plasmid 27, 72-79.

Smith, T.P., Alexander, M.J., Enterline, D.S., **2003**, Delayed stenosis following placement of a polyethylene terephthalate endograft in the cervical carotid artery. Report of three cases. Journal of Neurosurgery 98, 421–425.

Sobczyński, A., Dobosz, A., **2001**, Water purification by photocatalysis on semiconductors. Polish Journal of Environmental Studies 10, 195-205.

Son, W.K., Youk, J.H., Lee, T.S., Park, W.H., **2004**, Electrospinning of ultrafine cellulose acetate fibers: studies of a new solvent system and deacetylation of ultrafine cellulose acetate fibers. Journal of Polymer Sciences: Part B Polymer Physics, 42, 5-11.

Srikar, R., Yarin, A.L., Megaridis, C.M., Bazilevsky, A.V., Kelly, E., **2008**, Desorption-limited mechanism of release from polymer nanofibers. Langmuir 24, 965-974.

Stammen, J. A., Williams, S., Ku, D.N., Guldberg, R.E., **2001**, Mechanical properties of a novel PVA hydrogel in shear and unconfined compression. Biomaterials 22, 799-806.

Stephen, A.M., **2006**, Food polysaccharides and their applications, CRC Press.

Stoimenov, P.K., Klinger, R.L., Marchin, G.L., Klabunde, K.J., **2002**, Metal oxide nanoparticles as bactericidal agents. Langmuir 18, 6679-6686.

Stuchell, Y.M., Krochta, J.M., **1994**, Enzymatic treatments and thermal effects on

edible soy protein films. Journal of Food Science 59, 1332–1337.

Sue, H.J., Wang, S., Jane, J.L., **1997**, Morphology and mechanical behavior of engineering soy plastics. Polymer 38, 5035-5040.

Truesdell, C., **1952**, The mechanical foundations of elasticity and fluid dynamics. J. Rat. Mech. Anal. 1, 125-300.

Truesdell, C., **1953**, The mechanical foundations of elasticity and fluid dynamics. Corrections and additions, ibid. 2. J. Rat. Mech. Anal. 2, 593-616.

Tuan, R.S., Boland, G., Tuli, R., **2003**, Adult mesenchymal stem cells and cell-based tissue engineering. Arthritis Research and Therapy 5, 32-45.

Valmikinathan, C.M., Defroda, S., Yu, X., **2009**, Polycaprolactone and bovine serum albumin based nanofibers for controlled release of nerve growth factor. Biomacromolecules 10, 1084–1089.

Vanholme, R., Demedts, K., Ralph, J., Boerjan, W., **2010**, Lignin biosynthesis and structure. Plant Physiology 153, 895-905.

Van Luyn, M.J.A., Van Wachem, P.B., Olde Damink, L.H.H., Dijkstra, P.J., Feijen, J., Nieuwenhuis, P., **1992**, Secondary cytotoxicity of cross-linked dermal sheep collagens

during repeated exposure to human fibroblast. Biomaterials 13, 1017-1024.

Vaz, C.M., Doeveren, P., Yilmaz, G., Graaf, L.A., Reis, R.L., Cunha, A., **2005**, Processing and characterization of biodegradable soy plastics: effects of crosslinking with glyoxal and thermal treatment. Journal of Applied Polymer Science 97, 604-610.

Vaz, C.M., Graaf, L.A., Reis, R.L., Cunha, A.M., **2003**, In vitro degradation behaviour of biodegradable soy plastics: effects of crosslinking with glyoxal and thermal treatment. Polymer Degradation & Stability 81, 65-74.

Vega-Lugo, A., Lim, L., **2009**, Controlled release of allyl isothiocyanate using soy protein and poly(lactic acid) electrospun fibers. Food Research International 42, 933-940.

Veleirinho B., Rei M.F., Lopes-da-Silva J.A., **2008**, Solvent and concentration effects on the properties of electrospun poly(ethylene terephthalate) nanofiber mats. Journal of Polymer Science: Part B:Polymer Physics 46, 460-471.

Verreck, G., Chun, I., Rosenblatt, J., Peeters, J., Van Dijck, A., Mensch, J., Noppe, M., Brewster, M.E., **2003**, Incorporation of drugs in an amorphous state into electrospun nanofibers composed of a water-insoluble, nonbiodegradable polymer. Journal of Controlled Release 92, 349-360.

Wall, J.S., **1971**, Disulfide bonds: determination, location, and influence on molecular properties of proteins. Journal of Agricultural and Food Chemistry 19, 619-625.

Wang, J., Huang, N., Yang, P., Leng, Y.X., Sun, H., Liu, Z.Y., Chu, P.K., **2004**, The effects of amorphous carbon films deposited on polyethylene terephthalate on bacterial adhesion. Biomaterials 25, 3163–3170.

Wang, X., Michielsen, S., **2002**, Morphology gradients in thermally point-bonded poly(ethylene terephthalate) nonwovens. Textile Research Journal 72, 394-398.

Wang, Z., Wan, L., Liu, Z., Huang, X., Xu, Z., **2009**, Enzyme immobilization on electrospun polymer nanofibers: an overview. Journal of Molecular Catalysis B: Enzymatic 56,189-195.

Wellen, R., Canedo, E., Rabello, M., **2012**, Effect of styrene-co-acrylonitrile on cold crystallization and mechanical properties of poly(ethylene terephthalate). Journal of Applied Polymer Science 125, 2701-2710.

Whelove O. E., Cozad M.J., Lee B.D., Sengupta S., Bachman S.L., Ramshaw B.J., Grant S.A., **2011**, Development and in vitro studies of a polyethylene terephthalate-gold nanoparticle scaffold for improved biocompatibility. Journal of Biomedical Materials Research B:Appiled Polymer Biomaterials 99B, 142-149.

Wise, D.L., Klibanov, A.M., Langer, R., Mikos, A.G., Peppas, N.A., Trantolo, D.J.,

Wnek, G.E., Yaszemski, M.J. (Eds.), **2000**, Handbook of Pharmaceutical Controlled Release Technology. Marcel Dekker, New York.

Yao, C., Li, X., Song, T., **2006**, Electrospinning and crosslinking of zein nanofiber mats. Journal of Applied Polymer Science 103, 380–385.

Yarin, A.L., **2008**, Stimuli-responsive polymers in nanotechnology: deposition and possible effect on drug release. Mathematical Modeling of Natural Phenomena 3, 1-15.

Yoo, H.S., Kim, T.G., Park, T.G., **2009**, Surface-functionalized electrospun nanofibers for tissue engineering and drug delivery. Advanced Drug Delivery Reviews 61, 1033-1042.

Zahedia, P., Rezaeiana, I., Ranaei-Siadatb, S.-O., Jafaria, S.-H., Supaphol, P., **2010**, A review on wound dressings with an emphasis on electrospun nanofibrous polymeric bandages. Polymers for Advanced Technologies 21, 77-95.

Zhang, Y.Q., **2002b**, Applications of natural silk protein sericin in biomaterials. Biotechnology Advances 20, 91-100.

Zhang, L., Kanki, T., Sano, N., Toyoda, A., **2003**, Development of TiO2 photocatalyst reaction for water purification. Separation and Purification Technology 31, 105-110.

Zhang, H., Magoshi, J., Magoshi, Y., Yoshida, H., Chen, J.Y., Saiki, K., **2002a**, Inorganic composition and thermal properties of cocoon fiber. International Journal of the Society of Materials Engineering for Resources 10, 113-116.

Zhang, J., Mungara, P., Jane, J., **2001**, Mechanical and thermal properties of extruded soy protein sheets. Polymer 42, 2569-2578.

Zhou, W., He, J., Du, S., Cui, S., Gao, W., **2011a**, Electrospun silk fibroin/cellulose acetate blend nanofibres: structure and properties. Iranian Polymer Journal 20, 389-397.

Zhou, W., He, J., Cui, S., Gao, W., **2011b**, Studies of Electrospun cellulose acetate nanofibrous membranes, The Open Materials Science Journal 5, 51-55.

Zhuang, X., Yang, X., Shi, L., Cheng, B., Guan, K., Kang, W., **2012**, Solution blowing of submicron-scale cellulose fiber. Carbohydrate Polymers 90, 982-987.

Ziabicki, A., **1976**, Fundamentals of fiber formation: The science of fiber spinning and drawing. Wiley, London.

Zielinska, B., Grzechulska, J., Morawski, A.W., **2003**, Photocatalytic decomposition of textile dyes on TiO2-Tytanpol A11 and TiO2-Degussa P25. Journal of Photochemistry and Photobiology A: Chemistry 157, 65-70.

VITA

NAME: Shahrzad Khansari

EDUCATION: Bachelor of Chemical Engineering,
Sharif University of Technology, Tehran, Iran, 2009

Ph.D., Mechanical Engineering,
University of Illinois at Chicago, Chicago, Illinois, USA, 2013

TEACHING: Teaching Assistant, University of Illinois at Chicago,
Chemical Engineering Department:
Chemical Engineering Thermodynamics (CHE 301)
Chemical Reaction Engineering (CHE 321)
Physics Department:
Introductory Physics Lab (PHYS 106)
Mechanical and Industrial Engineering Department:
Heat Transfer (ME 321)

HONORS: 'NSF CMMI Engineering Research & Innovation' fellowship, 2012

PROFESSIONAL MEMBERSHIP: American Institute of Chemical Engineers (AIChE)
American Society of Mechanical Engineers (ASME)
UIC Women in Engineering

PUBLICATIONS: Journals

Khansari, S., Sinha-Ray, S., Yarin, A.L., Pourdeyhimi, B., 2012. Stress-strain dependence for soy-protein nanofiber mats. Journal of Applied Physics. 111, 044906-1-13.

Sinha-Ray, S., Khansari, S., Yarin, A.L., Pourdeyhimi., B., 2012. Effect of chemical and physical cross-linking on tensile characteristics of solution-blown soy protein nanofiber mats. Industrial and Engineering Chemistry Research. 51, 15109-15121.

Zhang, Y., Lee, M.W., Sinha-Ray, S., Khansari, S., Joshi, B., Hong, S., Hong, J.H., Kim, J.J., Yoon, S.S., Yarin, A.L., Pourdeyhimi, B., 2013. Antibacterial activity of photocatalytic eletrospun Titania nanofiber mats

and solution-blown soy protein nanofiber mats decorated with silver nanoparticles. Catalysis Communications 34, 35-40.

Khansari, S., Duzyer, S., Sinha-Ray, S., Hockenberger, A., Yarin, A.L., Pourdeyhimi, B., 2013. Two-stage desorption-controlled release of fluorescent dye and vitamin from solution-blown and electrospun nanofiber mats containing porogens. Molecular Pharmaceutics (Submitted).